

University of Alberta

Identification of Small Molecule Inhibitors of the Human DNA Repair
Enzyme Polynucleotide Kinase/Phosphatase

by

Gary Freschauf

A thesis submitted to the Faculty of Graduate Studies and Research
in partial fulfillment of the requirements for the degree of

Master of Science
in
Experimental Oncology

Oncology

©Gary Freschauf
Fall 2011
Edmonton, Alberta

Permission is hereby granted to the University of Alberta Libraries to reproduce single copies of this thesis and to lend or sell such copies for private, scholarly or scientific research purposes only. Where the thesis is converted to, or otherwise made available in digital form, the University of Alberta will advise potential users of the thesis of these terms.

The author reserves all other publication and other rights in association with the copyright in the thesis and, except as herein before provided, neither the thesis nor any substantial portion thereof may be printed or otherwise reproduced in any material form whatsoever without the author's prior written permission.

ABSTRACT

Human polynucleotide kinase/phosphatase (hPNKP) is a bifunctional DNA repair enzyme that phosphorylates DNA 5'-termini and dephosphorylates DNA 3'-termini. hPNKP has been shown to be involved in both single- and double-strand break repair, and cancer cells depleted of hPNKP show significant sensitivity to ionizing radiation and various other genotoxic agents, including the chemotherapeutic drug camptothecin. Based on these findings, we hypothesized that small molecule inhibitors could also potentiate the sensitivity of human tumors to γ -radiation or camptothecin.

A12B4C3 was the most effective inhibitor and was able to enhance the radiosensitivity of human A549 lung adenocarcinoma and MDA-MB-231 breast carcinoma cells by a factor of two. Kinetic analysis of A12B4C3 showed it to be a noncompetitive inhibitor. Conformational investigation using circular dichroism, UV difference spectroscopy and fluorescence resonance energy transfer all indicate that A12B4C3 disrupts the secondary structure of PNKP causing an allosteric conformational change resulting in PNKP phosphatase inhibition.

Acknowledgments

I would like to acknowledge my whole family, especially my parents, for their patience and support over the past many years. Achieving a Master of Science degree would not have been possible without their help, because they were always there when things got tough and helped guide me through university.

Secondly, I would like to acknowledge my fiancée Amy for tolerating me these past few months and for helping me take my mind off school when things got rough.

In addition, I would like to thank my friends Todd Mereniuk, Mesfin Fanta, Jodi Wilkinson, Jennifer Dufour, Diana Carandang, Dr. Feridoun-Karimi-Busheri, Jane Lee, Ismail Abdou, and Darcy Robillard. Especially Mesfin for those interesting soccer conversations (Go MAN UTD), Todd for those great times on the golf course, Jennifer for all those Starbucks coffee runs, and finally to Darcy for always being there to have a pint or two.

Furthermore, I would like to thank Dr. Feridoun Karimi-Busheri and Dr. Rajam Mani for their guidance and input throughout my research project. Without their help this project would not have been possible.

Lastly, I would like to especially thank my supervisor, Dr. Michael Weinfeld, for allowing me to work in his lab and for his guidance and support on my project. And also for being there when I needed to talk about things other than science, thanks again.

TABLE OF CONTENTS

Chapter I: Introduction

1.1 DNA Repair

1.1.1 Single-Strand Break Repair

1.1.1.1 Base Excision Repair

1.1.1.2 Sugar Damage Repair

1.1.1.3 Topoisomerase 1 Single-Strand Break Repair

1.1.2 Double-Strand Break Repair

1.1.2.1 Non-Homologous End-Joining

1.2 Polynucleotide Kinase/Phosphatase

1.2.1 Biological Importance of Polynucleotide Kinase/Phosphatase in Cells

1.2.2 Mechanism of Action of Polynucleotide Kinase/Phosphatase

1.3 Cancer

1.3.1 Radiotherapy

1.3.2 Radiation Induced DNA damage

1.3.3 Chemotherapy

1.3.4 Topoisomerase I Inhibitors/ Topoisomerase I inhibitor Induced DNA Damage

1.4 Treating Cancer with Small Molecule Inhibitors

1.4.1 Small Molecule Inhibitors to DNA Repair Enzymes

1.4.2 Small Molecule Inhibitors to Signaling Kinases

1.4.3 Small Molecule Inhibitors of Cell Cycle Proteins

1.5 Synthetic lethality

1.6 Thesis Focus

Chapter II: Identification of a Small Molecule Inhibitor of the Human DNA Repair Enzyme Polynucleotide Kinase/Phosphatase.

2.1 Abstract

2.2 Introduction

2.3 Materials and Methods

2.3.1 Enzymes

2.3.2 Cells

2.3.3 Optimization of fluorescence quenching-based assay for PNKP 3-phosphatase activity

2.3.4 Acquisition and screening of the small molecule library

2.3.5 Assay for 3'-phosphatase activity based on the release of inorganic phosphate

2.3.6 Conventional radio-gel assay for hPNKP 3'-phosphatase activity

2.3.7 PP-1cy and calcineurin phosphatase inhibition assay

2.3.8 DNA kinase assay

2.3.9 Cell proliferation assay

2.3.10 Cytotoxicity studies

2.4 Results

2.4.1 Screening of the library by fluorescence-based assay

2.4.2 Confirmation of inhibition of PNKP phosphatase activity

2.4.3 Inhibitory activity and specificity of A12B4C3

2.4.4 Specificity of A12B4C3

2.4.5 Cytotoxicity of A12B4C3 and cellular radiosensitization by A12B4C3

2.5 Discussion

2.6 Acknowledgements

Chapter III: Mechanism of Action of an Imidopiperidine Inhibitor of Human Polynucleotide Kinase/Phosphatase.

3.1 Abstract

3.2 Introduction

3.3 Materials and Methods

3.3.1 Reagents

3.3.2 Cells

3.3.3 Cytotoxicity Studies

3.3.4 DNA Strand-break repair measured by single-cell gel electrophoresis

3.3.5 DNA Ligase III Assay

3.3.6 DNA Polymerase β Assay

3.3.7 Assay for 3'-phosphatase activity based on the release of inorganic phosphate (Pi)

3.3.8 Inhibition (Lineweaver-burk plot) assay

3.3.9 UV difference spectroscopy

3.3.10 Circular dichroism spectroscopy

3.3.11 Steady-state fluorescence spectroscopy

3.3.12 Fluorescence resonance energy transfer measurements

3.4 Results

3.4.1 Cellular chemosensitization by A12B4C3

3.4.2 Influence of A12B4C3 on DNA strand-break repair

3.4.3 Influence of A12B4C3 on DNA polymerase β and DNA ligase III

3.4.4 Mode of PNKP phosphatase inhibition by A12B4C3

3.4.5 A12B4C3 has no effect on ATP binding to PNKP

3.4.6 Effect of A12B4C3 binding on PNKP conformation

3.4.6.1 Circular dichroism

3.4.6.2 Ultraviolet difference spectroscopy

3.4.6.3 Fluorescence resonance energy transfer

3.4.8 Localization of A12B4C3 interaction site with PNKP

3.5 Discussion

3.6 Acknowledgments

Chapter IV: Discussion, Future Directions and Significance

4.1 Discussion

4.2 Future Directions

4.2.1 Studying A12B4C3's effect on SSBR and DSBR complexes

4.2.2 Pharmacological and Animal Studies for A12B4C3

4.2.3 Development of a Drug Delivery System for A12B4C3

4.2.4 Testing a sub-library of A12B4C3

4.3 Significance

Chapter V: References

Appendix A – Supplementary Material and Analysis from Chapter II (Kinase Inhibitors)

A.1 Introduction

A.2 Results

A.2.1 Screen of imidopiperidine compounds for PNKP Kinase Inhibitors

A.2.2 Confirmation of Kinase Inhibition

A.2.3 Specificity of AUH-7-71-2, MLH-1-14-8, A27B14C5, and AUH-7-193-34

A.2.4 Cytotoxicity of MLH-14-8 and A27B14C5

A.2.5 Radiosensitization by MLH-1-14-8

A.3 Discussion

LIST OF TABLES

TABLE	TITLE	PAGE
2.1	Inhibition by A12B4C3 of other related DNA phosphatases...	57
3.1	Fluorescence energy transfer parameters of AC-labeled PNKP-WFX 402 mutant.....	101
3.2	Effect of A12B4C3 binding on wild-type and mutant PNKP phosphatase activity and Trp fluorescence.....	105

LIST OF FIGURES

FIG.	TITLE	PAGE
1.1	Single-strand break repair pathways.....	6
1.2	Non-homologous end-joining pathway.....	11
1.3	Depiction of the three PNKP subdomains.....	12
1.4	Crystal structure of murine PNKP.....	13
1.5	Mechanism of 5'-DNA Phosphorylation by PNKP.....	14
1.6	Mechanism of 3'-DNA dephosphorylation by PNKP.....	14
1.7	Covalent linkage's of Top type IA and type IB enzymes.....	20
1.8	Mechanism of action of Top1 type IB.....	21
2.1	Screening of the library by a fluorescence-based assay.....	49
2.2	Chemical structures and names of PNKP phosphatase inhibitors.....	52
2.3	Confirmation of inhibition of PNKP phosphatase activity.....	53
2.4	Inhibitory activity and specificity of A12B4C3.....	54
2.5	Specificity of A12B4C3.....	58
2.6	Cytotoxicity of A12B4C3 and cellular radiosensitization by A12B4C3..	59
3.1	Structure of the PNKP inhibitor A12B4C3.....	71
3.2	Chemosensitization by A12B4C3.....	82
3.3	Categorization of comets for alkaline and neutral Comet assay.....	84
3.4	Single strand break slowing by A12B4C3 measured by single cell gel electrophoresis (comet) assay under alkaline conditions.....	85
3.5	Double strand break slowing by A12B4C3 measured by comet assay under neutral conditions.....	88
3.6	Influence of A12B4C3 on human SSBR proteins.....	90
3.7	Lineweaver-Burk analysis of PNKP phosphatase activity.....	92
3.8	Fluorescence titration of PNKP with A12B4C3 and 3'-phosphatse oligonucleotide.....	94
3.9	Fluorescence titration of PNKP versus ATP in the presence and absence of A12B4C3.....	95
3.10	Influence of A12B4C3 binding on PNKP protein conformation.....	98
3.11	UV difference spectrum of PNKP with A12B4C3.....	98
3.12	Fluorescence emission spectra of PNKP.....	102
4.1	Crystal structure of murine PNKP with A12B4C3 Binding.....	116
4.2	Computer model of hPNKP with A12B4C3 Binding.....	117
A.1	Screening of the library for kinase inhibitors of hPNKP.....	136
A.2	Corroboration of kinase inhibition of hPNKP.....	138
A.3	Specificity of kinase inhibitors.....	139
A.4	Cytotoxicity of MLH-1-14-8 and A27B14C5.....	142
A.5	Radiosensitization of A549 lung adenocarcinoma cells by MLH-1-14-8	143

LIST OF ABBREVIATIONS

Abbreviation	Full name
%	percent
°C	degree celsius
⁶⁰ Co	cobalt 60 radiation source
³² P	phosphate 32 radio-isotope
A ₂₈₀	Absorbance 280 nanometers
A12B4C3	2-(1-hydroxyundecyl)-1-(4-nitrophenylamino)-6-phenyl-6,7a-dihydro-1Hpyrrolo[3,4- <i>b</i>]pyridine-5,7(2 <i>H</i> ,4 <i>aH</i>)-dione
AC	acrylodan
APE1	apurinic/aprimidinic endonuclease
APTX	aprataxin
ATM	ataxia telangiectasia-mutated
ATP	adenosine triphosphate
BSA	bovine serum albumin
BER	base excision repair
CaN	calcineurin
CD	circular dichroism
CHART	continuous accelerated hyperfractionated radiotherapy
CLL	chronic lymphocytic leukemia
CML	chronic myeloid leukemia
CO ₂	carbon dioxide
CT	computed tomography
d	days
DE3	BL21-Gold
DMSO	dimethyl sulfoxide
DNA-PK	deoxyribonucleic acid protein kinase
DNA-PKcs	deoxyribonucleic acid protein kinase catalytic subunit
DSB	double-strand break
DSBR	double-strand break repair
DTT	Dithiothreitol
<i>E</i>	efficiency of energy transfer
$\epsilon_A(\lambda)$	the molar extinction coefficient of the acceptor
EDTA	ethylenediaminetetraacetic acid
$F_D(\lambda)$	corrected fluorescence of the donor
FEN1	flap endonuclease 1
g	gravity (units)
Gy	gray (radiation unit)
h	hour
H ₂ O	water
HCl	hydrochloric acid
hAPTX	aprataxin
hPNKP	human polynucleotide kinase/phosphatase
HR	homologous recombination

IC ₅₀	concentration of inhibitor to obtain 50% inhibition
<i>J</i>	spectral overlap integral of donor fluorescence and acceptor absorbance
kDa	kilo-dalton
<i>k</i> ²	dipole orientation factor
<i>k_t</i>	rate of energy transfer from a specific donor to a specific acceptor
L	liter
LB	lysogeny broth
LIG1	DNA ligase 1
LIG3	DNA ligase 3
mer	oligomer
mg	milligram
MgCl ₂	magnesium chloride
min	minutes
ml	milliliter
mm	millimeter
mM	millimolar
MnCl ₂	manganese chloride
mPNKP	mouse polynucleotide kinase/phosphatase
MRI	magnetic resonance imaging
mTop1	mitochondrial topoisomerase I
<i>n</i>	the refractive index of the medium (taken to be 1.4)
NaCl	sodium chloride
NaH ₂ PO ₄	sodium phosphate
NEIL1	nei endonuclease VIII-like 1
NEIL2	nei endonuclease VIII-like 2
ng	nanograms
ng/ μl	nanogram/microliter
NH ₂	amino
NHEJ	non-homologous end-joining
nm	nanometer
NSCLC	non-small-cell lung cancer
NTCP	risk of normal tissue complication
Q _D	quantum efficiency of the donor
Q _D	quantum yield of the donor in absence of the acceptor
Q _{DA}	quantum yield of the donor in presence of the acceptor
P	phosphate
PAR	ADP-ribose
PARP1	poly(ADP-ribose) polymerase 1
PBS	phosphate-buffered saline
PCNA	proliferating cell nuclear antigen
PET	positron emission tomography
Pi	inorganic phosphate
PMSF	phenylmethylsulfonyl fluoride
PNKP	human polynucleotide kinase/phosphatase

PP-1 γ	protein phosphatase-1 gamma
PP-1 ϵ	protein phosphatase-1
PP-1	protein phosphatase-1
Pol β	DNA polymerase beta
Pol δ	DNA polymerase delta
Pol ϵ	DNA polymerase epsilon
R	distance between the donor and acceptor
RNAP	RNA polymerase
R ₀	characteristic distance called the “Förster critical distance”
ROS	reactive oxygen species
rpm	revolutions per minute
s	seconds
SEM	standard error of the mean
SSB	single-strand break
SSBR	single-strand break repair
<i>S. pombe</i> PNKP	<i>Schizosaccharomyces pombe</i> polynucleotide kinase/phosphatase
TBE	Tris/Borate/EDTA
TCP	probability of tumor control
T _d	lifetime of the donor in the absence of the acceptor
Tdp1	tyrosyl DNA-phosphodiesterase
TI	therapeutic index
Top1	topoisomerase I
Top1A	topoisomerase IA
Top1B	topoisomerase IB
TOP1-SSB	topoisomerase I-linked single-strand break
TopII	topoisomerase II
Tris-HCl	tris(hydroxymethyl)aminomethane-hydrochloric acid
Trp ⁴⁰²	tryptophan residue 402 of human polynucleotide kinase/phosphatase
T4 PNK	T4 Bacteriophage polynucleotide kinase/phosphatase
W402F	tryptophan residue 402 mutated to a phenylalanine in human polynucleotide kinase/phosphatase
W331F	tryptophan residue 331 mutated to a phenylalanine in human polynucleotide kinase/phosphatase
WFX402	all tryptophans of human polynucleotide kinase/phosphatase mutated to phenylalanine except tryptophan 402
μ g	microgram
μ g/ml	microgram/milliliter
μ l	microliter
μ M	micromolar
UV	ultraviolet
U/ μ l	units/microliter
XRCC1	X-ray repair cross complementing protein 1
XRCC4	X-ray repair cross complementing protein 4

XRT	radiotherapy
*p20	radiolabeled 5'-phosphate 20-mer oligonucleotide
*p20p	radiolabeled 5'-phosphate 20-mer oligonucleotide with 3'-terminal phosphate
α	alpha
β	beta
γ	gamma
δ	delta
λ	wavelength (cm)

Chapter I

Introduction

1.1 DNA Repair

One of the most essential features of living cells is the ability to maintain genomic stability through the process of DNA repair. This complex process requires the initial identification of the DNA damage followed by its subsequent repair. The complexity of DNA repair is due to the extensive variety of DNA alterations that can occur from both endogenous and exogenous sources.

DNA repair can be subdivided into numerous pathways based on the types of damage. For the purposes of this thesis, only single-strand break repair (SSBR) via base excision repair (BER), sugar damage repair, and topoisomerase I inhibitor single strand break repair (TOP1-SSB) and double-strand break repair (DSBR) via the Non-Homologous End-Joining (NHEJ) pathway will be discussed. Both SSBR and DSBR are vital to ensure genomic stability as everyday the cell encounters approximately 10 000 single strand lesions and ~ 10 double strand breaks (DSBs) under normal cellular processes (1). However, this number greatly increases if cells are exposed to exogenous DNA damaging agents such as radiation or environmental toxins, and the subsequent increase in DNA damage can lead to failure to repair all the lesions resulting in a mutation, cell killing or replication errors.

1.1.1 Single-strand Break Repair

Single strand breaks (SSBs) are commonly associated with loss of one or more nucleotides often resulting in damaged 5' and/or 3' termini. SSBs and damage to DNA nucleotides are the major source's of DNA damage in living cells as they occur at substantially higher rates than DSBs (2). Because of this

cells have developed several SSBR pathways to cope with the daily onslaught of SSBs and damaged bases. These include base excision repair (indirect SSB), sugar damage (direct SSB), and topoisomerase I-linked single-strand break (TOP1-SSB) repair pathways (Figure 1.1).

1.1.1.1 Base Excision Repair

All three SSBR pathways contain four similar steps in order to complete DNA repair. These consist of a detection, end processing, gap filling and ligation step. In BER, single-strand breaks are either detected by apurinic/apyrimidinic endonuclease 1 (APE1), Lyase or possibly by poly(ADP-ribose) polymerase 1 (PARP1) (2). Lyases break the phosphodiester backbone of DNA, creating a SSB and DNA glycosylases frequently have lyase activity (3). Importantly, PARP1 detection of indirect SSBs is unlikely because APE1/lyase activity is responsible for cutting the phosphodiester backbone (2). After detection of the SSB, the damaged termini need to be repaired and this requires the action of end processing enzymes. For indirect SSBs the end processing enzymes consist of APE1, polynucleotide kinase/phosphatase (PNKP), DNA polymerase β (Pol β), and aprataxin (APTX) (2). Following successful repair of the damaged termini the gap must be filled in order for the DNA ends to be ligated together. During indirect SSB repair gap filling can range from 1-12 nucleotides (nt) and a DNA polymerase will be selected depending on the size of the gap. Gaps of 1 nt are predominately filled by Pol β (short patch repair), while gaps of ~2-12 nt are filled by either Pol β , DNA polymerase δ (Pol δ) or DNA polymerase ϵ (Pol ϵ) (long patch repair) (2). Pol β fills the first nt then either Pol δ or Pol ϵ take over.

Subsequently the final step of ligation is completed by either DNA ligase III (LIG3) or DNA ligase I (LIG1) corresponding to short or long patch repair, respectively (2).

1.1.1.2 Sugar Damage Repair

Sugar damage (direct SSB) is very common in human cells due to their consumption of oxygen, which creates toxic metabolites called reactive oxygen species (ROS). ROS are present in large quantities in a cell and if left unresolved can directly cause SSBs by direct interaction with the deoxyribose groups in DNA (2). Direct SSBs are detected by PARP1, which binds to the site of damage activating it thereby allowing the repair complex to access the DNA lesion. Activation of PARP1 proceeds through process of rapid catalyzation of ADP-ribose units that are transferred from NAD⁺ to PARP1 thereby resulting in the formation of branched polymers of ADP-ribose (PAR) (4). These branched PAR units help signal downstream repair proteins to the DNA strand-break. The repair complex is composed of several proteins including x-ray repair cross complementing protein 1 (XRCC1), APE1, APTX, PNKP, and LIG3 (2). The repair complex's initial function is the correction of the damaged 5' and/or 3' termini into the correct 5' phosphate and 3'-hydroxyl termini. Following the successful remediation of the damaged termini a DNA polymerase inserts the missing nucleotides. The size of the gap will help determine which polymerase will be utilized. For gaps of 1 nt (short patch) Pol β is the polymerase of choice, however for long patches of missing nucleotide, ~2-12 nts, the operation can be performed by Pol β , Pol δ or Pol ϵ (2). Pol β adds the first nt then Pol δ or Pol ϵ take

over. Importantly, for direct SSBs requiring long patch repair an additional step is required called the flap removal step. The flap is generated by the addition of new nucleotides, which supplant the existing nucleotides. This 5' flap is removed by flap endonuclease 1 (FEN1), which must first be stimulated by PARP1 and proliferating cell nuclear antigen (PCNA) (2). Once gap filling has been completed short patch repaired gaps are ligated by LIG3 and long patch-repaired gaps are ligated by LIG1 (2).

1.1.1.3 Topoisomerase I-Linked Single-Strand Break Repair

The final SSB pathway is TopI-SSBR, which deals with SSBs that arise from aberrant topoisomerase I (TopI) activity. TopI enzymes function by cutting the phosphodiester backbone on one DNA strand and then the subsequent relaxing and reannealing of the strands (5). The Top1 reaction involving SSBs requires the formation of protein-DNA complex's whereby the damaged 3'-ends of the SSB are briefly covalently linked to Top1 through interaction with the tyrosine hydroxyl residue. TopI-SSBs transpire through two mechanisms; 1) improper interaction with RNA polymerase (RNAP) or 2) through interaction with DNA damage in close vicinity to Top1 activity (2). As with BER, the detection of TopI-SSBs is thought to be via the initial step, which is the cause of the TopI-SSB damage (2). End processing of TopI-SSBs is a three-step process; initially tyrosyl-DNA phosphodiesterase 1 (TDP1) removes the TopI enzyme from the 3' end resulting in a 3'phosphate terminus (2); second following TopI removal, PNKP cleaves off the 3'phosphate leaving a proper 3' hydroxyl terminus (2); and lastly PNKP phosphorylates the 5'-hydroxyl end at TOP1-SSBs.

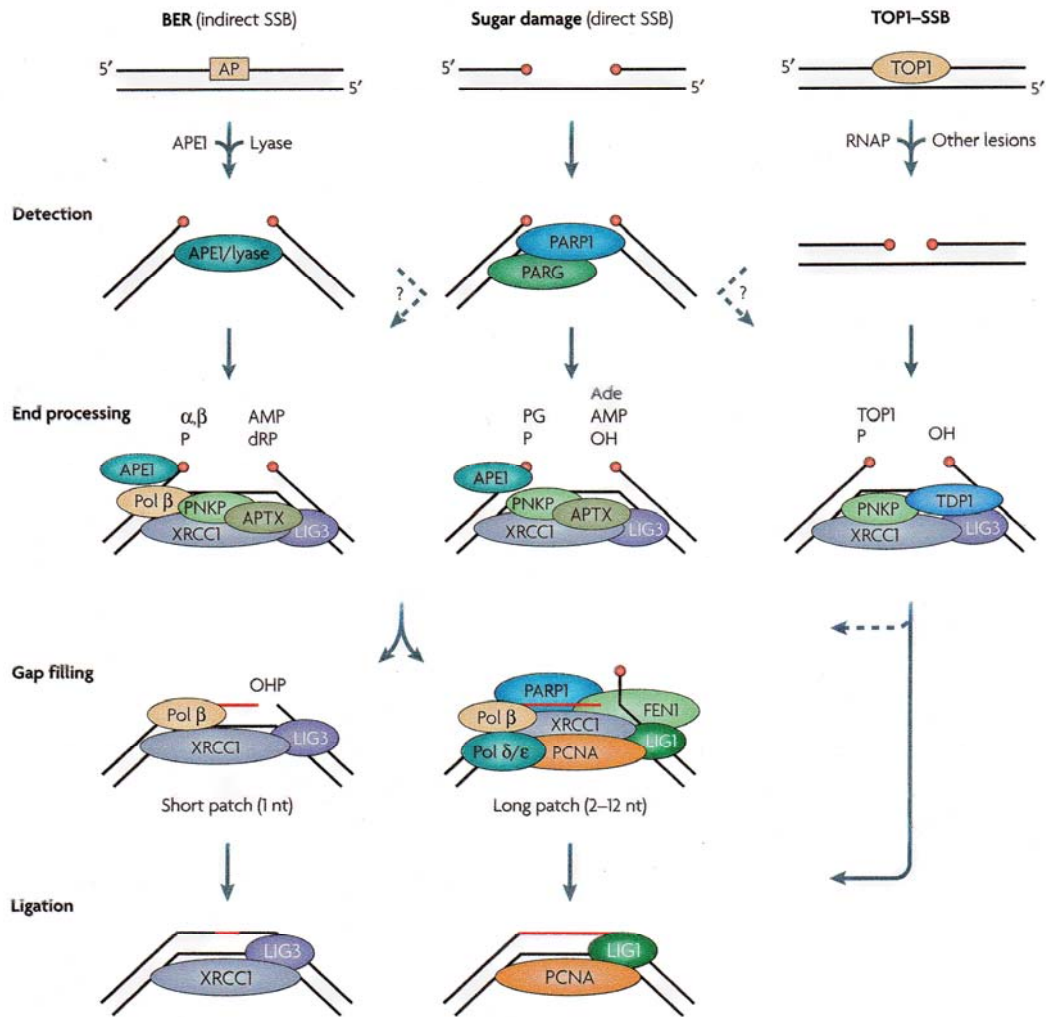


Figure 1.1. The complexity and variety of single strand break repair pathways in the cell. SSBR can be subdivided into 3 pathways depending on the type of DNA damage. BER normally deals with repair of apurinic or apyrimidinic damage. Direct SSB repair pathway manages sugar damage and TOP1-SSB pathway fixes DNA damage as a result of topoisomerase enzymatic activity. (Caldecott et al., 2008)

Importantly, TopI-SSBs may not require gap filling because they usually create DNA nicks (2). The gap filling (if required) and ligation steps are identical to those described for BER and sugar damage repair pathways.

1.1.2 Double-Strand Break Repair

DNA double-strand breaks (DSBs) are extremely detrimental to the cell and unless repaired lead to deleterious effects such as chromosomal rearrangements (translocations or deletions) or cell death. These deleterious effects help accelerate aging and promote carcinogenesis (6). DSBs can be introduced by the following agents, ionizing radiation, UV light, oxidative free radicals, replication across a nick, topoisomerase failures and mechanical stress (7). There are two main DSB repair pathways employed in human cells, nonhomologous end-joining (NHEJ) and homologous recombination (HR). For the purpose of this thesis we will only focus on NHEJ, shown in Figure 1.2, because PNKP is a recognized participant in this pathway.

1.1.2.1 Nonhomologous End-Joining

NHEJ repairs DSBs throughout the cell cycle, unlike HR which is only active during late S-phase and G₂ due to the requirement for a sister chromatid (8,9). NHEJ is an error prone pathway that joins DSB ends by a process that's mainly independent of DNA sequence homology (6). The chemical modifications at the DSB termini require processing in order for successful repair to take place. There are a host of enzymes that are responsible for correcting the damaged termini. NHEJ plays a more prominent role in DSBR than HR and is primarily active during G₀, G₁ and early S-phase component of the cell cycle (6,8). NHEJ

can be divided into a 4-step model, which includes a recognition, synapsis, end-processing/extension, and resolution step (Figure 1.2). DSBs are recognized by a heterodimer composed of Ku70/Ku80, which is responsible for recruiting DNA-dependent protein kinase catalytic subunit (DNA-PKcs) to the DSB ends and also acts as a scaffold protein to which other NHEJ proteins can bind (6). Ku is also responsible for triggering the kinase activity of DNA-PKcs (6). Interaction of the DNA-PKcs molecules allows the DSB ends to join up. Synapsis of DNA-PKcs triggers autophosphorylation of DNA-PKcs and phosphorylation is thought to induce a conformational change that allows end processing enzymes to access the ends of the DSB (10). These end-processing enzymes include Artemis, PNKP, or the X-family of DNA polymerases. Artemis interacts with DNA-PK and is responsible for repairing 5' or 3' overhangs (6). In addition, artemis possesses 5'-3' exonuclease activity (6). The X-family of DNA polymerases are responsible for filling gaps during NHEJ (11). Once the DSB ends are properly restored to normal the ligation (resolution) step can occur. Ligation requires the X4-L4 complex (composed of x-ray repair cross complementing protein 4 (XRCC4), DNA ligase 4 (LIG4) and XRCC4-like factor (XLF)) to ligate the ends and complete the NHEJ repair process (6).

1.2 Polynucleotide Kinase/Phosphatase

1.2.1 Biological Importance of Polynucleotide Kinase/Phosphatase in Cells

PNKP is required for the repair of both single- and double-strand breaks through the SSBR/BER and nonhomologous end-joining pathways, respectively (12-15). In the SSBR pathway, PNKP acts in concert with XRCC1, Pol β and

LIG3 (see section 1.1.1.2) (12,16). PNKP involvement in BER was observed after identifying NEIL1 and NEIL2 DNA glycosylase activity, which produces 3'-phosphate termini by the β,δ -elimination reaction (17). At DSBs, PNKP is dependent on DNA-PK and XRCC4 (see section 1.1.2.1) (18,19). Without the repair activities of PNKP, cells are highly sensitive to radiation and topoisomerase I poisons, which create incorrect 3'-phosphate and 5'-hydroxyl termini (15). Furthermore, A549 lung adenocarcinoma cells depleted of PNKP displayed a ~7-fold increase in the spontaneous mutation frequency compared to normal A549 cells due to endogenous DNA damage (19). Failure to properly remove the damaged 5' and 3' ends results in DNA mutations or cell death via apoptosis or necrosis. In addition, mutation of PNKP in humans causes a severe early onset neurological disorder, denoted MCSZ, characterized by seizures and microcephaly (20). Importantly, PNKP is expressed in many tissues throughout the body with the highest levels in the spleen, liver, heart, and kidney and the lowest expression in the small intestine (21).

1.2.2 Mechanism of Action of Polynucleotide Kinase/Phosphatase

Human polynucleotide kinase/phosphatase (PNKP) is a 57.1 kDa enzyme that phosphorylates DNA 5'-termini and dephosphorylates DNA 3'-termini (16,22,23). In 2006, Dobson et al., showed that the phosphatase activity of PNKP is more active compared to the kinase activity and that the phosphatase activity takes precedence when PNKP encounters SSBs possessing both 5'-hydroxyl and 3'-phosphate termini (78). PNKP is composed of three subdomains, the FHA subdomain followed by the two catalytically active phosphatase and kinase

subdomains (16,24) (Figure 1.3). Figure 1.4 shows the crystal structure of the murine PNKP, which is ~80% identical to human PNKP (24). The FHA subdomain has no catalytic function, however it is required for the interaction with the phosphorylated regions of two vital scaffold proteins XRCC1 and XRCC4 (17). The interaction between XRCC1 and XRCC4 with the FHA subdomain effects PNKP function at DNA strand breaks by helping turnover PNKP catalytic activity faster to increase the speed at which the repair reaction takes place (17). Importantly, PNKP's kinase and phosphatase subdomains share similarity to phage T4 PNK. The phosphatase subdomains of both proteins belong to the haloacid dehalogenase (HAD) superfamily (24-26) with a conserved DxDGT motif, where the first Asp forms a covalent phospho-aspartate intermediate with the substrate. The kinase subdomains of both proteins consist of a 5-stranded parallel β sheet, which belong to the adenylate family of kinases (15). PNKP kinase activity requires ATP binding, which is characterized by two Walker motifs, A and B (15). The Walker A motif interacts with the β - and γ -phosphates, while the Walker B motif utilizes Asp 421 and Ser 378 hydrogen bonding, which helps position Mg^{2+} (15). Figure 1.5 displays the mechanism of action of PNKP kinase activity, where activation of the 5'-OH for nucleophilic attack is provided by Asp396 (79). Figure 1.6 shows the mechanism of action for the 3' phosphatase activity of PNKP, where Asp170 is thought to make a covalent phospho-aspartate intermediate, which helps the reaction proceed (79).

1.3 Cancer

Cancer is a generic term for a debilitating disease in which cells

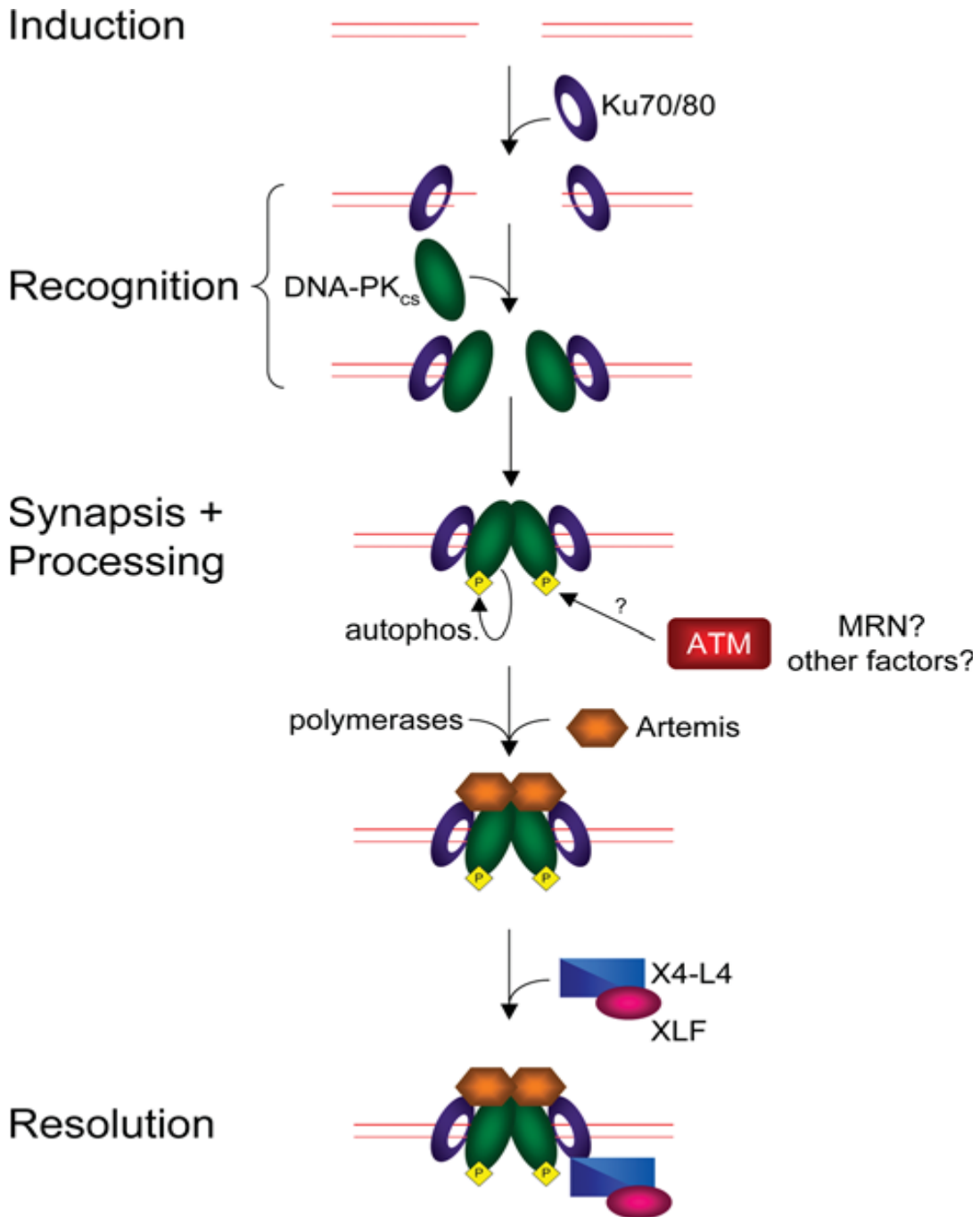


Figure 1.2. The majority of DNA DSBs are repaired by the NHEJ pathway (shown above). The damaged DNA ends are detected by Ku 70/80 heterodimers. Following detection, recognition of the damaged ends is by DNA-PKcs which bring the two damaged ends together. Once the DNA ends are in close proximity to one another DNA-PKcs autophosphorylates itself, thereby allowing recruitment of end-processing enzymes such as PNKP, polymerases, etc. Lastly, the X4-L4 complex including XLF ligates the ends. (Hartlerode et al., 2009)



Figure 1.3. A depiction of the three subdomains of PNKP. At the amino terminus is the FHA subdomain in purple, followed by the two catalytically active phosphatase and kinase subdomains in yellow and green, respectively. The numbers above the representation refer to the amino acid designation of each subdomain.

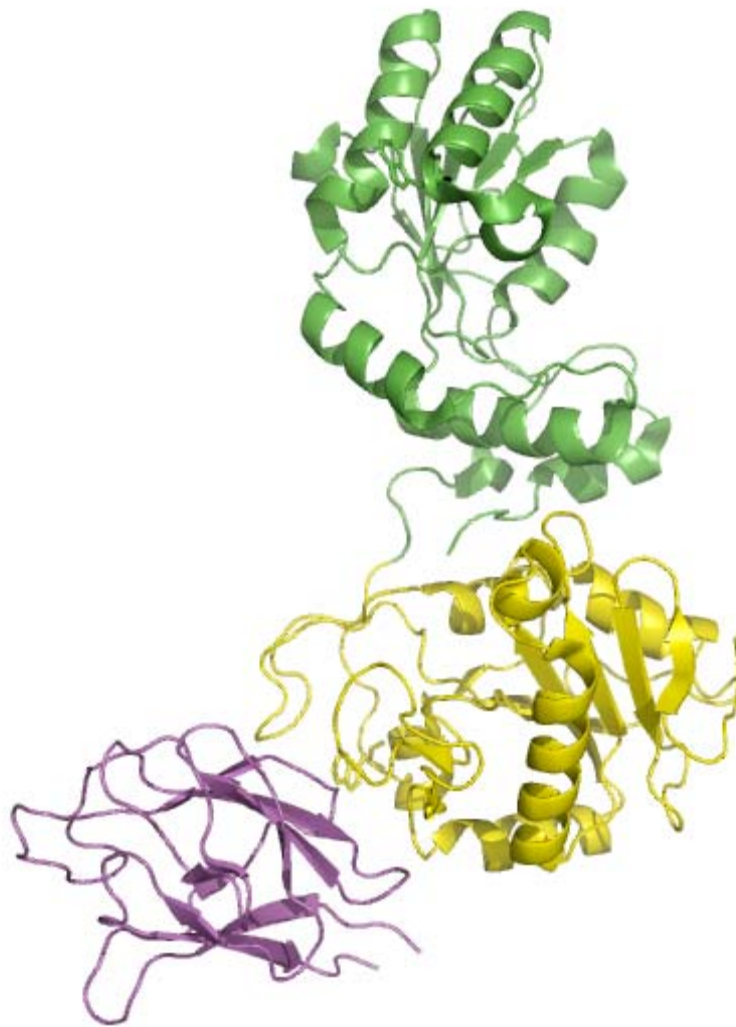


Figure 1.4. The crystal structure of murine PNKP. PNKP has three subdomains, the FHA subdomain in purple and the kinase and phosphatase catalytically active subdomains in green and yellow respectively. (Bernstein et al., 2005)

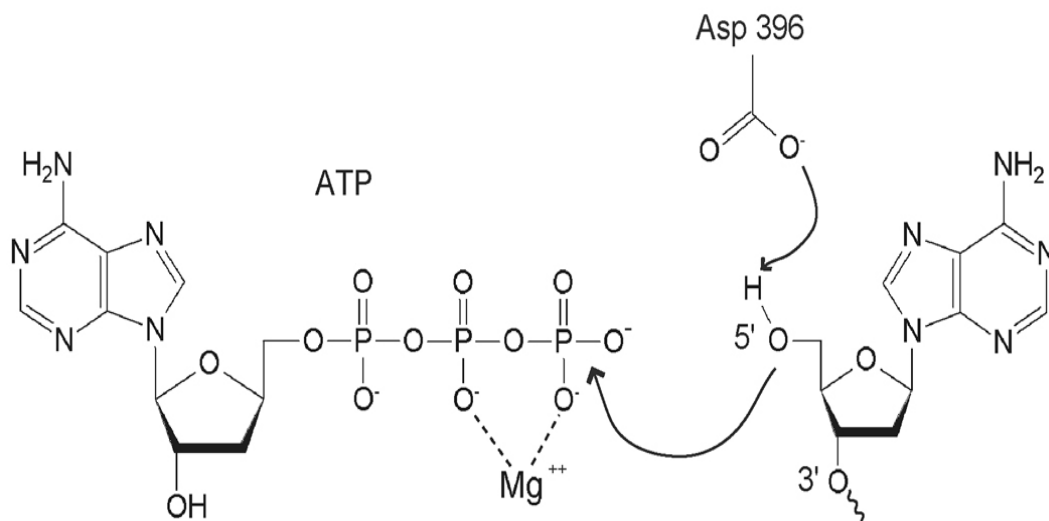


Figure 1.5. The mechanism of action of PNKP kinase activity. Asp 396 is thought to help catalyze the reaction (Bernstein et al., 2008).

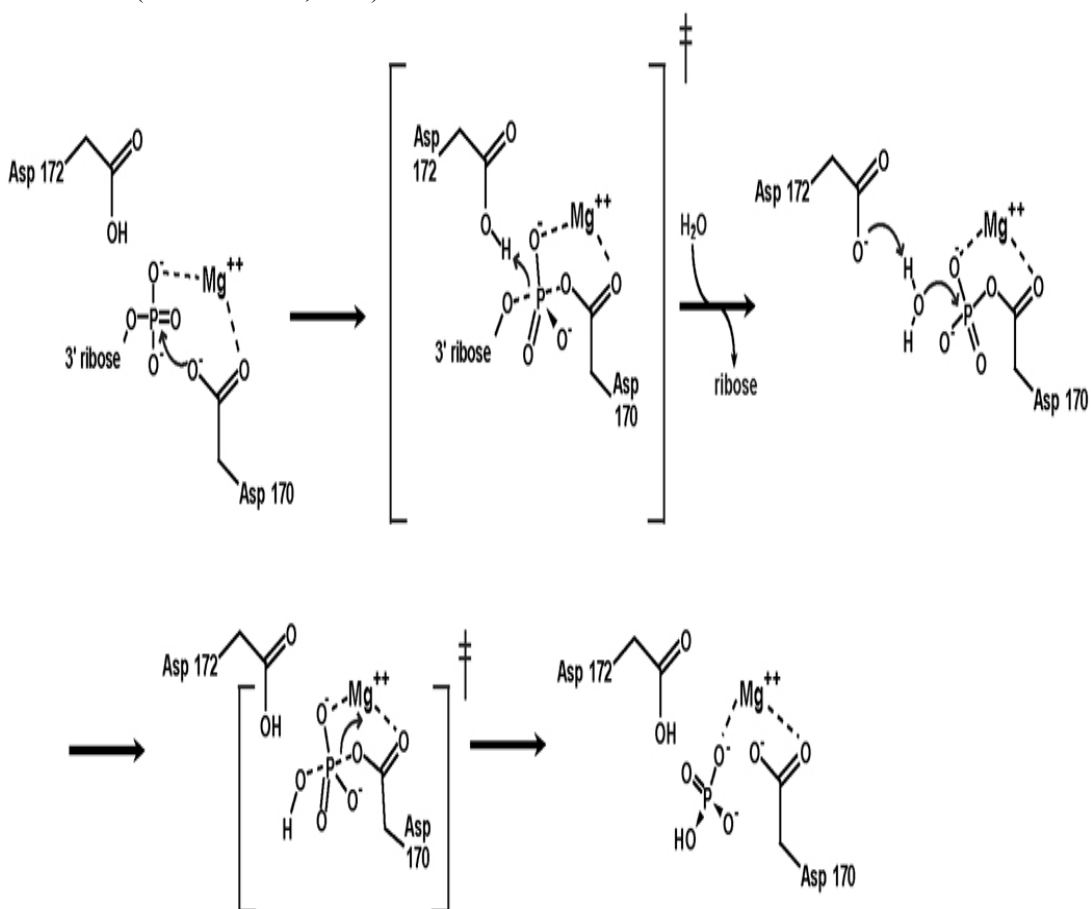


Figure 1.6. The 3'-DNA phosphorylation mechanism of action of PNKPs phosphatase subdomain. PNKP phosphatase activity is hypothesized to involve Asp 170, which is utilized to make a covalent phospho-aspartate intermediate (Bernstein et al., 2008).

display uncontrolled growth, invasion and sometimes metastasis. At present, approximately one in three people will be affected by cancer at some stage of their life, and this is expected to increase to one in two in the near future (27). It has been argued that the majority of cancers 90-95% are due to environmental factors such as smoking, diet, infections, obesity and exposure to toxins and 5-10% are due to genetics (28). The main cellular outcome of the exposure to environmental factors is damage to the DNA and this leads to frequent deleterious events such as amplifications, deletions, inversions, translocations and countless point mutations. These genetic alterations can affect two important classes of genes, proto-oncogenes and tumour suppressors. Oncogenes, which arise from mutation or activation of proto-oncogenes, act dominantly to transform cells through several important cellular mechanisms such as, evasion of apoptosis, increased cell growth and/or cell division, tissue invasion and metastasis (29). Tumor suppressors are recessive in nature and require the “two hit hypothesis”, which implies that both alleles that code for a particular gene must be affected before an effect is manifested (30). The regular physiologic functions of tumour suppressors include regulating the cell cycle, repairing damaged DNA, and initiating apoptosis (31). The development of cancer is a multistep process, which may require as many as 100 mutational events for cancer to arise (32). Once diagnosed with cancer, patients usually undergo treatment with a combination of surgery, radiation and/or chemotherapy.

1.3.1 Radiotherapy

After surgery, radiotherapy (XRT) is the second most commonly used treatment, with a high percentage of patients receiving XRT at some point in their management of cancer. XRT is the medical use of ionizing radiation and is often combined with surgery and/or chemotherapy to obtain optimal results. The most important factor in XRT is the therapeutic index (TI), which is defined “ as the probability of tumour control (TCP) and the risk of normal tissue complications (NTCP) (33)”. Complications from XRT are inevitable and the TI is utilized to allow patients to receive the most effective radiation dose while trying to minimize harmful side effects. However, finding ways to increase the TI is challenging because in most tumours when radiation dose is increased both tumour response and normal tissue injury increase in parallel (33). One of the main reasons for the small TI is because XRT necessitates the inclusion of a margin of normal tissue around the tumour to account for tumour infiltration and also to account for the inadequacies of tumour detection from positron emission tomography (PET), computed tomography (CT), or magnetic resonance imaging (MRI). Along with poor visualization techniques, internal movement of the tumour caused by breathing and unconscious bodily movement affect the arrangement of the tumour during radiation. These factors are the primary reason why the TI for XRT needs improvement.

In today’s cancer clinics standard radiotherapy is usually given in 35 fractions of 2 gray (Gy) during a 7-week program. However, variations of fractionated radiotherapy have been employed, for example hyperfractionated radiation encompasses using smaller doses of radiation more than once per day to

obtain the same total radiation dose as standard XRT. In other strategies, accelerated fractionation has been utilized where the total dose of radiation is given over a shorter period of time usually 3-4 weeks. Finally, both subsets of therapies can be combined to form continuous accelerated hyperfractionated radiotherapy (CHART), which involves multiple low doses of radiation per day over a shorter period of time. Studies indicated that all three non-standard radiation treatments worked better than the standard XRT and the combined accelerated hyperfractionated radiotherapy was most effective at treating cancer (34,35). In spite of this, CHART is not being implemented in cancer clinics because of the extraordinary costs to governments to run the radiation machines and to pay the employees to operate the machines.

1.3.2 Radiation Induced DNA Damage

The most important cellular target of radiotherapy is the nuclear DNA. XRT induces two main classes of DNA damage: 1) isolated DNA lesions and 2) clustered DNA damage (36). Multiple oxidized bases, abasic sites or strand breaks within a couple helical turns characterize clustered DNA damage and these closely spaced lesions are very difficult to correct (36-39). Inability to correct radiation induced clustered DNA lesions can result in cell death or accumulation of mutagenic damage (37-39), which may lead to aberrant cell growth. Conversely, isolated lesions being less complex than clustered damage are easier to repair. Isolated lesions such as SSBs, oxidized bases, or abasic sites, constitute a larger percentage of radiation-induced DNA damage than clustered DNA damage. The most detrimental isolated lesion is the DSB (described in section

1.1.2 and 1.1.2.1), which can kill the cell if not repaired. Furthermore, ionizing radiation produces several main types of strand break termini, such as 3'-phosphate, 3'-phosphoglycolate, and 5-hydroxyl termini (40).

1.3.3 Chemotherapy

Chemotherapy is the third most utilized cancer therapy in today's cancer clinics behind surgery and XRT. The main use of chemotherapy is in the treatment of malignancies and palliative treatment for many advanced cancers (41). Chemotherapy is commonly used both pre- and postoperatively to treat cancer. Neoadjuvant chemotherapy (preoperative) treats the tumour before local treatment (surgery or XRT) with the goal of shrinking the primary tumour (41). Adjuvant chemotherapy (postoperative) is used after local treatment to help eradicate any metastasis present and to help prevent the cancer from reoccurring (41). As with XRT, the TI of chemotherapeutic drugs limits the dose that can be given to the patient. The toxicity to patients usually occurs through dose-limiting toxicity of the bone marrow (41). Currently, chemotherapy is being improved by utilizing specific drug combinations, which act additively to increase the antitumour effects. However, these additive effects can only be observed when the drugs are able to be combined at close to full tolerated concentrations which may help achieve additive effects against the tumour and less than additive effects against normal tissue. Another major drawback is the development of drug resistance in the tumour. Drug-resistance is separated into two classes: intrinsic and acquired. Intrinsic resistance arises when patients do not respond to their initial chemotherapy due to underlying properties of the tumour, while acquired

resistance arises when patients initially respond to chemotherapy but then a sub-population of cancerous cells emerge that have a selective advantage, which will lead to their rapid emergence as the dominant tumour cell population and relapse (41). Drug resistance is hypothesized to be the result of both genetic (mutation or gene amplification) and epigenetic (change in DNA methylation) alterations in the tumour.

1.3.4 Topoisomerase I Inhibitors/ Topoisomerase I Inhibitor Induced DNA Damage

During normal cellular processes DNA may become highly supercoiled due to transcription or chromatid separation (42). Topoisomerases are responsible for the relaxation of these supercoils causing DNA strand breaks on either one (TopI) or both (TopII) DNA strands. TopI is further characterized according to its mechanism of action, where covalent linkages to the 5' termini of the DNA strand break are sub-classified as type IA TopI enzymes and covalent linkages to the 3' termini of the DNA strand break are sub-classified as type IB TopI enzymes (Figure 1.7) (43). The mechanism of catalysis of type IB Top1 is shown in Figure 1.8. To date, two type IB Top have been identified in mammals: a nuclear (Top1) and a mitochondrial enzyme (mTop1) (44). A main class of chemotherapeutic anticancer agents has been shown to target type IB Top. The first drug to target TopI was camptothecin, which was isolated from the *Camptotheca acuminata* tree in 1966 (43). Camptothecin inhibits the re-ligation of Top IB after DNA cleavage, which extends the life of the normal cleaved DNA intermediate (43,44). Camptothecin kills cancer cells by allowing the single strand DNA break to

Type I Topoisomerase

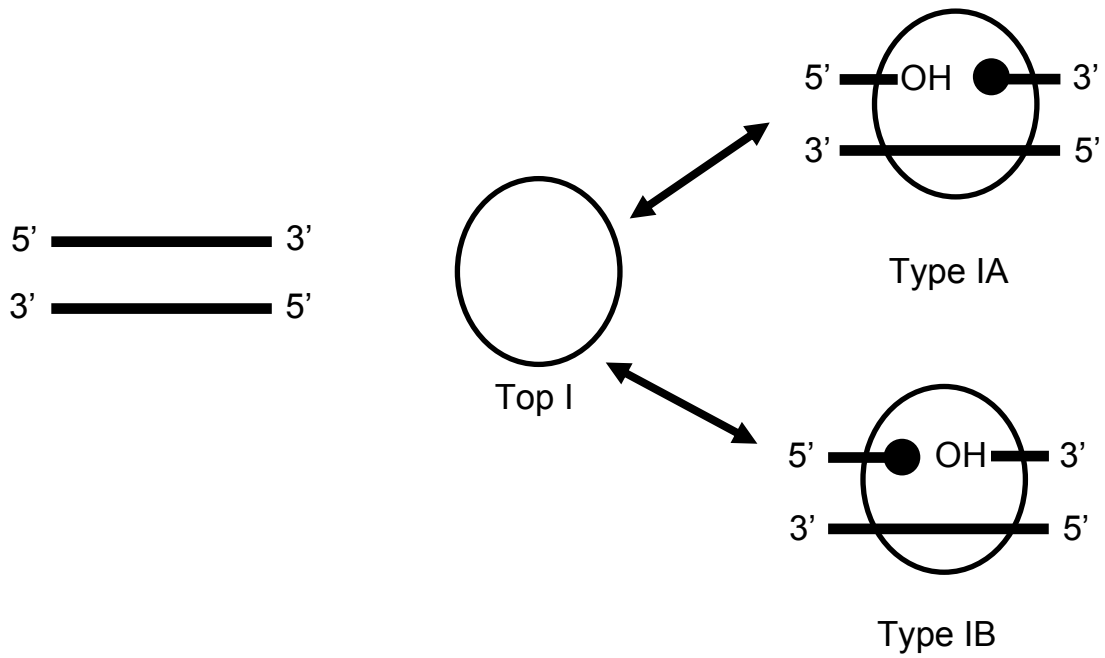


Figure 1.7. Covalent interactions with the DNA strand break for Topoisomerase IA and IB enzymes. Type IA Top forms a covalent linkage to the 5' terminus of the DNA strand break, while Type IB Top makes a covalent linkage to the 3' terminus of the DNA strand break. (Holden et al., 2001)

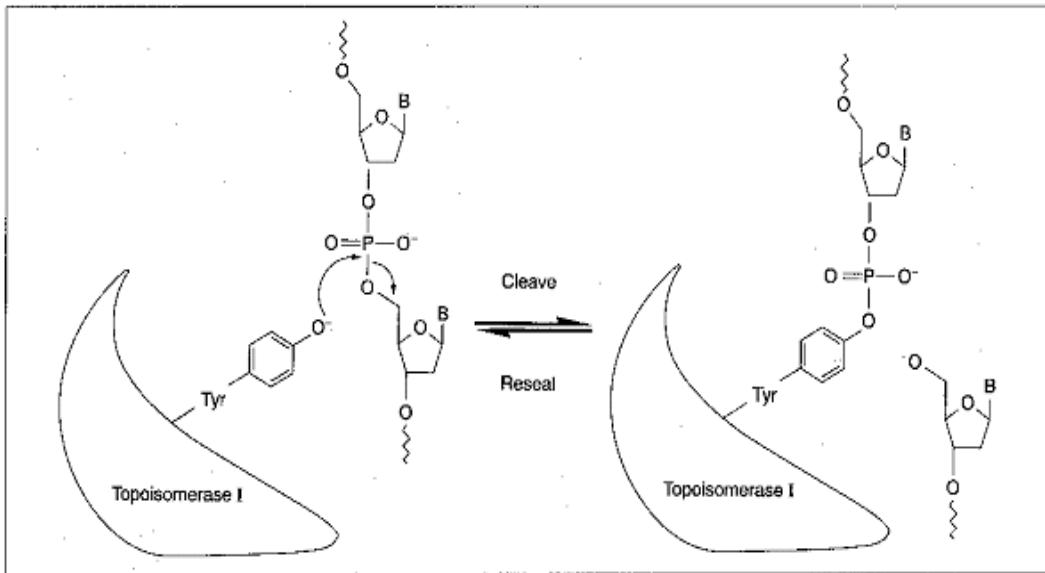


Figure 1.8. Type IB Top1 enzyme forming a covalent linkage to the 3'- terminus of the nicked DNA strand. Camptothecin works by inhibiting the resealing step, thereby extending the life of the nicked DNA strand.(cancernetwork.com, Dr. Allan Y. Chen, 1999)

encounter a replication fork and then the SSB is converted into a DSB, which can kill the cell if unrepaired (43,44). Initially camptothecin showed good anticancer properties, however, further research discovered a high level of toxicity and poor solubility forcing camptothecin to be discontinued as an anticancer drug (42,43). After the failure of camptothecin as a chemotherapeutic drug, scientists developed two derivatives called topotecan and irinotecan (45). Both topotecan and irinotecan go into solution more readily than camptothecin and have lower toxicity (43). Topotecan and irinotecan are commonly used against a number of malignancies, however the response rate is only ~20-40% in certain cancers and other cancers have shown no response at all (43). Several strategies have been suggested to try and increase the efficacy of TopI inhibitor treatment. One proposed method is the development of small molecule inhibitors that can increase the level of unrepaired DNA damage in the cancer cells thereby causing more cells to be killed

1.4 Treating Cancer with Small Molecule Inhibitors

The use of novel small molecule inhibitors to treat cancer is a relatively recent event in the ever-increasing arsenal of cancer therapies being developed. One of the first drugs created utilizing this technique was Imatinib, commonly referred to as Gleevec, which targeted the ATP binding pocket of the mutated BCR-ABL fusion protein that is almost exclusively identified in Chronic Myeloid Leukemia (CML) (46). Imatinib revolutionized cancer therapy because it allowed oncologist's to specifically target the mutation in CML. There is now an emphasis to identify inhibitors for specific cancers. Examples include PARP

inhibitors for breast cancer (47,48), Gefitinib for the treatment of non-small-cell lung cancer (NSCLC) (49), and Salirasib in the treatment of pancreatic cancer (50). The current explosion of interest in developing small molecule inhibitors to treat cancer is mainly due to a number of key factors that make small molecules effective means in the battle against cancer. First off, pharmaceutical companies can synthesize small molecules relatively easily and at relatively low cost. Second, small molecules can be easily administered to the patient, either orally or intravenously, allowing more people to receive this cancer treatment. This is in contrast to radiotherapy, which uses large machines in limited quantity, where the number of people who can receive treatment is significantly reduced compared to that of small molecule treatment. To this end, small molecules are less invasive than a significant proportion of other existing cancer therapies such as radiotherapy and surgery. And lastly, but most importantly, since most of the small molecule inhibitors are designed specifically to target an enzyme in a tumour cell, most produce lower side-effects than the commonly used cancer therapies of the past eg chemotherapy and radiotherapy.

As previously mentioned, there are currently many small molecules being developed to help treat cancer and many of them fall under three main categories: DNA repair, signaling kinases and cell cycle enzymes.

1.4.1 Small Molecule Inhibitors to DNA Repair Enzymes

The repair of DNA is a critical cellular process, which is mediated by a multitude of enzymes. These DNA repair enzymes enable the cell to maintain genomic stability. Due to the necessity of DNA repair enzymes in cell survival,

cancer researchers have begun to exploit this finding by developing small molecule inhibitors to a number of key DNA repair enzymes. The most heavily studied to date, are inhibitors of the SSBR enzyme PARP. PARP inhibitors were initially designed to enhance the chemosensitivity to tumour cells (51). Recent data has shown that PARP inhibitors in combination with chemotherapy in triple-negative breast cancers can enhance tumour cell killing (51). Other uses for PARP inhibitors have been described where the concept of synthetic lethality comes into play (see section 1.5 Synthetic lethality). To date, there are approximately eight PARP inhibitors in clinical trials around the world (51). However, a drawback of PARP inhibitors has been the limited use in only BRCA-mutated breast cancer or triple negative breast cancer (51). Both BRCA-mutated and triple negative breast cancers comprise a minor percentage of breast cancer cases reported. But recently, Alan Ashworth's lab discovered that PARP inhibitors could also be utilized to treat cancers with PTEN mutations (52). This is important because PTEN is lost or mutated in approximately 40% of all tumours, which greatly broadens the range of tumours that can be treated with PARP inhibitors (53).

The BER enzyme AP endonuclease 1 (APE1) is also a major candidate for development into a target for cancer therapy. The main reason for this is APE1 is irregularly expressed or has altered subcellular localization in many types of cancers, such as breast, head and neck, melanoma, cervical, ovarian and hepatocellular etc (54,55). In these cancers, APE1 has higher activity in tumour cells than in normal cells, making it an excellent candidate for small molecule inhibition (56). Furthermore, inhibition of APE1 by small molecule inhibitors

has been shown to significantly increase its cellular sensitivity to DNA base damaging agents (54). However, concerns have arisen regarding toxicity to the patients when APE1 inhibitors are combined with chemotherapy (54). Because of this, localized radiotherapy instead of chemotherapy is suggested along with APE1 inhibitors to try to reduce normal tissue toxicity. In either case, PARP and APE1 inhibitors have garnered significant attention and the use of these inhibitors in the clinic are now closer than ever before.

1.4.2 Small Molecule Inhibitors to Signaling Kinases

Signaling kinases represent one of the major classes of catalytic enzymes within the cell. There are approximately five hundred signaling kinases and each one plays an important role in relaying signals throughout the cell, including in the nucleus. Many cancers contain mutated signaling kinases that enable the cell to undergo aberrant unregulated cell growth i.e. cancer. The majority of these signaling mutations cause the cell to grow under less stringent control through upregulation of kinase activity. To try and counter this unregulated growth affect, small molecules inhibitors have been developed that target these kinases. One of the most well known cancers that contain an aberrant signaling kinase is CML. Almost all CML patients have a gross chromosomal translocation where part of chromosome nine is translocated to chromosome twenty-two, which generates a bcr-abl fusion protein that forms a constitutively active tyrosine signaling kinase. Researchers utilized this mutation to their advantage and identified a novel potent small molecule inhibitor called Imatinib (Gleevec, Novartis Pharmaceuticals, East Hanover, NJ) (46). Over the last few years newer more potent inhibitors to bcr-

abl have been developed for patients who failed to respond to Imatinib. Most of these patients contained a gatekeeper mutation in the ATP binding pocket of the bcr-abl fusion gene. These newer generations of bcr-abl kinase inhibitors, such as Dasatinib (Sprycel, Bristol-Myers Squibb, New York, NY), are more effective than imatinib on all CML patients whether they contain the gatekeeper mutation or not (57). Imatinib demonstrated the utility of targeting a major mutation in a type of cancer thereby improving patient outcome.

1.4.3 Small Molecule Inhibitors of Cell Cycle Proteins

Another major cellular process where small molecule inhibitors have shown to be advantageous in treating cancer is the cell cycle. The cell cycle is extremely important to ensure proper replication of genetic material and resultant formation of daughter cells. There are classically four stages to the cell cycle (G_1 , S, G_2 and mitosis) and numerous proteins regulate these stages. Many of these proteins provide checkpoints where abnormalities have time to be detected and corrected before the next stage of the cell cycle. Mutation of the cyclin dependent kinases cdk1, cdk2, and cdk9 is frequently seen in cancers including non-small cell lung carcinoma (NSCLC), breast carcinoma and hematologic malignancies such as chronic lymphocytic leukemia (CLL) (58). Cdk1, cdk2 and cdk9 are currently being targeted for inhibition by small molecules, for example, flavopiridol, AG024322, seliciclib, and dinaciclib (SCH727965) (58) The use of these cdk1, cdk2 or cdk9 inhibitors as anticancer drugs is mainly through combination therapy with DNA damaging agents to help increase the efficacy of chemotherapy.

Another key step in the cell cycle, mitosis, appears to be a promising target in cancer therapy. The primary target for inhibition in mitosis are the aurora kinases, which are responsible for spindle assembly, centrosome maturation, chromosomal segregation and cytokinesis (59). Irregular mitoses through mutation of aurora kinases can lead to tumorigenesis and hence inhibition of aurora kinase activity has been hypothesized to be a potential target in the treatment of cancer (59). There are currently thirteen aurora kinase inhibitors in clinical trials for multiple types of cancers (59). Many of these inhibitors are being tested on solid tumours; however further clinical testing is required to ensure their safety as commonly used anti-cancer drugs. These inhibitors are primarily used as single agent treatments and are not being combined with radio- or chemotherapy.

The use of small molecule inhibitors as anticancer agents is increasing at an exponential rate and the few listed here are just examples of the progress researchers have made in the past few decades to first identify the potential molecular target and then develop drugs that may be utilized in the clinic to help treat various types of cancer.

1.5 Synthetic lethality

The concept of synthetic lethality has been around since 1946, when the geneticist Theodosius Dobzhansky initially described the occurrence “where 2 non-lethal genetic mutations are harmless when they occur separately, however when used in combination are lethal (60,61).” The mutations arise through several means such as, change in genetic sequence, inactivation of protein expression through epigenetic mechanisms, or inhibition of protein activity. The changes can

arise in genes working in the same pathway or from genes in a related pathway, or by disruption of two genes in non-related pathways, where the combination results in significant stress to the cell. Initially, synthetic lethality was primarily used in yeast genetics to ascertain the function of proteins in the cell. This was until Allan Ashworth's and Tom Helleday's lab's simultaneously discovered that synthetic lethality could also be applied to treat cancer. They both identified that PARP inhibitors given to BRCA1 or BRCA2 mutated breast cancer cells caused them to die (62,63). The explanation for death of the tumour cell was the concept of synthetic lethality. The notion of synthetic lethality garnered in a new age in cancer therapy because it allowed oncologist's to target specifically the tumour cell while not harming the normal cells. In principle, synthetic lethality should have fewer side effects than standard cancer therapy because of its specific targeting to tumour cells. Since that discovery five years ago more potent derivatives of the original PARP inhibitors have been developed and these inhibitors are now in phase 3 clinical trials, which look very promising (48). The synthetic lethality relationship between PARP and BRCA1 and BRCA2 causes cells to die because with the incapacitation of two DNA repair proteins there is a abundance of SSBs and after replication these SSBs form lethal DSBs which overrun the cells repair capabilities and the cell undergoes programmed cell death or necrosis (62).

As mentioned in section 1.1.1.1, PARP is a signaling protein involved in the repair of single-strand breaks. PARP helps initiate the repair of SSBs, but many other proteins are also required to ensure proper repair of SSBs including

PNKP, LIG3 and Pol β . These other proteins were also hypothesized to have synthetically lethal partnerships with PARP and in 2008 PNKP and PARP were shown to be synthetically lethal (64). Unfortunately, to date, no tumours have been identified that lack PARP. Because of this, inhibitors to PNKP can't be utilized in the same manner as PARP inhibitors to BRCA1 or BRCA2 mutated breast cancers. However, we have recently discovered that PNKP is synthetically lethal with other proteins, besides PARP, that are absent in tumours. Due to this finding PNKP is regarded as a potential target for use in a clinical setting to treat cancer using a synthetic lethality approach. In order for this treatment to commence a small molecule inhibitor to PNKP must first be identified and characterized. Once an inhibitor to PNKP has been established pharmacokinetics and pharmacodynamics along with animal tumour studies must be performed in order to gauge the effectiveness of the PNKP inhibitor as an effective cancer therapy in a synthetic lethality approach.

1.6 Thesis Focus

The focus of this thesis will encompass the identification and characterization of a potent small molecule inhibitor to the human DNA repair enzyme polynucleotide kinase/phosphatase. In the next two chapters I will describe the experiments from the initial screening of compounds and identification of a potent inhibitor, A12B4C3, which can significantly enhance the radio-, and chemosensitivity of A549 lung adenocarcinoma and MDA-MB-231 breast carcinoma cells. This will be followed by illustrating the mechanism of action of the PNKP inhibitor through using both biophysical and molecular

techniques, which show that the PNKP inhibitor A12B4C3 is an excellent starting point in the development of potent derivatives from which a novel cancer drug may arise.

Chapter II

Identification of a Small Molecule Inhibitor of the Human DNA Repair Enzyme Polynucleotide Kinase/Phosphatase

Running title: Inhibitor of Polynucleotide Kinase/Phosphatase

Gary K Freschauf¹, Feridoun Karimi-Busheri¹, Agnieszka Ulaczyk-Lesanko², Todd R Mereniuk¹, Ashley Ahrens¹, Jonathan M Koshy¹, Aghdass Rasouli-Nia¹, Phuwadet Pasarj³, Charles F B Holmes³, Dennis G Hall², and Michael Weinfeld¹

¹Experimental Oncology, Cross Cancer Institute, and Departments of ²Chemistry and ³Biochemistry, University of Alberta, Edmonton, Alberta; and ⁴QTL Biosystems, Santa Fe, New Mexico

Corresponding author. Michael Weinfeld Department of Experimental Oncology, Cross Cancer Institute, 11560 University Avenue, Edmonton, Alberta, Canada.
Phone: 780-432-8438; Fax 780-432-8428; E-mail: michaelw@cancerboard.ab.ca

A version of this chapter has been published. Gary K Freschauf¹, Feridoun Karimi-Busheri¹, Agnieszka Ulaczyk-Lesanko², Todd R Mereniuk¹, Ashley Ahrens¹, Jonathan M Koshy¹, Aghdass Rasouli-Nia¹, Phuwadet Pasarj³, Charles F B Holmes³, Dennis G Hall², and Michael Weinfeld¹. (2009) Identification of a Small Molecule Inhibitor of the Human DNA Repair Enzyme Polynucleotide Kinase/Phosphatase. *Cancer Res.* 69:(19); 7739-46.

2.1 ABSTRACT

Human polynucleotide kinase/phosphatase (hPNKP) is a 57.1 kDa enzyme that phosphorylates DNA 5'-termini and dephosphorylates DNA 3'-termini. hPNKP is involved in both single- and double-strand break repair, and cells depleted of hPNKP show a marked sensitivity to ionizing radiation. Therefore, small molecule inhibitors of hPNKP should potentially increase the sensitivity of human tumours to γ -radiation. To identify small molecule inhibitors of hPNKP we modified a novel fluorescence-based assay to measure the phosphatase activity of the protein, and screened a diverse library of over 200 polysubstituted piperidines. We identified five compounds that significantly inhibited hPNKP phosphatase activity. Further analysis revealed that one of these compounds, 2-(1-hydroxy-undecyl)-1-(4-nitrophenylamino)-6-phenyl-6,7a-dihydro-1Hpyrrolo[3,4-b]pyridine-5,7(2H,4aH)-dione (A12B4C3), was the most effective, with an IC_{50} of 0.06 μ M. When tested for its specificity, A12B4C3 displayed no inhibition of two well known eukaryotic protein phosphatases, calcineurin and protein phosphatase-1, or aprataxin, another human DNA 3'-phosphatase, and only limited inhibition of the related PNKP from *Schizosaccharomyces pombe*. At a non-toxic dose (1 μ M), A12B4C3 enhanced the radiosensitivity of human A549 lung carcinoma and MDA-MB-231 breast adenocarcinoma cells by a factor of two, which was almost identical to the increased sensitivity resulting from shRNA-mediated depletion of hPNKP. Importantly, A12B4C3 failed to increase the radiosensitivity of the hPNKP-depleted cells, implicating hPNKP as the principal cellular target of A12B4C3 responsible for increasing the response to

radiation. A12B4C3 is thus a useful reagent for probing hPNKP cellular function and will serve as the lead compound for further development of PNKP-targeting drugs.

2.2 INTRODUCTION

Radiation and systemic chemotherapy continue to be important therapeutic modalities for the treatment of cancer. Nuclear DNA is considered to be the major cellular target responsible for the cytotoxicity of ionizing radiation and many conventional antineoplastic drugs. As a consequence, the levels of DNA damage and its repair are likely to influence cell survival and affect clinical outcome (65), and the manipulation of DNA repair systems has recently become the focus of considerable interest as a means of enhancing the efficacy of radio- and chemotherapy. Particular emphasis has been placed on single and double-strand break repair pathways (66). Small molecule inhibitors have now been developed that target enzymes such as poly(ADP-ribose) polymerase (PARP) and apurinic/apyrimidinic endonuclease (APE1), which are involved in the repair of damaged bases and single-strand breaks induced by many agents including ionizing radiation and alkylating agents (65,67,68), tyrosyl DNA-phosphodiesterase (Tdp1), which is required for the repair of strand breaks introduced by topoisomerase 1 inhibitors such as camptothecin and irinotecan (69), and ATM and DNA-PK, which regulate the response to DNA double-strand breaks (70,71). Inhibitors of PARP are now in clinical trial (72).

Ionizing radiation and other genotoxic agents often generate strand breaks with incompatible termini that must be processed in order for single and double-

strand break repair pathways to complete the repair. Among the frequently observed termini are 3'-phosphate and phosphoglycolate and 5'-hydroxyl groups (73-75). These lesions create a barrier for DNA polymerases and ligases to replace missing bases and seal the breaks because these enzymes have a strict requirement for the presence of a 3'-hydroxyl group and in addition DNA ligases require a 5'-phosphate group (76,77). It is now clear that the major enzyme responsible for the phosphorylation of 5'-hydroxyl termini and dephosphorylation of 3'-phosphate termini in human cells is polynucleotide kinase/phosphatase (hPNKP) (16,22). In the single-strand break (SSB) repair pathway hPNKP acts in concert with XRCC1, DNA polymerase β and DNA ligase III (12,78,79), while PNKP-mediated DNA end-processing at double-strand breaks is a component of the nonhomologous end-joining (NHEJ) pathway and is dependent on DNA-PKcs and XRCC4 (14,18,80). In addition to its role in the repair of strand breaks produced directly by genotoxic agents, hPNKP has been implicated in the repair of strand breaks produced by DNA glycosylases such as NEIL1 and NEIL2 (13,81), and the topoisomerase I inhibitor camptothecin (82). Given the involvement of hPNKP in several repair pathways, it is not surprising that its down-regulation by RNAi sensitized cells to a variety of genotoxic agents including ionizing radiation, camptothecin, methyl methanesulfonate and hydrogen peroxide (15). It remains to be determined which of hPNKP's activities, 5'-kinase or 3'-phosphatase (or both), is responsible for sensitization to each agent. The two activities are independent with each active site containing its own DNA binding domain (24), but the phosphatase reaction appears to proceed ahead

of the kinase reaction (83).

It has recently been suggested that PNKP could be a potential target for small molecule inhibitors (66,84). We report here the development of a fluorescence-based assay for screening chemical libraries for inhibitors of the phosphatase activity of PNKP and its application in the screening of a library of drug-like polysubstituted piperidines. The compound scaffold in this library possesses a range of stable functionalities such as imide, hydroxyl and basic amino groups that confer hydrogen bond donor/acceptor capabilities that could promote interaction with proteins (85). We have identified several compounds that inhibit hPNKP phosphatase activity and further show that one of these compounds sensitized cells to ionizing radiation. It thus has the potential to be a useful laboratory reagent for studying the role of hPNKP in the cellular response to ionizing radiation and other genotoxins, and act as the initial compound in the development of a drug targeting hPNKP in the course of cancer therapy.

2.3 MATERIALS & METHODS

2.3.1 Enzymes

Recombinant hPNKP was purified as described previously (16,86). The bacteria were grown at 37 °C in 4 L of LB medium containing ampicillin (50 $\mu\text{g}/\text{mL}$) and kanamycin (30 $\mu\text{g}/\text{mL}$) to an OD_{600} of 0.6, and protein expression was then induced by overnight incubation at room temperature in the presence of 100 μM isopropyl-1-thio- β -D-galactopyranoside (Sigma, St. Louis, MO). Cells were harvested by centrifugation to separate the soluble fraction from the insoluble fraction. Protein in the supernatant was precipitated and centrifuged

once again. The pellet was first resuspended in 40 mL of buffer A (50 mM Tris-HCl, pH 8.00, 1 mM EDTA, 0.1% β -mercapthoethanol, and 0.5 mM PMSF) and then the solution was loaded onto a 10-mL HiPrep 16/10 Butyl FF column (Amersham Pharmacia BioTech, Baie d'Urfe, PQ). Fractions containing the highest concentration of hPNKP were pooled, and the sample was then applied to a 5-mL SP Sepharose Fast Flow cation-exchange column (Amersham Pharmacia BioTech). The column was washed, and the enzyme was eluted. Fractions containing hPNKP activity eluted between 0.4 and 0.5 M NaCl. The active fractions were pooled and concentrated using a 30-kDa cutoff Millipore ultrafree concentrator.

Mouse PNKP (mPNKP) was purified using the following protocol by Bernstein et al., 2005 (24). The bacteria were grown at 37 °C in 4 L of LB medium containing ampicillin (50 μ g/mL) and kanamycin (30 μ g/mL) to an OD₆₀₀ of 0.6, and protein expression was then induced by overnight incubation at room temperature in the presence of 100 μ M isopropyl-1-thio- β -D-galactopyranoside (Sigma, St. Louis, MO). Cells were harvested by centrifugation on ice for 30 min at 30 °C, and then the bacteria were disrupted by sonication. The soluble fraction was separated from the insoluble fraction by centrifugation and the salt concentration of the soluble fraction was raised to 500 mM. The sample was stirred on ice for another 20 min and then centrifuged again. The pellet was first resuspended in 40 mL of buffer A (50 mM Tris-HCl, pH 8.00, 1 mM EDTA, 0.1% β -mercapthoethanol, and 0.5 mM PMSF), and then the salt concentration was increased to 1.5 M by adding an additional 80 mL of buffer A. The solution

was loaded onto a 10-mL HiPrep 16/10 Butyl FF column (Amersham Pharmacia BioTech, Baie d'Urfe, PQ). The protein was eluted and the fractions containing the highest concentration of mPNKP were pooled, and the buffer exchanged with buffer B (50 mM HEPES, pH 7.0, 0.1% β -mercapthoethanol, 1 mM EDTA and 0.5 mM PMSF) using a 30-kDa cutoff Ultrafree concentrator (Millipore, Bedford, MA). The sample was then applied to a 5-mL SP Sepharose Fast Flow cation-exchange column (Amersham Pharmacia BioTech). Fractions containing mPNKP activity eluted between 0.4 and 0.5 M NaCl. The active fractions were pooled and concentrated using a 30-kDa cutoff Millipore ultrafree concentrator. The sample was applied on a gel filtration column (Amersham Pharmacia BioTech), and purified protein was eluted. The final protein concentration was adjusted to the desired level using a 30-kDa cutoff Millipore ultrafree concentrator.

Purification of Recombinant *Schizosaccharomyces pombe* PNKP (Pnk1) was performed using the protocol described by Meijer et al., 2002 (87). The bacteria were grown at 37 °C to an A_{600} of 0.6 in 100 ml of Luria-Bertani medium containing 50 μ g/ml ampicillin and 12.5 μ g/ml tetracycline. Protein expression was induced at 30 °C for 3 h by the addition of 0.1 mM final concentration of isopropyl-1-thio- β -D-galactopyranoside (Sigma). The cells were then harvested by centrifugation and resuspended in extraction buffer (50 mM Tris-HCl, pH 7.5, 0.015 mM ZnCl₂, 4 mM 2-mercaptoethanol). The bacteria were then disrupted by sonication, and the soluble fraction was separated from the insoluble fraction by centrifugation. The soluble fraction was subjected to a 65% ammonium sulfate precipitation followed by centrifugation at 10,000g for 15 min. The pellet was

resuspended and dialyzed overnight. The solution was applied on a 25-ml SP-Sepharose fast flow cation exchange column (Amersham Biosciences, Inc.). The column was washed, and the enzyme was eluted. The active fractions were pooled and concentrated by 65% ammonium sulfate. The precipitate was dissolved and loaded onto a Superdex-75 PC 3.2/30 gel filtration column attached to a SMART micropurification system (Amersham Biosciences, Inc.). The active fractions coeluted with a purified protein at an estimated molecular mass of 40–50 kDa.

Phage T4 polynucleotide kinase (T4 PNK) was purchased from Roche Diagnostics (Indianapolis, IN).

The catalytic subunit of the human PP1 ζ was purified using the protocol described by Misik et al., 2005 (88). The bacteria were grown overnight at 37 °C, this culture was used to inoculate 1 L of LB medium containing 1 mM MnCl₂ and 54 μ M ampicillin and was grown to an optical density of 0.5 at 600 nm.

Expression was then induced with 1 mM IPTG for up to 18 h. Cells were harvested by centrifugation and were resuspended in 80 mL of buffer A [50 mM imidazole (pH 7.5), 100 mM NaCl, 0.5 mM EDTA, 0.5 mM EGTA, 2 mM MnCl₂, 3 mM DTT, 2 mM benzamidine, 0.5 mM PMSF, and 10% (v/v) glycerol]. The solution was disrupted by sonication and the lysate was then centrifuged. The supernatant was then loaded onto an 80 mL heparin-Sepharose column (Pharmacia). The solution was added to a column and fractions were assayed for activity using *p*-nitrophenyl phosphate (pNPP) as a substrate. The active fractions were pooled and diluted 2:1 with buffer B [50 mM imidazole (pH 7.5), 0.5 mM

EDTA, 0.5 mM EGTA, 3 mM MnCl₂, 3 mM DTT, 2 mM benzamidine, 0.5 mM PMSF, and 10% (v/v) glycerol] and loaded onto a MonoQ 10/10 column (Pharmacia). The solution was further run on a column and the active fractions were pooled and concentrated. The concentrated solution was then loaded onto a HiLoad 26/60 Superdex 75 prep grade column (Pharmacia). The column was run with a 180 mL isocratic gradient, and 0.6 mL fractions were collected for the final 54 mL at a flow rate of 0.2 mL/min. Active fractions were pooled and concentrated to a volume of 1-3 mL. Glycerol was added to a final concentration of 50%, and PP1 was then stored at -20 °C.

Rat δ -calcineurin protein was purified by the following protocol (89). Bacteria were grown overnight at 37 °C, this culture was used to inoculate 1 L of LB medium containing 1 mM MnCl₂ and 54 μ M ampicillin and grown to an optical density of 0.5 at 600 nm. Expression was then induced with 1 mM IPTG for up to 18 h. Cells were harvested by centrifugation. The cultures were resuspended in 80 mL of buffer A [50 mM imidazole (pH 7.5), 100 mM NaCl, 0.5 mM EDTA, 0.5 mM EGTA, 2 mM MnCl₂, 3 mM DTT, 2 mM benzamidine, 0.5 mM PMSF, and 10% (v/v) glycerol] and disrupted by sonication. The lysate was then centrifuged and the supernatant was then loaded onto an 80 mL heparin-Sepharose column (Pharmacia). The column was run with a 400 mL linear gradient from 0.1 to 0.5 M sodium chloride, and 5 mL fractions were collected at a flow rate of 5 mL/min. The active fractions were pooled and concentrated to a volume of 1.5-10 mL using Amicon ultracentrifugal filter devices (Millipore) and loaded onto a HiLoad 26/60 Superdex 75 prep grade column (Pharmacia). The

column was run with a 180 mL isocratic gradient, and 0.6 mL fractions were collected for the final 54 mL at a flow rate of 0.2 mL/min. Active fractions were pooled and concentrated to a volume of 1-3 mL. Glycerol was added to a final concentration of 50%, and calcineurin was then stored at -20 °C.

Human recombinant aprataxin (APTX) protein with an N-terminal 6x His tag was expressed in BL21-Gold (DE3) *E. coli* competent cells (Stratagene, La Jolla, CA) using the QIAgene expression construct (Qiagen, Mississauga, ON, Canada). A single colony of kanamycin resistant *E. coli* was used to inoculate a 200-ml overnight culture in Luria6 Bertani (LB) media containing 30 µg/ml kanamycin. Four 50-ml fractions of overnight culture were then subcultured into 4 x 1 L LB without kanamycin. Once the culture reached an optical density of ~0.6 at 600 nm, protein expression was induced using 0.2 mM isopropyl-1-thio-β-galactopyranoside (Sigma, St Louis, MO) at 37 °C for 2 hours. Cells were harvested by centrifugation at 10,000 rpm for 10 minutes at 4 °C and resuspended in 40 ml buffer (50 mM NaH₂PO₄, 250 mM NaCl, 1 mM PMSF, at pH 7.9). The solution was then stirred on ice for 30 minutes in the presence of 30 mg lysozyme and 4 mg PMSF, 1 µg/ml each of pepstatin and leupeptin. The bacteria were then sonicated 6 x 30 sec allowing 30 sec between intervals to cool down. The cell debris was then spun down at 15,000 rpm for 15 minutes at 4 °C and the supernatant collected. The supernatant was then stirred on ice in the presence of 4 ml Probond resin (Invitrogen, Burlington, ON, Canada) for 1 h and then loaded onto a column. The resin was washed with 3 x 5 ml 20 mM imidazole and 5 ml fractions were collected. Then, 25 ml of 150 mM imidazole was loaded onto the

column and 1 ml fractions were collected. Fractions were run on a 10% SDS-PAGE and stained with Coomassie Brilliant Blue R-250 (Invitrogen). 150 mM fractions showing high concentrations and single bands were then combined and concentrated using a 30 kDa cutoff Amicon Ultra-15 centrifugal filter (Millipore, Etibicoke, ON, Canada) and dialyzed with 50 mM Tris-HCl (pH 7.5), 100 mM NaCl, and 5 mM MgCl₂. His-APTX concentration was then determined using the Bio-Rad Protein assay (Bio-Rad, Mississauga, ON, Canada).

2.3.2 Cells

A549 (human lung carcinoma cells) and MDA-MB-231 (human breast adenocarcinoma cells) were obtained from the American Type Culture Collection (Manassas, VA). Cells were cultured in a 1:1 mixture of Dulbecco's modified Eagle's medium/nutrient mixture F-12 (DMEM/F-12) supplemented with 10% fetal calf serum (FCS), penicillin (50 U/ml), streptomycin (50 µg/ml), L-glutamine (2 mM), non-essential amino acids (0.1 mM) and sodium pyruvate (1 mM), and maintained at 37 °C under 5% CO₂ in a humidified incubator. All culture supplies were purchased from Invitrogen. A549δPNKP cells were generated by the following method: A549 cells were plated in 60-mm culture dishes a day before transfection to grow to 50-70% confluent at the time of infection. To reduce expression of hPNKP an oligonucleotide (5'-ACAGATGACGG-ACTCCTCT-3') directed against nucleotides 1391-1410 of hPNKP cDNA (GenBank accession no. AF125807) was designed. The duplex produced by annealing the forward and reverse oligonucleotides 5'-GATCCCAGAGATGACGGACTCCTCTTTCAAGAGAAGAGGAGTCCGTC-

ATCTCTTTTTTGGAA-3' and 5'-AGCTTTTCCAAAAAAGAGATGACGGA-CTCCTCTTCTCTTGAAAGAGGAGTCCGTCATCTCTGGG-3' was incorporated between *Bgl*III and *Hind*III sites in the pSUPER.neo vector (OligoEngine), which was carrying the neomycin resistance gene (neo) and was transfected into A549 cells using Lipofectamine 2000 (Invitrogen). The transfection complex containing 2 µg of pSUPER.neo was added to 100 µl of Opti-MEM and 6 µl of Lipofectamine 2000 was diluted in 100 µl of Opti-MEM and left at room temperature for 5 min. The two tubes were then combined and incubated at room temperature for 30 min. Then the transfection complexes were added to A549 cells and left for 24 h at 37 °C. The next day cells were passaged 1:10 into DMEM/F12 without antibiotics. 24 h later the media was aspirated and complete DMEM/F12 + 650 µg/ml of G418 was added. The cells were then grown for 2 weeks under selection and media was replaced every 4 days. Colonies were then picked and expanded and tested for their PNKP status using western blotting as well as cell survival after radiation treatment. MDA-MB-231δPNKP cells were generated in a comparable manner except only 400 µg/ml of G418 was added to the complete media and not 650 µg/ml of G418 as with A549 cells. The PNKP-depleted MDA-MB-231 cells were generated in a similar fashion except that the shRNA-expressing pSUPER vector used on this occasion (pSUPER.neo, OligoEngine, Seattle, WA) also contained the cDNA for the G418 selectable marker.

2.3.3 Optimization of fluorescence quenching-based assay for PNKP 3'-phosphatase activity

We modified the Lightspeed™ assay developed originally for protein kinases and phosphatases by QTL Biosystems (Santa Fe, NM). [This reagent is no longer produced or distributed by QTL Biosystems]. The standard substrate used for this assay was a 20mer oligonucleotide (5'-TAMRA-AAT ACG AAT GCC CAC ACC GC-P-3') labelled with 5-(6-carboxytetramethylrhodamine) (TAMRA) at the 5'-end and bearing a terminal 3'-phosphate (Integrated DNA Technologies, Coralville, IA). The TAMRA-labelled oligonucleotide lacking a 3'-phosphate served as a control. Four calibration solutions, consisting of 0, 25, 50 and 100% 3'-phosphorylated oligonucleotide, were prepared by mixing the two oligonucleotides (i.e. 3'-phosphorylated and non-phosphorylated oligonucleotides) in respective proportions (0.5 μ M total oligonucleotide concentration). The assay was performed in 384-well white Optiplate microplates (PerkinElmer, Woodbridge, ON, Canada) in 70 mM Tris-HCl, pH 7.4, 60 mM MgCl₂, 5 mM MnCl₂, 0.3% BSA, 0.09% sodium azide. Reaction buffer was prepared by adding 1 mM DTT immediately prior to use. Five μ l of 3'-phosphatase substrate (final concentration 0.5 μ M) was used per well. In duplicate, 10 μ l of each concentration of hPNKP was added per well. Plates were incubated for 1 h at 37 °C and then 15 μ l of sensor solution (provided by QTL) was added to each well and incubated for 30 min at room temperature. Fluorescence (485 nm excitation and 520 nm emission wavelengths) of each well was read in a FLUOstar Optima® (BMG Labtech Inc, Durham, NC). Data were analyzed using GraphPad Prism® Software (San Diego, CA).

2.3.4 Acquisition and screening of the small molecule library

A previously described library of 244 polysubstituted piperidines encompassing a diversity of functional groups and substituents was synthesized as described (85) and used for screening. Small molecules were provided in powder form and were dissolved in 100% DMSO and a final concentration of 100 μ M was added to each well and assays were performed as described above.

After obtaining an optimum calibration curve and enzyme concentration curve, we employed a simplified form of the assay to test the library in a short time. Only one concentration of hPNKP, 50 ng, was tested and compared with the control well with no enzyme. The assay was conducted in the same way as described above with respect to oligonucleotides, buffer, controls, incubation lengths/temperatures, centrifugations and sensor addition.

2.3.5 Assay for 3'-phosphatase activity based on the release of inorganic phosphate (Pi)

hPNKP phosphatase reactions (20 μ l total volume) were setup as follows: 1 μ l hPNKP (100 ng), 2 μ l 10X phosphatase buffer (500 mM Tris-HCl, pH 7.4, 0.1 mM EDTA, 1 mM spermidine and 2.5 mM DTT), 15 μ l distilled H₂O and 1 μ l small molecule (varying concentrations) were incubated at 37 °C for 5 min and then 2 μ l of 1 mM 3'-P 20mer oligonucleotide was added, (The oligonucleotide had the same sequence as that used in the fluorescence quenching assay, but without the TAMRA substituent). The reactions were then transferred to a clear polystyrene colorimetric 384-well plate and incubated at 37 °C for 30 min. PiColorlock Gold reagent (Innova Biosciences Ltd., Cambridge, UK) was prepared shortly before use by addition of 1/100 vol. of accelerator to PiColorlock

Gold reagent as directed by the manufacturer. The Gold mix was then added to Pi-containing samples in a volume ratio of 1:4 and the samples were incubated at room temperature for 30 min before the absorbance was read at 620 nm using a FLUOstar Optima® plate reader (BMG Labtech Inc. Durham, NC).

2.3.6 Conventional radio-gel assay for hPNKP 3'-phosphatase activity

hPNKP phosphatase activity was determined by monitoring the removal of the 3'-phosphate from a 5'-³²P-labeled 20mer oligonucleotide containing a 3'-phosphate (5'-ATT ACG AAT GCC CAC ACC GC-P-3'). Briefly, the 5'- end of the oligomer was labelled (*p20P) by incubation with phage T4 phosphatase-free polynucleotide kinase (Roche Diagnostics, Indianapolis, IN) and [γ -³²P]ATP (PerkinElmer). To the labelled oligomer was added 50 ng of hPNKP that had been pre-incubated for 5 min at 37 °C with varying concentration of small molecule inhibitor in 1X phosphatase buffer (70 mM Tris-HCl, 10 mM MgCl₂, 5 mM dithiothreitol, pH 7.6) and the reaction was allowed to proceed with the addition of 10 pmol of *p20p oligo for 20 min. The level of 3'-dephosphorylation was monitored by electrophoresis on a 12% polyacrylamide/7M urea sequencing gel for 3 h in 1 X TBE buffer. Gels were scanned with a Typhoon 9400 Variable Mode Imager (GE Healthcare, Little Chalfont, UK), and quantified using Image Quant 5.2 Software (GE Healthcare).

2.3.7 PP-1cy and calcineurin phosphatase inhibition assay

PP-1cy and calcineurin activity was analyzed, using a colorimetric *p*-nitrophenol phosphate (pNPP) assay. Inhibition reactions were carried out in a 96-well microplate with a final volume of 60 μ l containing 40 μ l of pNPP assay

buffer (50 mM Tris, pH 7.4, 0.1 mM EDTA, 30 mM MgCl₂, 0.5 mM MnCl₂, 1 mg/ml BSA, 0.2% β mercapto-ethanol), 0.03 μg PP-1 γ (specific activity >30 units per mg) or a catalytically equivalent quantity of calcineurin and 10 μl of 0.5 mM or 10 μl of 50 μM A12B4C3 in DMSO, or control solvent. After a 10 min incubation at 37 °C, 10 μl of 30 mM pNPP was added to each well and incubated for an additional of 60 min and 45 min for PP-1 γ and calcineurin, respectively. The absorbance at 405 nm was measured using a SOFTmax 2.35 kinetic microplate reader (Molecular Devices, Sunnyvale, CA).

2.3.8 DNA kinase assay

Kinase reactions (20 μl final volume) were set up as follows: 1 μg hPNKP was pre-incubated with increasing concentration of A12B4C3 in the kinase buffer (80 mM succinic acid (pH 5.5), 10 mM MgCl₂, and 1.0 mM DTT) at 37 °C for 5 min and then 20mer oligonucleotide substrate (20 nmol) and 3.3 pmol of [γ - ³²P]ATP were added and the reaction mixture was incubated at 37 °C for 20 min. The reaction was stopped by addition of an equal volume of DNA loading dye (90% formamide, 0.02% bromophenol blue, 0.02% xylene cyanol in 1X TBE). Samples were boiled for 5 min and the products separated on a 12% polyacrylamide/8M urea gel. Gels were scanned with a Typhoon 9400 Variable Mode Imager (GE Healthcare), and quantified using Image Quant 5.2 Software (GE Healthcare).

2.3.9 Cell proliferation assay

To determine the effect of the inhibition of PNKP by small molecule inhibitors on cell proliferation we used the CellTiter 96™ AQueous Non-

Radioactive Cell Proliferation Assay (Promega, Madison WI), better known as the MTS assay. Approximately 2.5×10^3 A549 cells were plated in triplicate in a 96-well plate with different concentrations of A12B4C3 inhibitor. After 72 h, 20 μ l of CellTiter 96 Aqueous One Solution Reagent was added to each well and cells were incubated for 4 more hours at 37 °C. The absorbance recorded at 490 nm on a FLUOstar Optima plate reader was used as a representation of the relative number of living cells in culture.

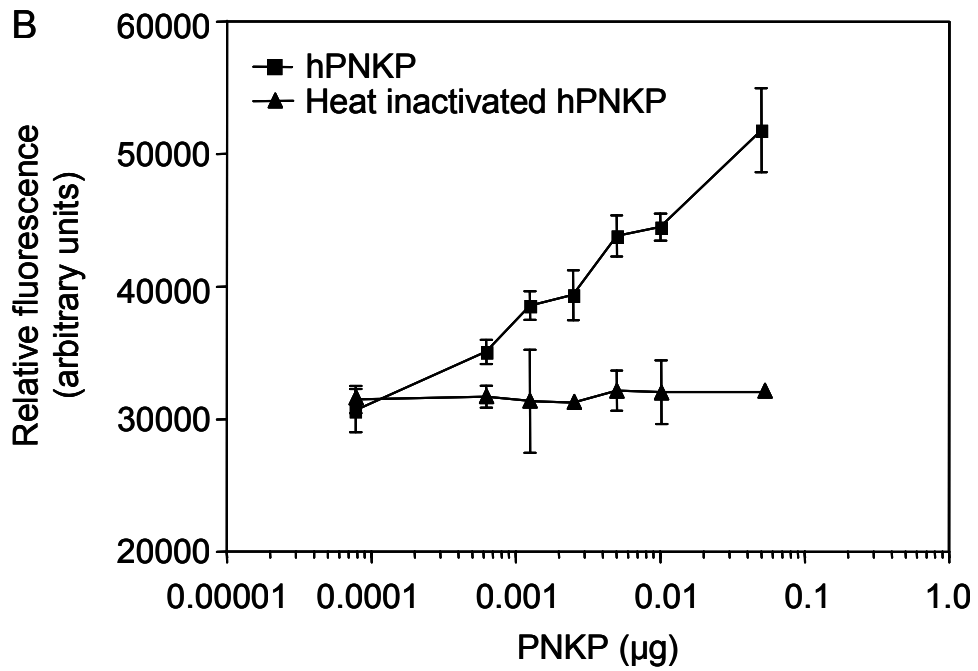
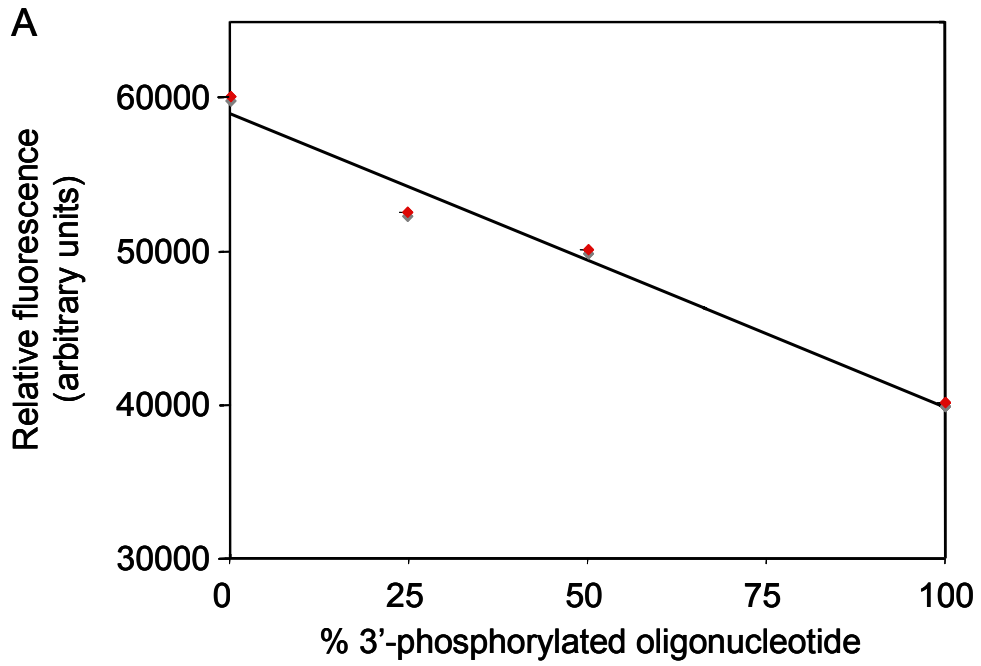
2.3.10 Cytotoxicity studies

The effect of hPNKP inhibition by A12B4C3 on cellular survival following exposure to ionizing radiation was measured in A549, A549 δ PNKP and MDA-MB-231 and MDA-MB-231 δ PNKP cells by clonogenic assays. Cells were seeded on 60-mm tissue culture plates at various concentrations to give between 100-1000 colonies per plate and returned to the incubator overnight to allow the cells to attach. For radio-sensitization studies, the cells were incubated with or without 1 μ M A12B4C3 for 2 h before irradiation and then exposed to increasing doses of γ -radiation (^{60}Co Gammacell; Atomic Energy of Canada Limited, Ottawa). After irradiation, cells were incubated for a further 24 h in the same media and then washed twice with phosphate-buffered saline (PBS) and incubated in fresh media without the inhibitor. Colonies were stained with crystal violet after 10 to 14 days and counted with an automated Colcount colony counter (Oxford Optronix, Oxford, UK).

2.4 RESULTS

2.4.1 Screening of the library by a fluorescence-based assay

The fluorescence-based phosphatase assay that we adapted was originally developed to monitor protein phosphatase activity (90). The assay involves a fluorescent sensor molecule coupled with trivalent metal ions which bind to phosphate groups. When the sensor is brought into close proximity with a phosphorylated and dye (TAMRA)-labeled substrate, superquenching of the sensor occurs. Removal of the phosphate leads to an elevation of fluorescence because the sensor is not brought close enough to TAMRA for its signal to be quenched. We modified the buffer conditions so that the internucleotide phosphate groups of a DNA substrate would not interfere strongly with the process of measuring the presence of a terminal phosphate group as shown by the standard curve of 0, 25, 50 and 100% phosphorylated oligo solutions (Figure 2.1A). We then determined the amount of hPNKP required for near complete dephosphorylation of the oligonucleotide by measuring the fluorescence signal as a function of hPNKP present in the reaction (Figure 2.1B), and as a result we chose 50 ng as the standard quantity of hPNKP for each reaction in the screen. Heat inactivated hPNKP was used as a control. We screened a small molecule library consisting of over 200 polysubstituted imidopiperidines (85) for their capacity to inhibit the phosphatase activity of human PNKP. Five of the compounds, A12B4C3, A1B4C3, A6B4C3, A26B11C2 and A39B1C2, were observed to cause significant inhibition as shown in Figure 2.1C. Also shown are the data for three other compounds, A4B8C2, A28B3C1 and A24B12C3, as examples of the majority of compounds that failed to inhibit hPNKP. The formal.



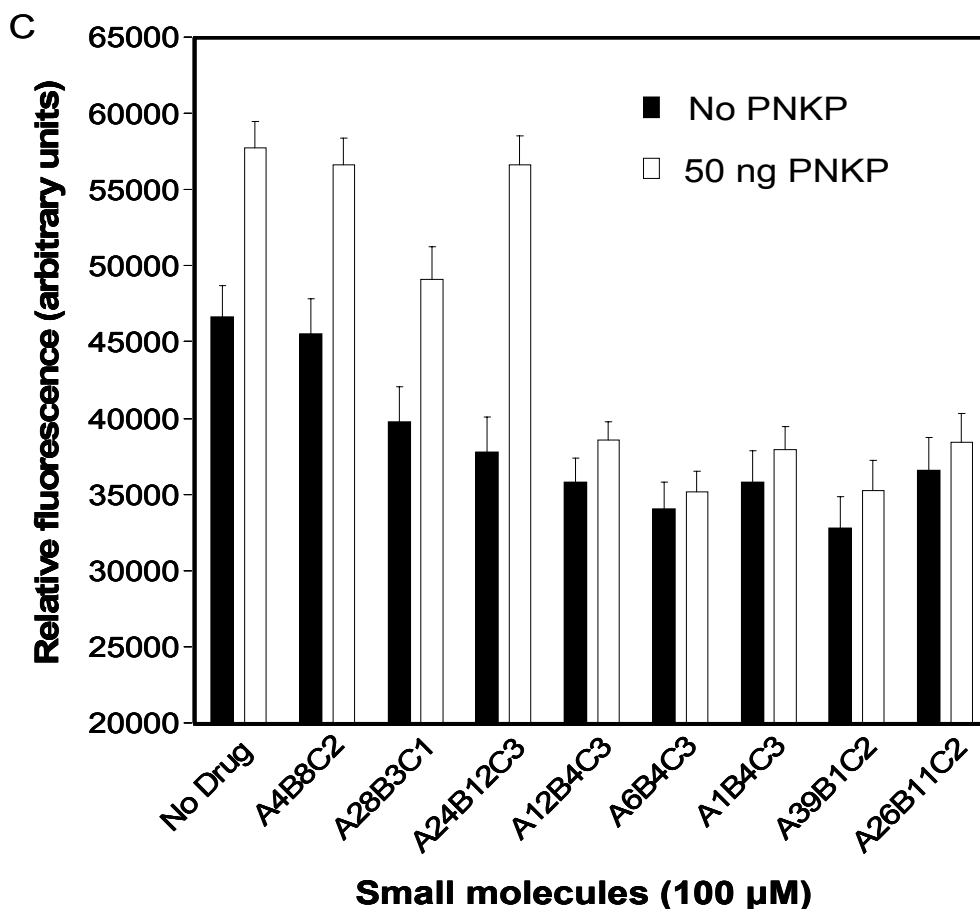


Figure 2.1. (A) Typical phosphatase standard curve for the fluorescence quenching-based phosphatase assay. Readings were taken for solutions consisting of 0, 25, 50 and 100 % phosphorylated oligonucleotides ($r = 0.99$). A fresh standard curve was generated each time the screening assay was performed. (B) Loss of fluorescence quenching resulting from increased removal of the 3'-phosphate group from the substrate with increasing quantity of hPNKP in the reaction. The data are combined from three independent determinations \pm S.E.M. (C) Results of the screening assay for eight of the small molecules tested. Compounds A4B8C2, A28B3C1 and A24B12C3 failed to show any quenching of the sensor molecule as a result of hPNKP inhibition, while A12B4C3, A1B4C3, A6B4C3, A26B11C2 and A39B1C2 all displayed marked inhibition of substrate dephosphorylation. The data are combined from three independent determinations \pm S.E.M.

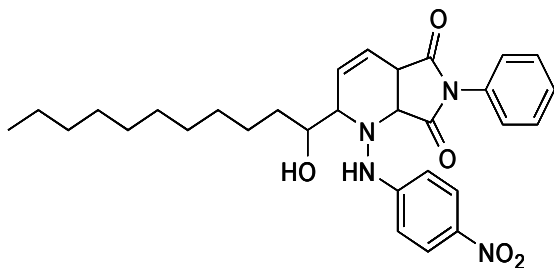
names and chemical structures of the active compounds are shown in Figure 2.2

2.4.2 Confirmation of inhibition of PNKP phosphatase activity

A conventional radio-gel assay was used to verify the inhibition of hPNKP phosphatase activity by these small molecules. This assay shows a shift on an acrylamide sequencing gel that corresponds to 3'-phosphate removal from a 20mer single-stranded oligonucleotide (23). We confirmed that all five of the positively identified compounds inhibited hPNKP phosphatase activity. We also examined a number of small molecules shown by the screening assay not to be inhibitors of hPNKP phosphatase activity, and they also failed to show inhibition by the radio-gel approach. Examples of the assay are shown in Figure 2.3.

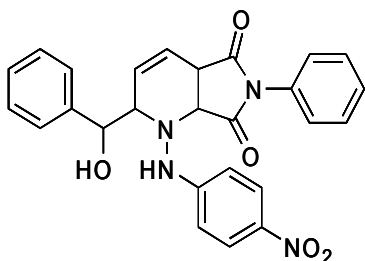
2.4.3 Inhibitory activity and specificity of A12B4C3

To further assess the activity of the five inhibitory molecules we made use of a proprietary colorimetric reagent (PiColorLock Gold) that measures release of inorganic phosphate. A drawback encountered with the fluorescence-based approach can be fluorescence quenching arising from direct interaction of the small molecule with the sensor agent. (Note in Figure 2.1C the lower fluorescence signal of the sensor caused by exposure to some compounds in the absence of PNKP). This problem is avoided in the colorimetric assay, which measures the release of inorganic phosphate (Pi) from a 20mer 3'-P oligonucleotide based on the change in absorbance of malachite green in the presence of molybdate. Based on the standard curve obtained using 0, 25, 50, and 100% phosphorylated substrates (Figure 2.4A), we found that A12B4C3 was the most potent of the five PNKP inhibitors (Figure 2.4B) and obtained an IC₅₀ dose of 0.06 μM and near



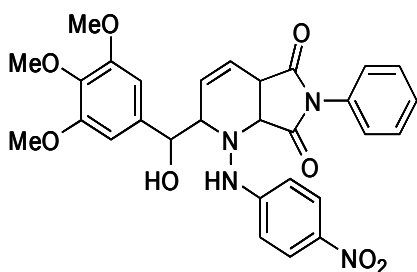
A12B4C3

2-(1-hydroxyundecyl)-1-(4-nitrophenylamino)-6-phenyl-6,7a-dihydro-1*H*-pyrrolo[3,4-*b*]pyridine-5,7(2*H*,4*aH*)-dione



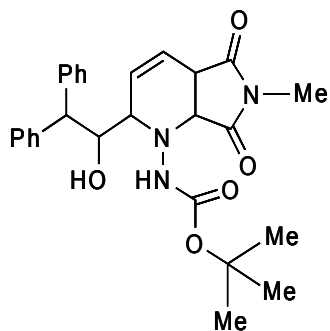
A1B4C3

2-(hydroxy(phenyl)methyl)-1-(4-nitrophenylamino)-6-phenyl-6,7a-dihydro-1*H*-pyrrolo[3,4-*b*]pyridine-5,7(2*H*,4*aH*)-dione



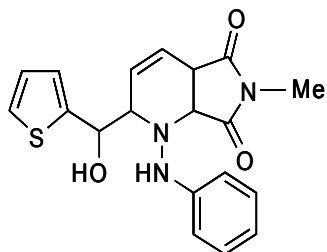
A6B4C3

2-(hydroxy(3,4,5-trimethoxyphenyl)methyl)-1-(4-nitrophenylamino)-6-phenyl-6,7a-dihydro-1*H*-pyrrolo[3,4-*b*]pyridine-5,7(2*H*,4*aH*)-dione



A26B11C2

tert-butyl 2-(1-hydroxy-2,2-diphenylethyl)-6-methyl-5,7-dioxo-2,4*a*,5,6,7,7*a*-hexahydro-1*H*-pyrrolo[3,4-*b*]pyridin-1-ylcarbamate



A39B1C2

2-(hydroxy(thiophen-2-yl)methyl)-6-methyl-1-(phenylamino)-6,7a-dihydro-1*H*-pyrrolo[3,4-*b*]pyridine-5,7(2*H*,4*aH*)-dione

Figure 2.2. Chemical structures and names of the compounds found to inhibit hPNKP phosphatase activity.

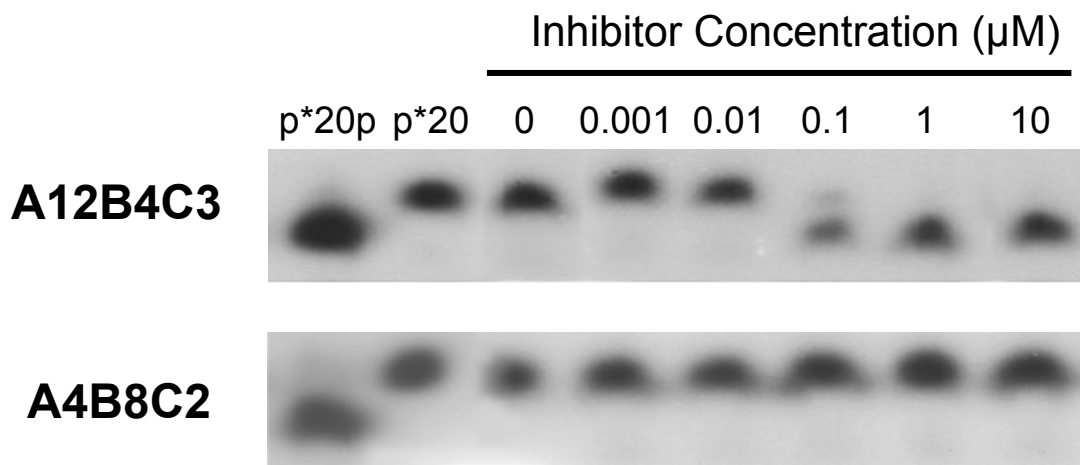
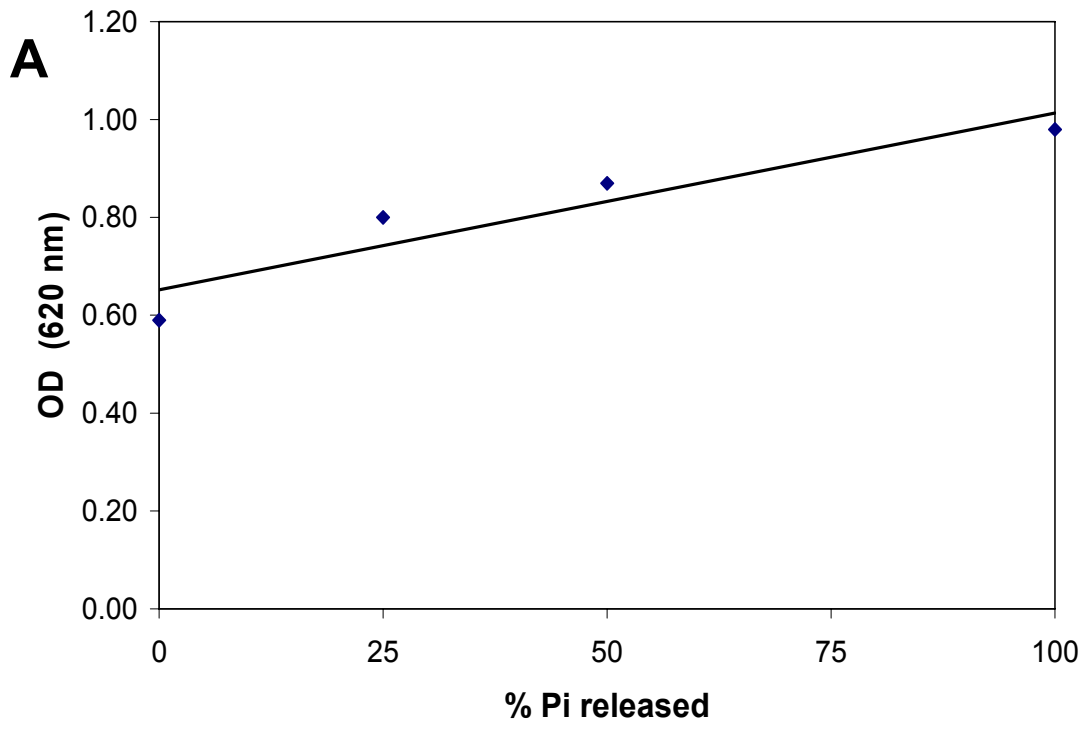


Figure 2.3. Corroboration of inhibition of hPNKP 3'-phosphatase activity by conventional radio-gel assay. A 20mer oligonucleotide with a 3'-phosphate was labelled at the 5'-terminus with [γ - ^{32}P]ATP (*p20p), which was acted on by hPNKP, resulting in the removal of the 3'-phosphate. This produced *p20, which has a slower mobility in the gel. Addition of the small molecule inhibitors reduces the conversion of *p20p to *p20. The figure confirms that A12B4C3 strongly inhibits hPNKP phosphatase activity, while A4B8C2 is inactive (see Figure 2.1C).



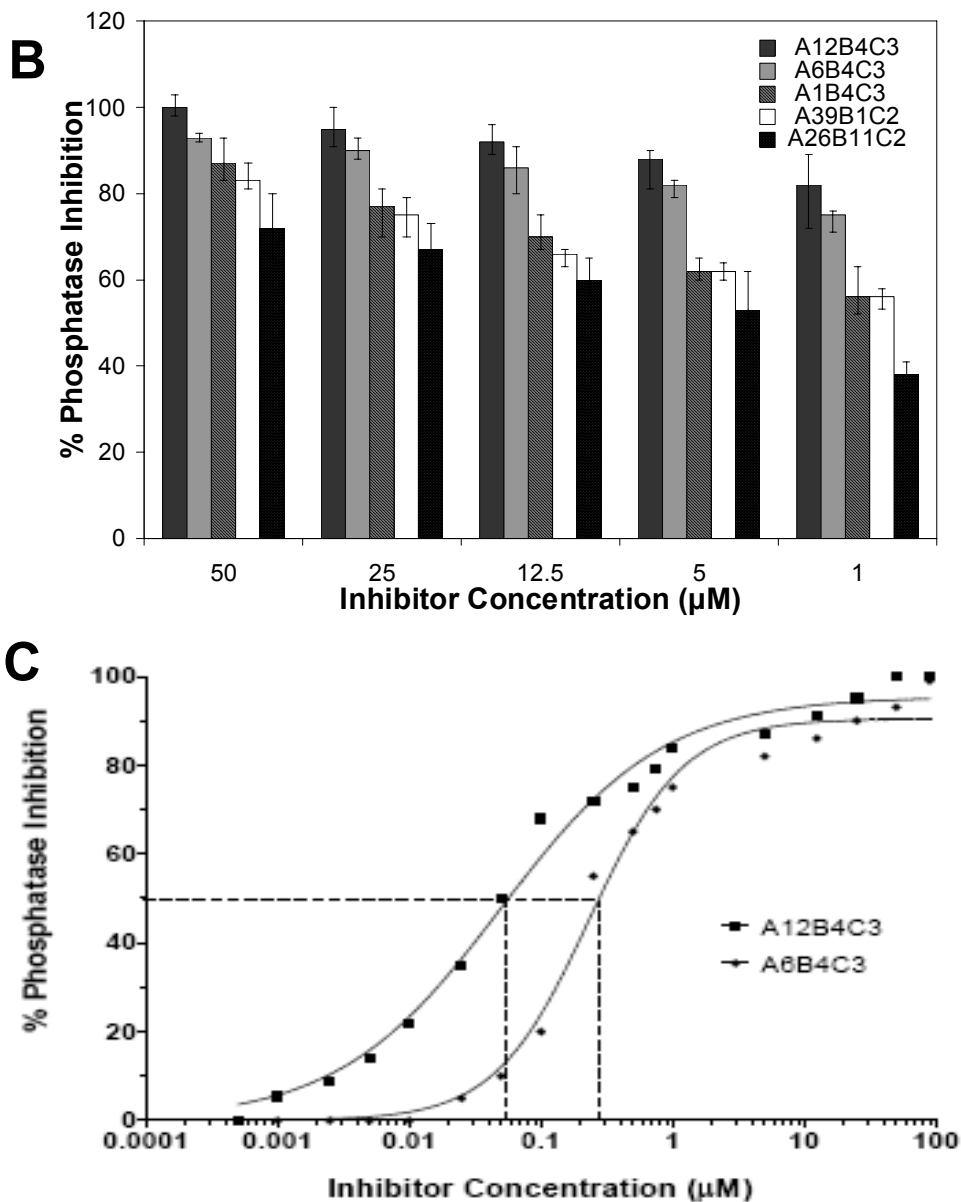


Figure 2.4. Measurement of 3'-phosphatase activity by the PiColorlock Gold assay. (A) Typical standard curve generated by mixing specific ratios of 3'-phosphorylated and nonphosphorylated 20-mer oligonucleotides (final concentration of oligonucleotide, 100 µM) in four separate tubes, which were then treated with hPNKP for 30 min at 37 °C, conditions that lead to complete 3'-dephosphorylation of the oligonucleotide. (B) Concentration dependence of phosphatase inhibition by the five identified compounds: A12B4C3 (dark grey), A6B4C3 (light grey), A1B4C3 (grey), A39B1C2 (white), A26B11C2 (black). The data are drawn from three independent assays. Error bars indicate the S.E.M. (C) Determination of the IC₅₀ values of the two most potent inhibitory compounds derived from three independent assays. The curves were fitted using GraphPad Prism software (GraphPad Software Inc., La Jolla, CA)

maximal inhibition with a concentration of 10 μM (Figure 2.4C). The curve was fitted to conform to a single site-specific binding with Hill slope. Deviation from the curve at high concentration of inhibitor most likely reflects the limitation of the assay when measuring low levels of released inorganic phosphate. The IC_{50} value for the next most active inhibitor, A6B4C3, was determined and found to be somewhat higher ($\sim 0.3 \mu\text{M}$).

2.4.4 Specificity of A12B4C3

To determine the specificity of A12B4C3 for human PNKP phosphatase activity we examined a number of closely related phosphatases such as the PNKP enzymes isolated from bacteriophage T4, *Schizosaccharomyces pombe* and mouse, as well as human aprataxin (APTX). We observed that 50 μM A12B4C3 inhibited phage T4 and the *S. pombe* PNKPs by ~ 15 and $\sim 30\%$, respectively, compared to complete inhibition of human PNKP (Table 2.1). Not surprisingly, the compound significantly inhibited mouse PNKP (which shares $\sim 80\%$ identity to human PNKP). We also tested whether A12B4C3 could inhibit APTX, which is another human DNA 3'-phosphatase. For this experiment, the oligonucleotide substrate was incubated with equal quantities of the two enzymes that were purified from bacteria on the same day. We observed that APTX has a robust phosphatase activity that was totally refractory to 50 μM A12B4C3 (Table 2.1). We then broadened our examination to look at two well known protein phosphatases, calcineurin and PP-1 γ . Neither enzyme displayed any inhibition when treated with an A12B4C3 concentration as high as 83.3 μM , whereas the control inhibitor microcystin LR reduced the activity of PP1 $\sim 65\%$ (Figure 2.5A).

Table 2.1

Inhibition by A12B4C3 of other related DNA phosphatases

% Phosphatase Activity

Protein	Enzyme Concentration	No Inhibitor	50 μM A12B4C3
hPNKP	5 ng/ μ l	100 \pm 0.5	0 \pm 1.3
mPNKP	5 ng/ μ l	96 \pm 2.8	6 \pm 2.6
<i>S. Pombe</i> PNKP	5 ng/ μ l	94 \pm 1.7	68 \pm 5.2
T4 PNK	0.05 U/ μ l	92 \pm 2.4	79.5 \pm 3.8
hAPTX	50 ng/ μ l	70 \pm 0.9	70 \pm 1.2

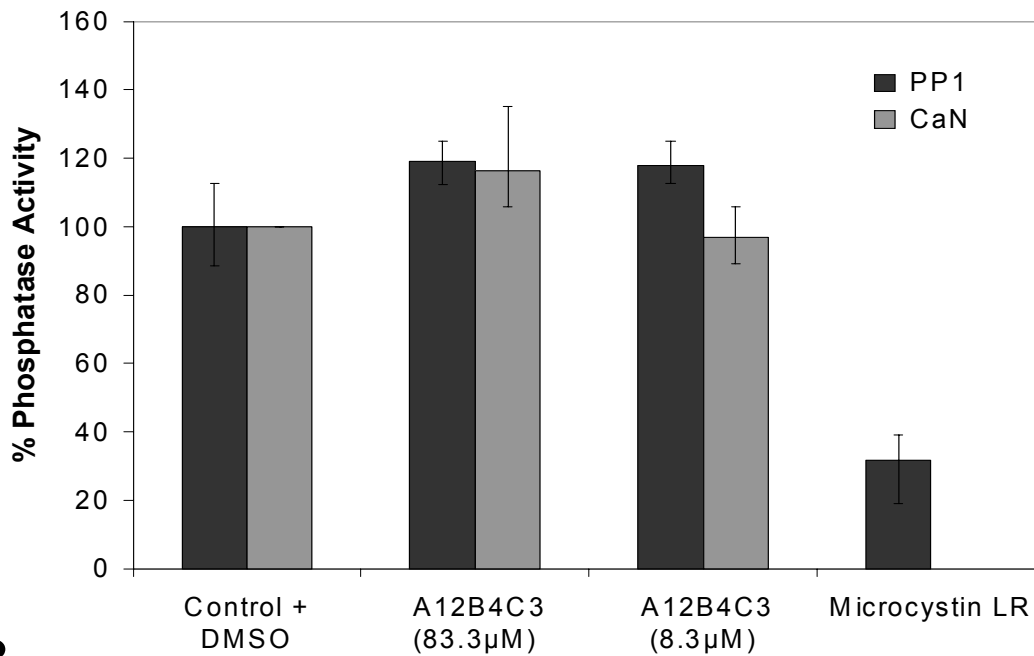
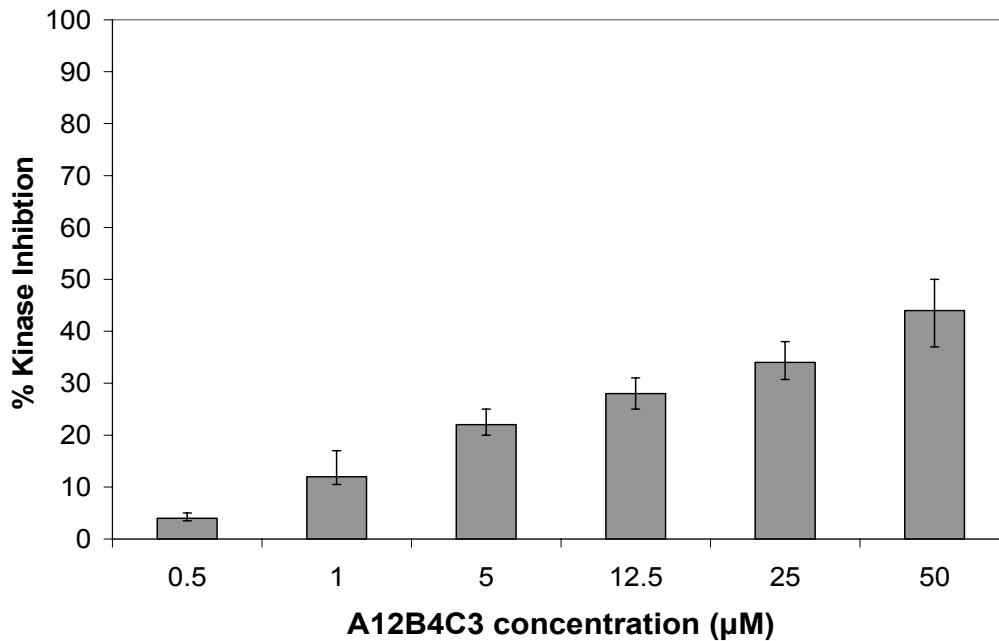
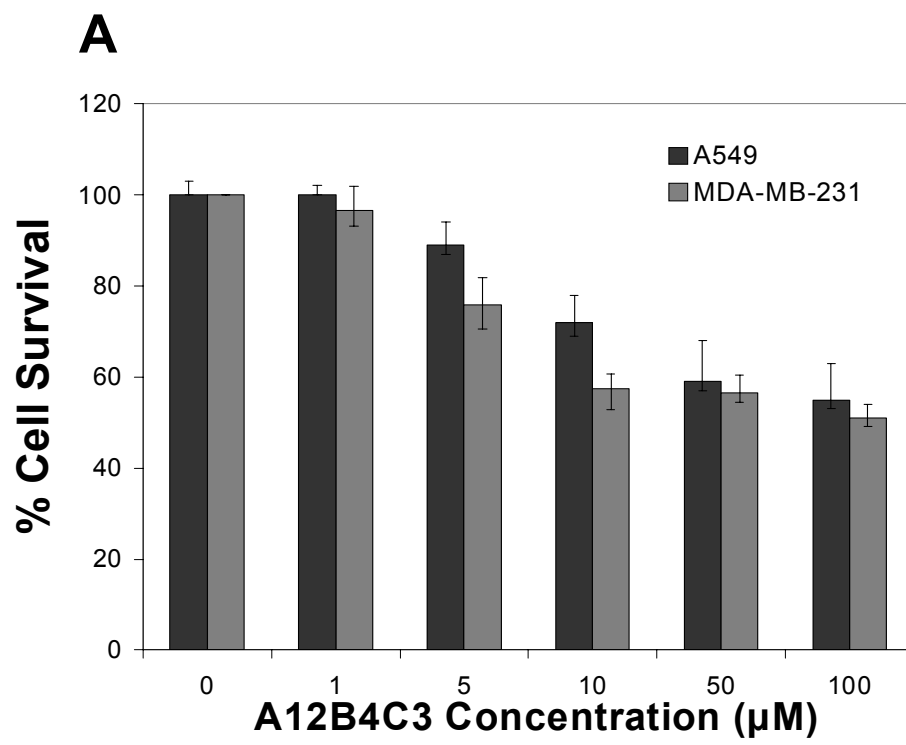
A**B**

Figure 2.5. Specificity of inhibition by A12B4C3. (A) The influence of A12B4C3 on protein phosphatases was examined as described in Material and Methods. No inhibition by A12B4C3 of PP-1c or calcineurin (CaN) was observed. In comparison, the potent PP-1 inhibitor microcystin LR effectively inhibited PP-1c at low nanomolar concentrations [12 nM], as expected. (B) Dose-dependent inhibition of hPNKP DNA kinase activity by A12B4C3 measured by the transfer of radiolabeled phosphate from $[\gamma\text{-}^{32}\text{P}]\text{ATP}$ as described in Materials and Methods. Data for each figure were compiled from three independent assays for each activity measured. The error bars show the S.E.M.



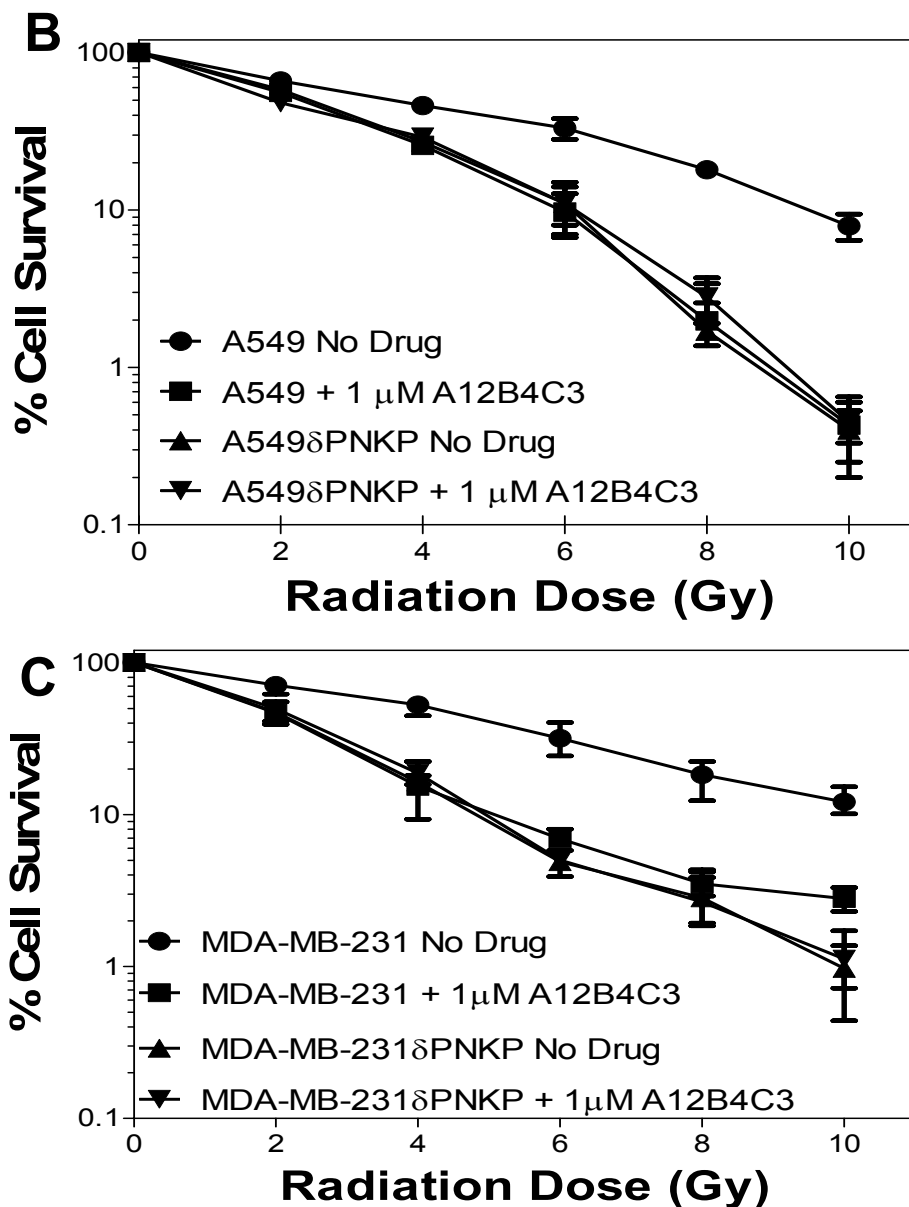


Figure 2.6. Radiosensitization by A12B4C3. (A) Cytotoxicity of A12B4C3 alone measured by 72-h exposure of A549 lung cancer cells and MDA-MB-231 breast cancer cells to increasing concentrations of the compound and determination of cell proliferation as described in Materials and Methods. The data are drawn from three independent determinations \pm S.E.M. (B) Influence of A12B4C3 on the radiosensitivity of wild-type A549 cells and PNKP-deficient cells (A549 δ PNKP). Cells were exposed to 1 μ M A12B4C3 two hours prior to irradiation and then maintained in the same media for a further 24 h. The media was then replaced with fresh media without the drug. Cytotoxicity was determined by the colony forming assay as described in Materials and Methods. The survival curves (\pm S.E.M.) are based on four independent sets of determinations. (C) Influence of A12B4C3 on the radiosensitivity of wild type MDAMB-231 cells and PNKP-depleted MDA-MB-231 cells (MDA-MB-231 δ PNKP) using identical conditions to those described in Figure 2.6B. The survival curves (\pm S.E.M.) are based on five independent sets of determinations.

Finally, the effect of A12B4C3 on the kinase activity of human PNKP was examined by quantifying the transfer of ^{32}P -labeled phosphate from radiolabeled ATP to an oligonucleotide. As shown in Figure 2.5B, there was a concentration-dependent increase in inhibition of the PNKP kinase activity up to ~45% at 50 μM A12B4C3. However, the inhibition of the kinase and phosphatase activities cannot be directly compared because the standard assay for kinase activity employs ten-fold more enzyme than the assay for phosphatase activity.

2.4.5 Cytotoxicity of A12B4C3 and cellular radiosensitization by A12B4C3

The data presented indicated that A12B4C3 is a potent inhibitor of human PNKP *in vitro*. It was therefore important to assess the compound's effectiveness as a radiosensitizer. A12B4C3 was first tested for its inherent toxicity.

Cytotoxicity was measured by cell proliferation assay after exposure of A549 human lung carcinoma cells and MDA-MB-231 breast adenocarcinoma cells to increasing doses of the compound for 72 h (Figure 2.6A). We observed a dose-dependent reduction in cell proliferation up to ~50% at 100 μM A12B4C3, which is close to the limit of solubility of the compound. No significant effect on cell proliferation was detected after exposure of either cell line to 1 μM A12B4C3.

The lack of cytotoxicity at this dose was confirmed by clonogenic survival assay following exposure to A12B4C3 up to 24 h (data not shown). We then examined the capacity of A12B4C3 to act as a radiosensitizer. A549 cells were incubated with 1 μM A12B4C3 for 2 h prior to irradiation and then maintained in the presence of the compound for a further 24 h. The survival curves indicated that exposure to A12B4C3 almost doubled the radiosensitivity of A549 cells based on

the dose required to achieve the same level of cell killing (Figure 2.6B). This radiation response was nearly identical to that seen with cells depleted of PNKP by stable expression of shRNA (A549 δ PNKP). On the other hand, A12B4C3 failed to sensitize the PNKP-depleted cells. Similar data were obtained with wild type and PNKP-depleted MDA-MB-231 breast cancer cells (Figure 2.6C).

2.5 Discussion

In this report, we describe the initial steps towards the generation of a selective human PNKP inhibitor because our previous observations indicated that PNKP depletion, mediated by shRNA, sensitizes cells to ionizing radiation (15), and would therefore be an appropriate target for small molecule inhibition. PNKP possesses 5'-kinase and 3'-phosphatase activity. For this study we chose to target the latter activity, because 3'-phosphate termini are frequently generated by ionizing radiation (73,75). This necessitated the development of a suitable screening assay for inhibitors of the phosphatase activity. Most fluorescence-based high throughput screening assays for phosphatase activity have been directed towards protein phosphatases and rely on immunodetection using antibodies to the phosphorylated peptide substrate. The superquenching assay, originally devised by Rininsland et al. (90), presented an alternative approach that depended on the presence of a phosphate group for chemical recognition. It required some optimization involving protonation of the substrate to enhance the influence of the terminal phosphomonoester group over the internucleotide phosphodiester groups of the DNA substrate. Using this protocol a Z-factor of 0.68 was obtained, which is considered sufficient for identification of inhibitors in

high throughput screens (91). The inhibitory activity of compounds identified by the superquenching assay could be corroborated by the conventional radio-gel assay and by the PiColorlock colorimetric assay.

The chemical library of polysubstituted piperidines proved a relatively rich source of inhibitory compounds. Noticeably, the three most active compounds contain a para-nitrophenyl hydrazine substituent on the ring nitrogen of the six membered piperidines ring, as well as an N-phenyl imide unit (Figure 2.2). The importance of these substituents to the binding of the inhibitor to PNKP remains to be determined through further structure-activity relationship studies. The library features less chemical diversity at the position of the N-phenyl imide, which could be the target of future structure-activity optimization. A12B4C3 was clearly the most effective inhibitor of PNKP with an IC_{50} of 0.06 μ M compared to \sim 0.3 μ M for the next most active compound A6B4C3 (Figure 2.4C). In addition to the para-nitrophenyl hydrazine substituent, A12B4C3 also features a long hydrophobic alkyl chain, which may at least be partly responsible for the greater inhibitory activity displayed by this compound. However, as seen from the structures of the active compounds shown in Figure 2.2, all the compounds have different substituents at this position, suggesting that this site may be less critical and consequently it could be a potential site for bioconjugation required in radiolabeling and mechanistic studies.

An important issue with all small molecule inhibitors is their specificity. We examined the response of a number of other phosphatases to A12B4C3. Phage T4 polynucleotide kinase and human PNKP share similar nucleic acid

kinase and phosphatase activities. However, with the exception of the enzyme active sites, the proteins bear no recognizable homology (24,84). The phosphatase domains of both proteins belong to the haloacid dehalogenase (HAD) superfamily (24-26) with a conserved Dx DGT motif, where the first Asp forms a covalent phospho-aspartate intermediate with the substrate. The fact that A12B4C3 poorly inhibited T4 PNK (Table 2.1) suggests that the small molecule does not directly interact with this conserved HAD motif. The catalytic domain (phosphatase and kinase) of *S. pombe* PNKP, on the other hand, shares considerably more structural similarity with human PNKP than the T4 enzyme, with 127 identical residues, including the HAD motif (87). Despite this level of sequence overlap, the inhibition of *S. pombe* PNKP by A12B4C3 was limited (~30%), even at 50 μ M inhibitor concentration (Table 2.1), suggesting that the compound interacts primarily with a region specific to mammalian PNKP, hence the strong inhibition of human and mouse PNKP (Table 2.1). Since A12B4C3 also inhibits the kinase activity of hPNKP (Figure 2.5B), it is possible that the compound acts as a non-competitive inhibitor disrupting the structure of the enzyme. Indeed evidence suggests that this is the case (see chapter III).

Given the low level of inhibition of related PNKPs, it is not surprising that A12B4C3 displayed no inhibition (Figure 2.5A) of either of the two protein phosphatases tested, protein phosphatase 1 (PP-1) and calcineurin (protein phosphatase 2B), which are important members of the eukaryotic serine/threonine family involved in a broad range of signal transduction pathways (92). Of course, we cannot rule out the possibility that A12B4C3 interacts with other protein

phosphatases or indeed other enzymes, but our tests for radiosensitization by A12B4C3 (Figure 2.6B and 2.6C) indicated not only that the compound effectively sensitized wild type cells to ionizing radiation, but also revealed that PNKP is most likely the cellular target for A12B4C3 in human cells because it failed to sensitize the PNKP-deficient cells. In summary, we have made use of several analytical approaches to identify a set of polysubstituted piperidine molecules that inhibit mammalian PNKP in the μM range and may prove to be useful tools in the study of DNA repair. The most potent of these compounds, A12B4C3, will serve as a useful lead compound for future development of potential clinical radiosensitizers.

Acknowledgements

I must acknowledge Ashley Ahrens and Jonathon Koshy for their initial identification of the phosphatase inhibitors, and to Dr. Feridoun Karimi-Busheri whose idea it was to screen for inhibitors to PNKP. Special thanks also go to Todd Mereniuk who created the PNKP stable knockdown in A549 cells and to Dr. Aghdass Rasouli-Nia who created the PNKP stable knockdown in MDA-MB-231 cells. In addition, I must acknowledge Dr. Charles Holmes (Department of Biochemistry, University of Alberta) and his graduate student Phuwadet Pasarj for their contribution on testing A12B4C3 on PP1 and calcineurin. Furthermore, I would like to thank Dr. Dennis Hall (Department of Chemistry, University of Alberta) and his post-doctoral fellow Dr. Agnieszka Ulaczyk-Lesanko who created the small molecule library. And lastly I would like to acknowledge my supervisor Dr. Michael Weinfeld for his significant contribution in helping to

brainstorm and design experiments to test the inhibitors effectiveness.

Chapter III

Mechanism of Action of an Imidopiperidine Inhibitor of Human Polynucleotide Kinase/Phosphatase

Running title: Inhibitor of Polynucleotide Kinase/Phosphatase

Gary K Freschauf¹, Rajam S Mani¹, Todd R Mereniuk¹, Mesfin Fanta¹, Caesar A Virgen¹, Grigory L Dianov³, Jean-Marie Grassot², Dennis G Hall², and Michael Weinfeld¹

¹Experimental Oncology, Cross Cancer Institute, and Department of ²Chemistry, University of Alberta, Edmonton, Alberta; and ³the Gray Institute for Radiation Oncology and Biology, University of Oxford, Oxford

Corresponding author. Michael Weinfeld Department of Experimental Oncology, Cross Cancer Institute, 11560 University Avenue, Edmonton, Alberta, Canada.

Phone: 780-432-8438; Fax 780-432-8428; E-mail: michaelw@cancerboard.ab.ca

A version of this chapter has been published. Gary K Freschauf¹, Rajam S Mani¹, Todd R Mereniuk¹, Mesfin Fanta¹, Caesar A Virgen¹, Grigory L Dianov³, Jean-Marie Grassot², Dennis G Hall², and Michael Weinfeld¹. (2010) Mechanism of Action of an Imido-piperidine Inhibitor of Human Polynucleotide Kinase/Phosphatase J Biol. Chem. 285; (4): 2351-60.

3.1 ABSTRACT

The small molecule, 2-(1-hydroxyundecyl)-1-(4-nitrophenylamino)-6-phenyl-6,7a-dihydro-1*H*-pyrrolo[3,4-*b*]pyridine-5,7(2*H*,4*aH*)-dione (A12B4C3), is a potent inhibitor of the phosphatase activity of human polynucleotide kinase/phosphatase (PNKP) *in vitro*. Kinetic analysis revealed that A12B4C3 acts as a non-competitive inhibitor, and this was confirmed by fluorescence quenching, which showed that the inhibitor can form a ternary complex with PNKP and a DNA substrate, i.e. A12B4C3 does not prevent DNA from binding to the phosphatase DNA binding site. Conformational analysis using circular dichroism, UV-difference spectroscopy and fluorescence resonance energy transfer all indicated that A12B4C3 disrupts the secondary structure of PNKP. Investigation of the potential site of binding of A12B4C3 to PNKP using site directed mutagenesis pointed to interaction between Trp402 of PNKP and the inhibitor. Cellular studies revealed that A12B4C3 sensitizes A549 human lung cancer cells to the topoisomerase I poison, camptothecin, but not the topoisomerase II poison, etoposide, in a manner similar to siRNA against PNKP. A12B4C3 also inhibits the repair of DNA single and double-strand breaks following exposure of cells to ionizing radiation, but does not inhibit two other key strand break repair enzymes, DNA polymerase β or DNA ligase III, providing additional evidence that PNKP is the cellular target of the inhibitor.

3.2 INTRODUCTION

The successful repair of DNA strand breaks is crucial to ensure the stability and survival of the cell. In the absence of correct and efficient repair,

cells can accumulate mutations or undergo cell death. Several repair pathways are responsible for handling various classes of DNA lesions, such as damaged bases and single- and double-strand breaks, which can be generated by endogenous and exogenous genotoxic agents. In mammalian cells, polynucleotide kinase/phosphatase (PNKP) plays a role in the base excision/single-strand break repair pathway and the nonhomologous end-joining (NHEJ) double-strand break repair pathway (12-15,93) because of its function in restoring the chemistry of strand breaks to a form suitable for DNA polymerases and ligases to complete the repair process, i.e. 3'-hydroxyl and 5'-phosphate termini. PNKP catalyzes the phosphorylation of 5'-OH termini and dephosphorylation of 3'-phosphate termini (16,22). In the single-strand break repair (SSBR) pathway, PNKP acts in concert with XRCC1, DNA polymerase β (Pol β) and DNA ligase III (12,79,93). At double-strand breaks, PNKP is dependent on DNA-PKcs and XRCC4 (14,18), which are components of the NHEJ pathway. In addition, PNKP has been implicated in the repair of damaged termini generated by the topoisomerase inhibitor I camptothecin (15,82), which forms a "dead-end" complex in which topoisomerase I remains covalently attached to a 3'-phosphate group, thereby preventing topoisomerase I from resealing the DNA strand after the incision step (94). The inhibited enzyme can be cleaved from the phosphate group by the action of tyrosyl-DNA phosphodiesterase (Tdp1), leaving a break with 3'-phosphate and 5'-hydroxyl termini, which requires the subsequent action of PNKP (82). In contrast PNKP does not appear to play a role in the DNA repair of topo II-dead-end complexes generated by treatment with etoposide (15).

Cancer cells in which PNKP expression has been depleted by targeted shRNA display a noticeable decrease in cell survival when exposed to a number of genotoxic agents, including ionizing radiation, camptothecin and the alkylating agent, methyl methanesulphonate (15). This suggests that PNKP plays an important role in countering exogenous DNA damage and it was proposed that PNKP may be a suitable target for small molecule inhibitors in order to enhance the toxicity of genotoxic therapeutic agents, especially ionizing radiation and topoisomerase I inhibitors (66,84). We have recently identified a series of compounds from a library of polysubstituted imido-piperidines that inhibit the 3'-phosphatase activity of PNKP(95). The most potent of these inhibitors, 2-(1-hydroxyundecyl)-1-(4-nitrophenylamino)-6-phenyl-6,7a-dihydro-1*H*-pyrrolo[3,4-*b*]pyridine-5,7(2*H*,4*aH*)-dione (A12B4C3), (Figure 3.1), was shown to be non-toxic to A549 human lung cancer and MDA-MB-231 human breast cancer cells at 1 μ M concentration, but increased the sensitivity of these cells to ionizing radiation to almost the same extent as stable shRNA-mediated PNKP depletion (95). On the other hand, A12B4C3 failed to enhance the sensitivity of the shRNA-mediated PNKP-depleted cells, indicating that PNKP is probably the major cellular target for the inhibitor.

This study describes the further characterization of the inhibitor at the cellular and molecular levels. We have compared its chemo-sensitizing properties on cells treated with topoisomerase I and II inhibitors to further substantiate the likelihood that PNKP is the cellular target for A12B4C3. At the molecular level, we have examined the influence of A12B4C3 on strand break repair and

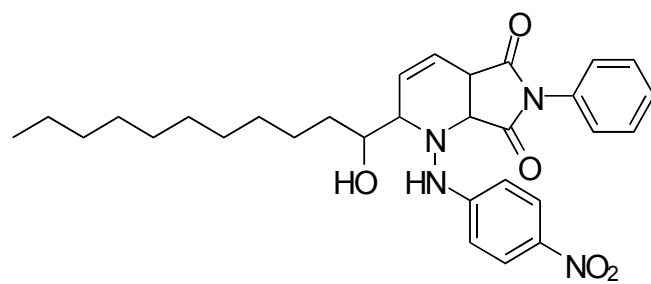


Figure 3.1. Structure of the PNKP inhibitor A12B4C3.

identified its mechanism of inhibition. Finally, we have obtained information regarding the perturbation of PNKP by A12B4C3 and the site of interaction of the protein with the inhibitor.

3.3 Materials and Methods

3.3.1 Reagents

The imidopiperidine A12B4C3 was resynthesized and purified as described in chapter II section 2.3.4. Recombinant human PNKP was purified as described previously in chapter II section 2.3.1 and stored in 50 mM Tris-HCl, pH 7.4, 100 mM NaCl, 5 mM MgCl₂, 0.5 mM dithiothreitol. Histidine-tagged human DNA ligase III α cloned in pET28b was expressed in bacterial cells and purified on a Ni²⁺-charged His-Bind resin (Novagen) as described by the manufacturer. Human Pol β was kindly provided by Dr. Sam Wilson, NIEHS, Research Triangle Park, NC. The his-tagged PNKP single mutants W402F and W331F were generated using the QuikChange Site-Directed Mutagenesis Kit (Stratagene, La Jolla, CA). Each reaction contained 50 ng of template pBluescript SK⁺/PNKP and 125 ng of sense and antisense primers. Eighteen PCR cycles were performed using an extension temperature of 65 °C. No further modifications were made to the protocol. The his-tagged mutant WFX402, in which all the tryptophans except 402 were replaced by phenylalanine, was generated with four rounds of mutagenesis using the QuikChange Multi Site-Directed Mutagenesis Kit (Stratagene). For each reaction, 50 ng of pBluescript SK⁺/PNKP was used as a template together with 100 ng of the appropriate primer. The plasmids were sequenced on an ABI 310 genetic analyzer (ABI-Inc, Ramsey, MN). The PNKP

mutants were subcloned from the cloning vector into pET16b (Novagen/EMD Chemicals Inc, Gibbstown, NJ) using the BamHI and XbaI cleavage sites and transfected into *Escherichia coli* DE3 (BL21) pLysS (Novagen) for expression. Recombinant his-tagged mutant PNKP proteins were purified from *E. coli* grown at 37 °C in 1-4 liters of LB medium supplemented with 50 µg ampicillin. At an OD₆₀₀ of 0.6, 0.1 mM isopropyl-1-thio-β-D-galactopyranoside (Sigma) was added and the culture was incubated for 24 h at 16 °C. The bacteria were spun down at 15 000 x g at 4 °C for 20 min. The pellet was resuspended in 40 ml his-PNKP binding buffer (50 mM NaH₂PO₄, 250 mM NaCl, 1mM PMSF at pH 7.9). The solution was stirred on ice for 30 min in the presence of 30 mg lysozyme and 4 mg PMSF. The bacteria were sonicated at 50 % of maximum for 3 x 60 sec with 60 sec intervals in between. The bacteria were then spun at 15000 rpm for 20 min at 4 °C. The supernatant was loaded into a beaker with 4 ml ProBond Resin (Invitrogen) and mixed slowly for 1 h at 4 °C. Then the slurry was loaded into a column and the resin was washed with 20 ml of 20 mM imidazole, before eluting the protein with 20 ml of 150 mM imidazole (4 x 5 ml fractions). The protein was concentrated using a 30 kDa cutoff Amicon Ultra-15 centrifugal filter (Millipore) and dialyzed with 50 mM Tris-HCl (pH 7.5), 100 mM NaCl and 5 mM MgCl₂. His-PNKP concentration was estimated by OD_{280nm} where 1.2 units were equivalent to 1.0 mg of protein.

3.3.2 Cells

A549 (human lung carcinoma cells) were obtained from the American Type Culture Collection (Manassas, VA). Cells were cultured in a 1:1 mixture of

Dulbecco's modified Eagle's medium/nutrient mixture F-12 (DMEM/F-12) supplemented with 10% fetal calf serum (FCS), penicillin (50 U/ml), streptomycin (50 µg/ml), L-glutamine (2 mM), non-essential amino acids (0.1 mM) and sodium pyruvate (1 mM), and maintained at 37 °C under 5% CO₂ in a humidified incubator. All culture supplies were purchased from Invitrogen. The generation of PNKP-depleted A549 cells (A549δPNKP) has been previously described in chapter II section 2.3.2.

3.3.3 Cytotoxicity studies

The effect of PNKP inhibition by A12B4C3 on cellular survival following exposure to topoisomerase I and II poisons, camptothecin and etoposide, respectively, was measured in A549 and A549δPNKP cells using the clonogenic survival assay. Cells were seeded on 60-mm tissue culture plates at various cell densities to give between 100 - 1000 colonies per plate and returned to the incubator overnight to allow the cells to attach. For chemosensitization studies, the cells were incubated with or without 1 µM A12B4C3 for 2 h before exposure to different doses of camptothecin or etoposide (Sigma, St. Louis, MO). After addition of topoisomerase poisons, cells were incubated for a further 24 h in the same media and then washed twice with phosphate-buffered saline (PBS) and incubated in fresh media without the drug or PNKP inhibitor. Colonies were stained with crystal violet after 10 to 14 days and counted with an automated Colcount colony counter (Oxford Optronix, Oxford, UK).

3.3.4 DNA strand-break repair measured by single-cell gel electrophoresis

A549 and A549 δ PNKP cells were grown in 60-mm plates to form a confluent monolayer. A12B4C3 (1 μ M) was added to the plates 2 h before irradiating cells. Cells were irradiated at 5 Gy (60 Co Gammacell; Atomic Energy of Canada Limited, Ottawa) and incubated at 37 °C for 0, 10, 30, 60 and 120 min. To analyze SSBs we utilized the alkaline comet assay. For each slide, 1×10^5 cells were trypsinized and mixed with 0.1% molten low-melting-point agarose at 42 °C at a 1:10 ratio (10 μ l cells per 100 μ l of agarose). The mixture (50 μ l) was spread immediately on a comet slide (Trevigen, Gaithersburg, MD) and kept at 4 °C for 25 min to allow the agarose to solidify. Slides were immersed in prechilled lysis solution (2.5 M NaCl, 100 mM Na₂-EDTA, pH 10, 10 mM Tris base, 1% SDS, 1% Triton X-100), kept on ice for 30 min, and then immersed in an alkaline solution (300 mM NaOH, 1 mM Na₂-EDTA) for 30 min at 23°C. Slides were then placed in an electrophoresis apparatus filled with fresh alkaline solution and run at 1 V/cm and ~300 mA at 4 °C for 25 min. The slides were then washed in 70% ethanol for 5 min. The DNA was stained with SYBR Green I (Invitrogen, San Diego, CA) and viewed with an AxioScope 2 fluorescence microscope (Zeiss). For each data point a minimum of 100 random cell images were visually analyzed and categorized according to the National Institutes of Health LISTSERV (Comet Assay Interest Group web site; <http://cometassay.com/introduction.htm>). To analyze DSBs, we utilized the neutral comet assay, which has the same protocol as described above for SSBs, however with the addition of a 10 min immersion step with 1X TBE buffer. The 1X TBE buffer was step was administered immediately before the slides were electrophoresed. After the 10 min immersion

step the 1X TBE buffer was removed and alkaline solution was added and the slides were electrophoresed.

3.3.5 DNA ligase III assay

The substrate for this assay was composed of two short oligonucleotides, a 21-mer 5'-ATTACGAATGCCACACCGCC-3' and a 5'-phosphorylated 24mer 5'-pGGCGCCCACCACCACTAGCTGGCC-3', annealed to a 45mer 5'-GGCC-AGCTAGTGGTGGGCGCCGGCGGTGTGGGCATTCGTAAT-3' (IDT, Coralville, IA). Prior to annealing, the 21mer was radiolabeled with [γ -³²P]ATP (PerkinElmer) by incubation with 1 unit of T4 PNK (New England Biolabs) for 20 min at 37 °C. After the labeling, the T4 PNK was inactivated by boiling for 10 min. The oligonucleotides were annealed by adding equal molar concentrations of the oligonucleotides with 1/10 volume of 10X annealing buffer (100 mM Tris-HCl, pH 7.4, 1 M NaCl, and 10 mM EDTA) and boiled for 10 min and then allowed to cool to room temperature. DNA ligase III reactions were set up as follows: 6 μ l distilled water, 2 μ l 10X ligase buffer (500 mM Tris-HCl, pH 7.5, 10 mM MgCl₂, 1 mM ATP, and 10 mM DTT), 4 μ l A12B4C3 (to a final concentration of 1, 5, 12.5, 25 or 50 μ M dissolved in DMSO) or DMSO, and 4 μ l human DNA ligase III (50 ng). The samples were incubated for 5 min at 30 °C and then 4 μ l annealed substrate (6.6 μ M final concentration) was added and the samples incubated at 30 °C for a further 30 min, before the reactions were stopped by addition of 3X gel loading dye (Fisher Scientific, Ottawa, ON) and boiled for 10 min. Samples were loaded on a 12% polyacrylamide/7 M urea sequencing gel and subjected to electrophoresis for 3 h in 1 X TBE buffer. Gels were scanned

with a Typhoon 9400 Variable Mode Imager (GE Healthcare, Little Chalfont, UK), and quantified using Image Quant 5.2 Software (GE Healthcare).

3.3.6 DNA polymerase β assay

The assay for Pol β activity utilized a similar substrate to that described for the ligase reaction except that a radiolabeled 20mer replaced the 21-mer to generate a 1-nucleotide gap in place of a nick. Pol β reactions were set up as follows: 6 μ l distilled water, 2 μ l 10X polymerase buffer (500 mM Tris-HCl, pH 8.0, 100 mM MgCl₂, 20 mM DTT, 200 mM NaCl, 10 % glycerol), 2-4 μ l A12B4C3 (to a final concentration of 1, 5, 12.5, 25, or 50 μ M) or DMSO, 2 μ l dNTP mixture (500 μ M), and Pol β (100 ng). The sample was incubated for 5 min at 37 °C before addition of 4 μ l annealed substrate (6.6 μ M final concentration). The samples were incubated at 37 °C for an additional 30 min and the reactions stopped by addition of 3X gel loading dye (Fisher Scientific) and boiled for 10 min. Samples were loaded on a 15% polyacrylamide/7 M urea sequencing gel and the products separated by electrophoresis for 3 h in 1 X TBE buffer. Gels were scanned with a Typhoon 9400 Variable Mode Imager and quantified using Image Quant 5.2 Software. Failure of the 5'-phosphorylated 20mer to undergo conversion to a 21mer was indicative of inhibition of Pol β activity.

3.3.7 Assay for 3'-phosphatase activity based on the release of inorganic phosphate (Pi)

PNKP phosphatase reactions (20 μ l total volume) were setup as follows: 1 μ l wild type or mutant PNKP (100 ng), 2 μ l 10X phosphatase buffer (500 mM Tris-HCl, pH 7.4, 0.1 mM EDTA, 1 mM spermidine and 2.5 mM DTT), 2 μ l of 1

mM 3'-P 20mer oligonucleotide, 15 μ l distilled H₂O and 1 μ l A12B4C3 (1, 5, 12.5, 25 and 50 μ M). The reactions were then transferred to a clear polystyrene colorimetric 384-well plate and incubated at 37 °C for 30 min. PiColorlock Gold reagent (Innova Biosciences Ltd., Cambridge, UK) was prepared shortly before use by addition of 1/100 vol. of accelerator to PiColorlock Gold reagent as directed by the manufacturer. The Gold mix was then added to Pi-containing samples in a volume ratio of 1:4 and the samples incubated at room temperature for 30 min before the absorbance was read at 620 nm using a FLUOstar Optima® plate reader (BMG Labtech Inc. Durham, NC).

3.3.8 Inhibition (Lineweaver-Burk plot) assay

PNKP phosphatase reactions (20 μ l total volume) were set up as follows: 1 μ l PNKP (100 ng), 2 μ l 10X phosphatase buffer (500 mM Tris-HCl, pH 7.4, 0.1 mM EDTA, 1 mM spermidine and 2.5 mM DTT), 2 μ l of 0, 50, 100, 150, 200, 250, 300, or 500 mM 3'-P 20mer oligonucleotide, 15 μ l distilled H₂O and 1 μ l A12B4C3 (5, 10, or 20 μ M). The reactions were then transferred to a clear polystyrene colorimetric 384-well plate and incubated at 37 °C for 30 min. Phosphatase activity was measured by the PiColorLock Gold reagent as described above.

3.3.9 UV difference spectroscopy

UV difference spectra were recorded on a PerkinElmer Lambda 40 spectrophotometer over the wavelength range 320-250 nm with a 1 cm path length cells as described previously (96). To generate a UV difference spectrum, both the sample cell and the reference cell contained A12B4C3 (3 μ M) and PNKP

(0.5 mg/ml), but only the contents of the sample cell were mixed, thereby allowing the interaction between PNKP and A12B4C3 to proceed.

3.3.10 Circular dichroism spectroscopy

Circular Dichroism (CD) measurements were performed in an Olis DSM 17CD spectropolarimeter (Bogart, GA) calibrated with a 0.06% solution of ammonium d-camphor-10-sulfonate. The temperature in the sample chamber was maintained at 5 °C. Each sample was scanned seven times and the experiments were carried as described previously (97). CD spectra were analyzed for secondary structures according to Chen et al (98).

3.3.11 Steady-state fluorescence spectroscopy-

Steady-state fluorescence spectra were measured at 4 °C on a Perkin-Elmer Life Sciences LS-55 spectrofluorometer with 5 nm spectral resolution for excitation and emission as described in earlier studies (79,97). Protein fluorescence was excited at 295 nm, and fluorescence emission spectra were recorded in the 300-400-nm range; changes in fluorescence were usually monitored at the emission maximum (332 nm). Binding data were analyzed by nonlinear regression analysis using Prism (GraphPad Software Inc., La Jolla, CA). The oligonucleotide used for these studies (5'-biotin/ATT ACG AAT GCC CAC ACC GCP_{hos}-3') containing a biotinylated 5'-terminus and a 3'-phosphate terminus was obtained from IDT.

3.3.12 Fluorescence resonance energy transfer measurements

Nonradiative energy transfer between Trp residue 402 of mutant PNKP WFX402 and acrylodan (AC) was followed in these experiments. Addition of

AC to PNKP WFX402 mutant resulted in quenching of Trp 402 fluorescence, and this was accompanied by the appearance of AC fluorescence around 500 nm. The estimation of molecular distances by intermolecular energy transfer between the emission transition dipole of a donor molecule and the absorption transition dipole of an appropriate acceptor is based on the theory of Förster (99). The rate of energy transfer from a specific donor to a specific acceptor (k_t) is given by

$$k_t = (1/T_d) (R_0/R)^6 \quad (1)$$

where T_d is the lifetime of the donor in the absence of the acceptor, R is the distance between the donor and acceptor, and R_0 is a characteristic distance called the “Förster critical distance” at which the efficiency of transfer is 50%. R_0 , which is dependent on spectral properties and the relative orientation of the donor–acceptor pair, can be evaluated from

$$R_0 = (9.79 \times 10^3) (J \kappa^2 Q_D n^{-4})^{1/6} \text{ \AA} \quad (2)$$

where J is the spectral overlap integral of donor fluorescence and acceptor absorbance, Q_D is the quantum efficiency of the donor, n is the refractive index of the medium (taken to be 1.4), and κ^2 is a dipole orientation factor. The value of $2/3$ for κ^2 was used on the basis of the assumption of random rotation of the fluorophores (100). The overlap integral was approximated by eqn 3,

$$J = \sum F_D(\lambda) \epsilon_A(\lambda) \lambda^4 \Delta \lambda / \sum F_D(\lambda) \Delta \lambda \quad (3)$$

where $F_D(\lambda)$ is the corrected fluorescence of the donor, $\epsilon_A(\lambda)$ is the molar extinction coefficient of the acceptor, and λ is the wavelength in centimeters. The terms were summed over 2 nm intervals. The efficiency of energy transfer (E) was calculated from changes in fluorescence as follows:

$$E = 1 - (Q_{DA} / Q_D) \quad (4)$$

where Q_D and Q_{DA} are the quantum yields of the donor in the absence and presence of acceptor, respectively. The distances between the donor and acceptor were calculated from eqn 5,

$$E = (R_0 / R)^6 / [1 + (R_0 / R)^6] \quad (5)$$

3.4 RESULTS

3.4.1 Cellular chemo-sensitization by A12B4C3.

We have previously shown that a non-toxic dose of A12B4C3 (1 μ M) was able to sensitize cells to ionizing radiation. To examine the capacity of A12B4C3 to act as a chemosensitizer to topoisomerase inhibitors, clonogenic survival assays were performed to measure the response of A549 human lung cancer cells and A549 cells depleted of PNKP by stable expression of shRNA (A549 δ PNKP) to the topoisomerase inhibitors in the presence and absence of A12B4C3. The cells were incubated with 1 μ M A12B4C3 for 2 h prior to addition of either camptothecin (topoisomerase I inhibitor) or etoposide (topoisomerase II inhibitor), and then maintained in the presence of the drugs for an additional 24 h before being replaced with fresh media. The survival curves (Figure 3.2A) indicated that exposure to A12B4C3 significantly increased the sensitivity of A549 cells to camptothecin, and this response was nearly identical to that seen with A549 δ PNKP cells treated with camptothecin alone. A12B4C3 failed to further sensitize the PNKP-depleted cells to camptothecin. On the other hand, the survival curves for the response to etoposide (Figure 3.2B) indicated that PNKP phosphatase inhibition did not sensitize cells to etoposide-induced DNA damage.

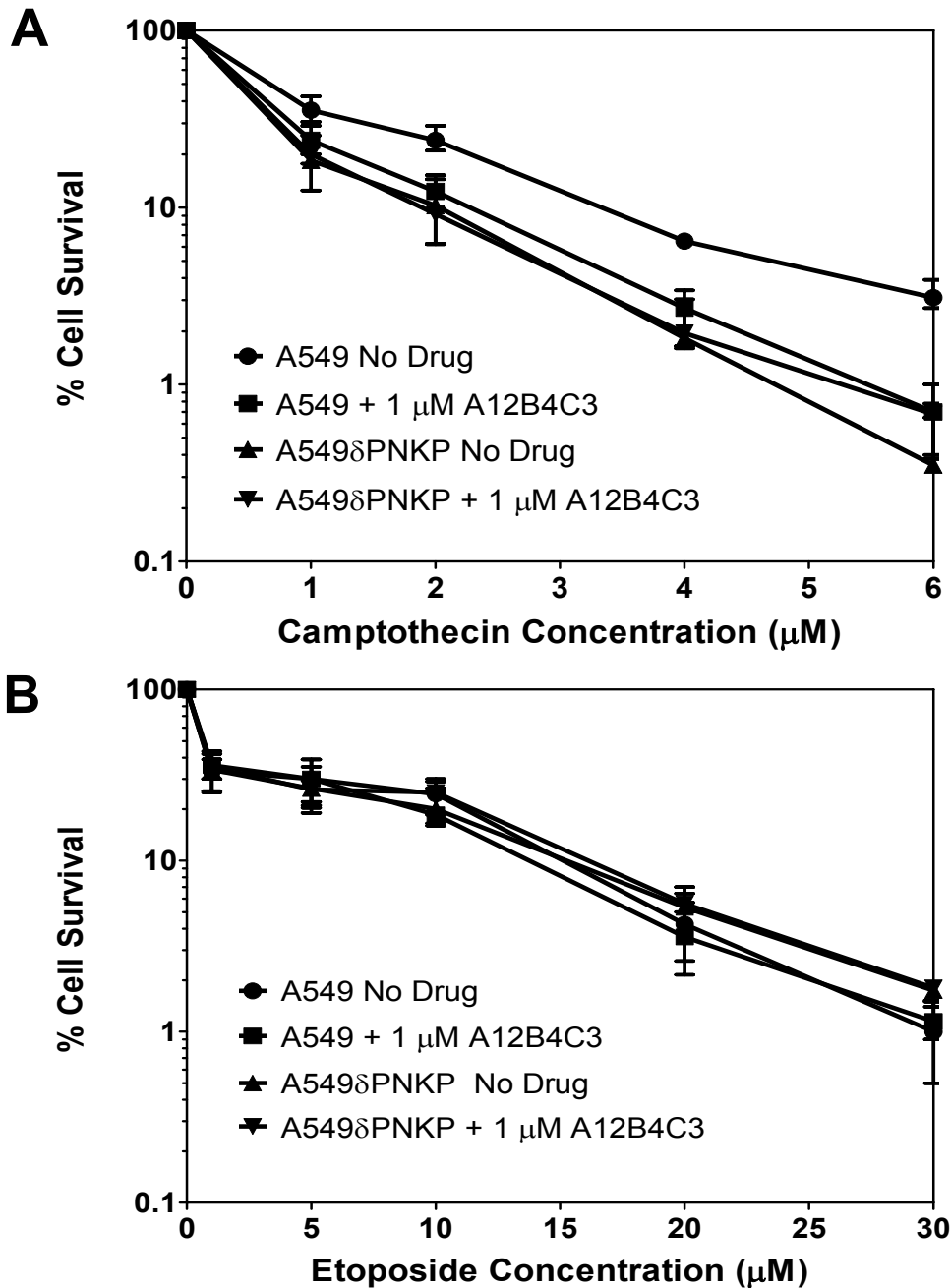


Figure 3.2. Chemosensitization by A12B4C3. (A) Influence of A12B4C3 on the chemosensitivity of wild-type A549 cells and PNKP-depleted cells (A549 δ PNKP) to Camptothecin. Cells were pre-incubated with 1 μM A12B4C3 for two hours prior to addition of camptothecin and then maintained in the same media for an additional 24 h. The media was then replaced with fresh media without the drug. The survival curves (\pm S.E.M.) are based on four independent sets of determinations. (B) Influence of A12B4C3 on the chemosensitivity of wild-type A549 cells and PNKP-depleted cells (A549 δ PNKP) to Etoposide using identical conditions to those described in Figure 3.2A. The survival curves (\pm S.E.M.) are based on four independent sets of determinations.

3.4.2 Influence of A12B4C3 on DNA strand-break repair.

PNKP-depleted cells have previously been shown to have a reduced capacity for repair of radiation-induced single and double-strand breaks. To determine if A12B4C3 can mimic shRNA-mediated down-regulation of PNKP expression, we monitored the influence of A12B4C3 on strand break repair in irradiated cells. For this experiment we utilized the comet assay, which can detect both single and double strand breaks depending on the experimental conditions. A549 cells were pretreated with 1 μ M A12B4C3 for 2 h prior to 5-Gy irradiation and maintained in the presence of the inhibitor during the course of repair. SSBR was followed by single-cell gel electrophoresis (comet assay) under alkaline conditions over 2 h and double-strand break repair (DSBR) by comet assay under neutral conditions over 24 h. The alkaline comet assay is performed under denaturing conditions to denature dsDNA to detect SSBs, while the neutral comet assay is performed under non-denaturing conditions to detect DSBs. For comparison, we also examined strand break repair in A549 δ PNKP cells. Figure 3.3 displays the appearance of the comets under the microscope. The comets were visually scored using a 5-point scale which reflects the amount of undamaged DNA retained in the nucleus of the cell (head of the comet) to damaged DNA which migrates out of the nucleus under electrophoresis (tail of the comet). Type 1 comets represent cells with undetectable levels of damage, while type 5 comets represent cells with very little intact DNA. The assessment of the comets indicated that the DNA in the A549 cells irradiated and incubated in the absence of inhibitor was approaching complete restoration to its initial (unirradiated)

Comet
Type

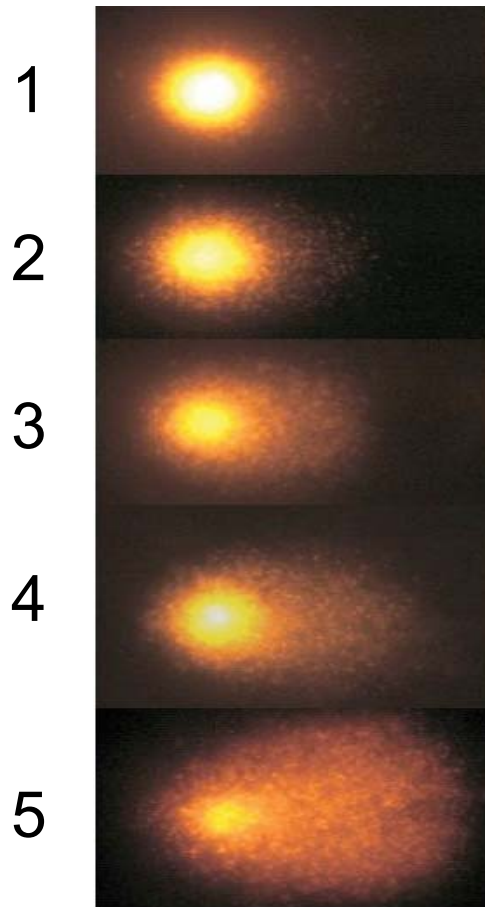
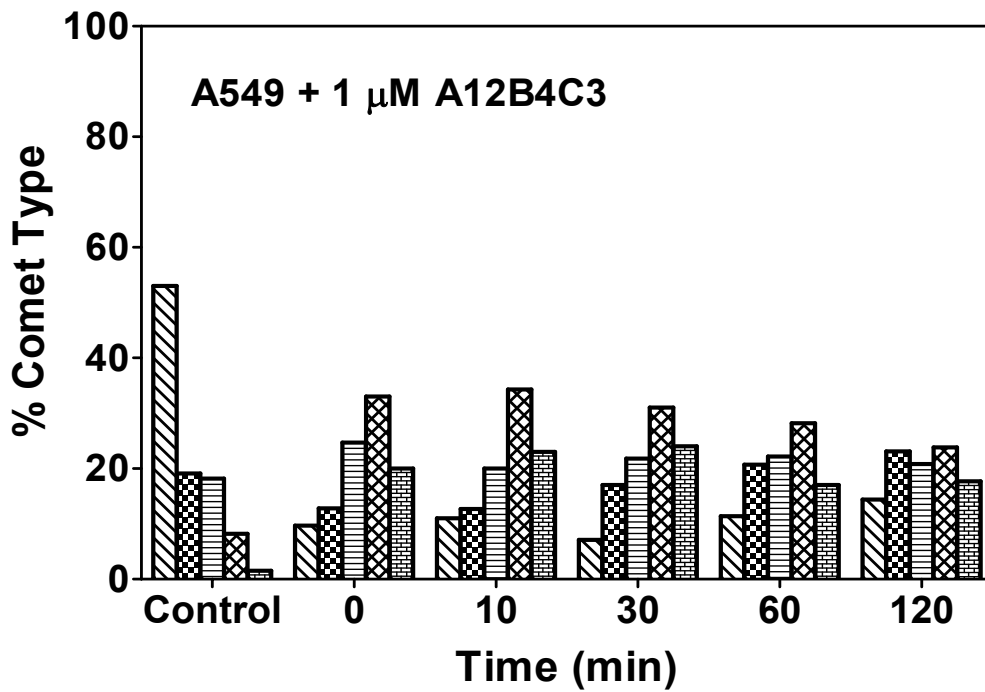
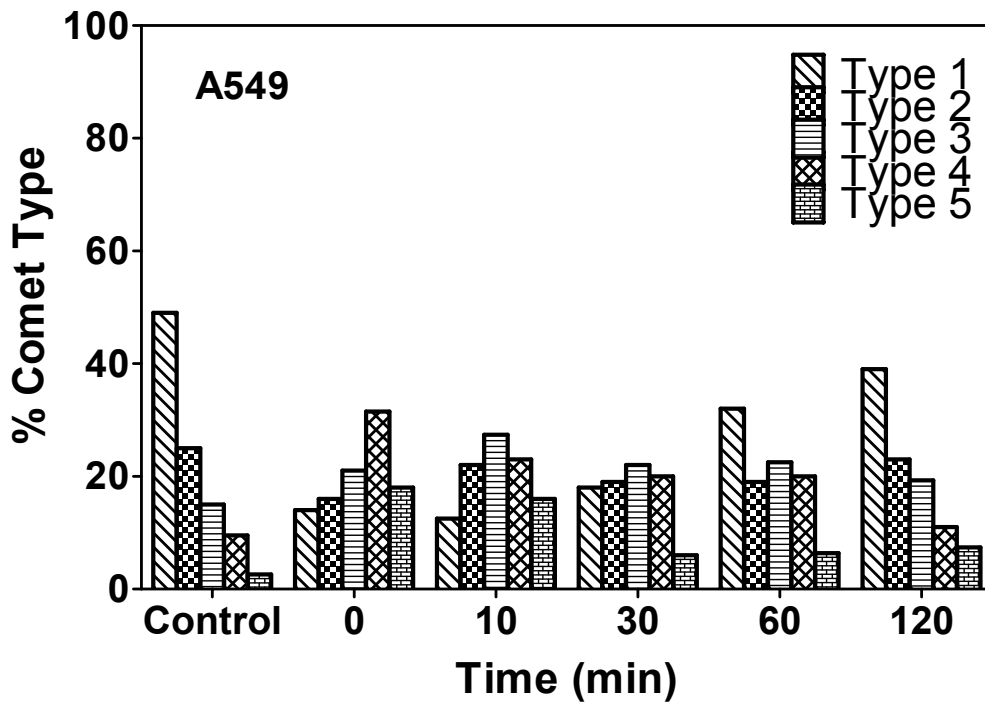


Figure 3.3. Categorization of comets for alkaline and neutral comet assay. Type 1 comets have the least amount of damage, while type 5 comets have the most amount of damage. (www.medgadget.com/archives/img/66553345g)



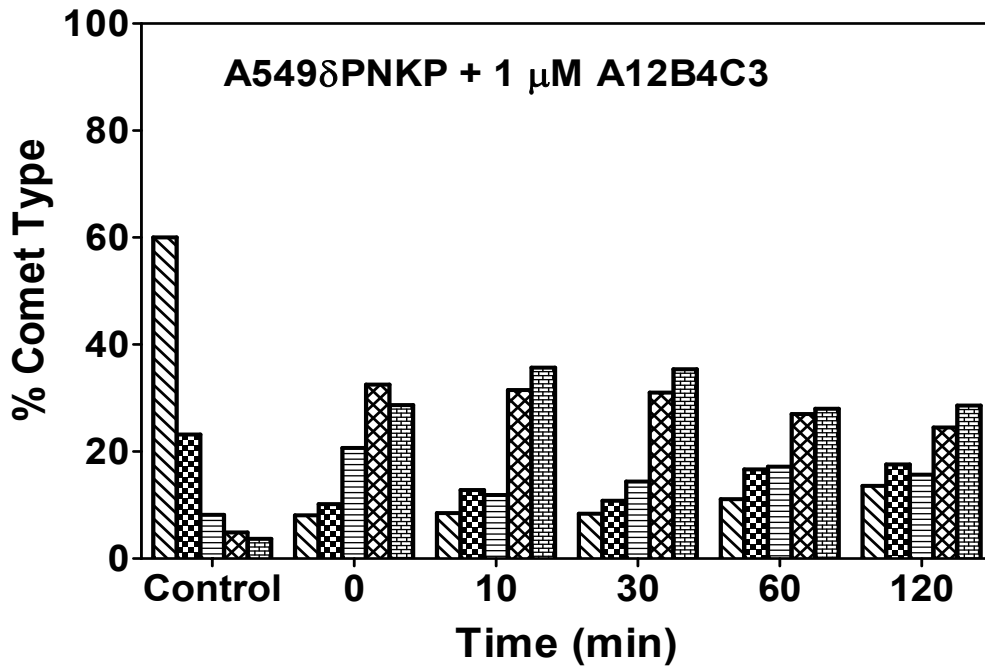
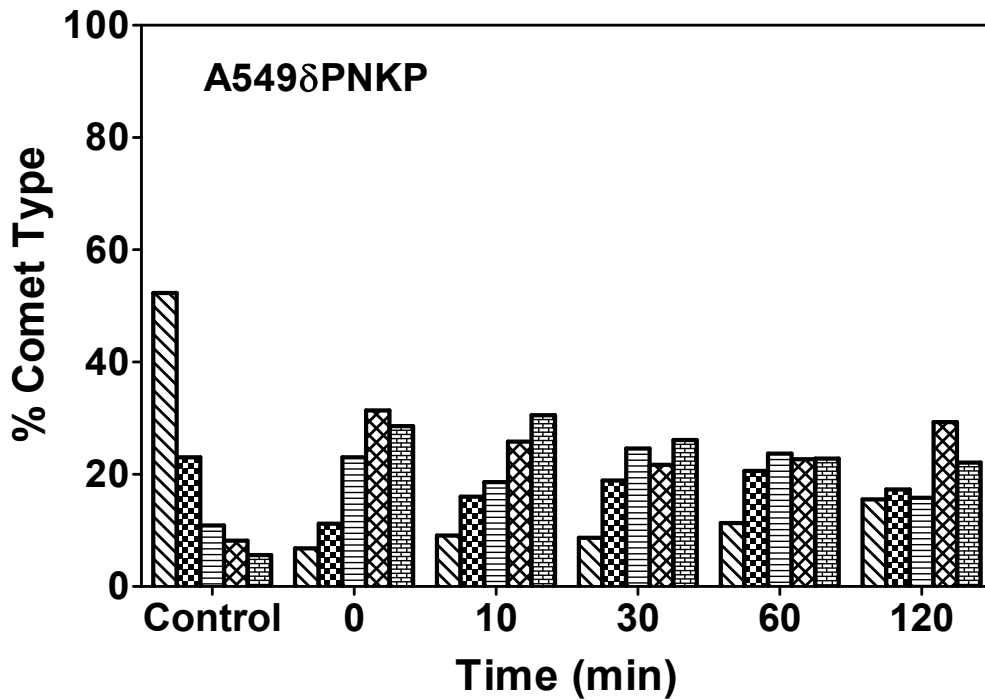
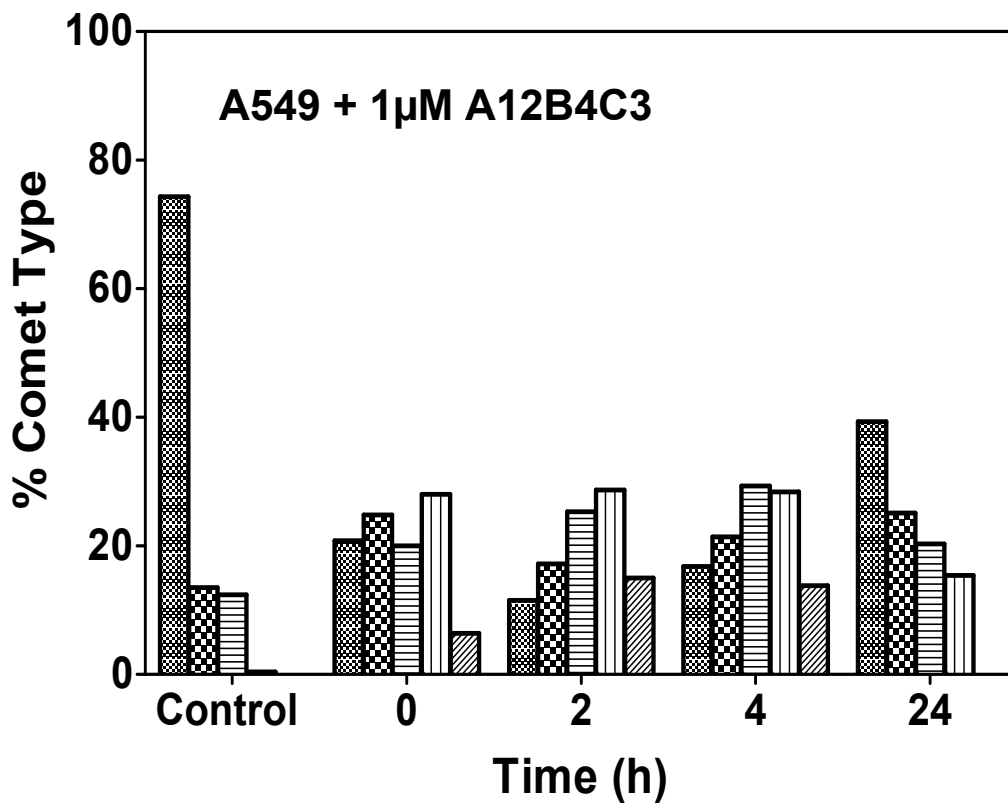
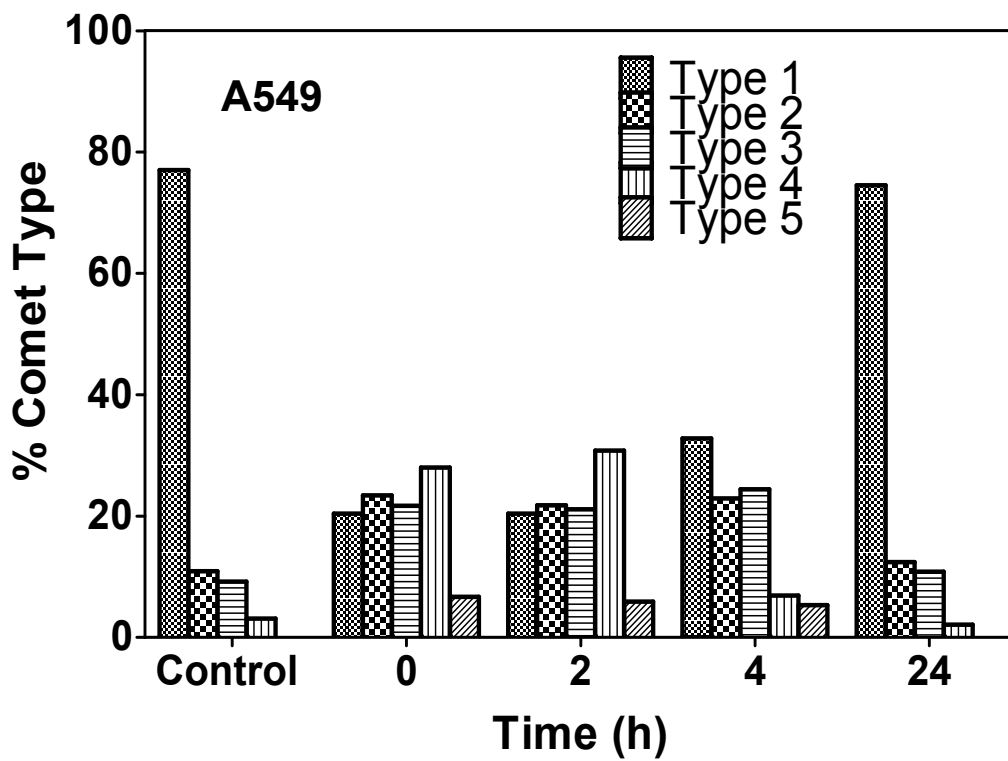


Figure 3.4. Single strand breaks plus alkali-labile sites before (Control) and at the indicated times after 5-Gy irradiation measured by single-cell gel electrophoresis (comet) assay under alkaline conditions. Comets were categorized according to the National Institutes of Health LISTERV (Comet Assay Internet Group web site), type 1 comets having the least damage and type 5 comets having most damage.

state by 2 h (Figure 3.4), i.e. the majority of cells were scored as type 3-5 comets immediately after irradiation, but type 1 and 2 comets after 2 h. In the presence of A12B4C3, however, we still observed a high frequency of type 3-5 comets after 2 h, implying only limited SSBR. The low level of repair was comparable to that seen in the A549 δ PNKP in the absence of A12B4C3. When the inhibitor was applied to the A549 δ PNKP cells, the degree of repair appeared to be even more attenuated. A very similar set of results were observed for DSBR over 24 h (Figure 3.5), with clear evidence for delayed repair in A12B4C3 exposed cells.

3.4.3 Influence of A12B4C3 on DNA polymerase β and DNA ligase III

To determine if A12B4C3 was reducing cellular SSBR by selectively inhibiting PNKP, we examined the ability of A12B4C3 to inhibit human DNA Pol β and DNA ligase III, which are two other enzymes involved with PNKP in the SSBR complex (12). Double-stranded substrates carrying either a 1-nucleotide gap or a nick were used to test for Pol β and DNA ligase III activity, respectively. Pol β activity was measured on the basis of addition of a nucleotide at the site of the gap, while DNA ligase III activity was measured on the basis of linking the two short oligonucleotides flanking the nick to create a 45mer. As shown in Figure 3.6, compared to the positive control in the absence of inhibitor, there was no significant inhibition of incorporation of the missing nucleotide by Pol β or joining of the two shorter oligonucleotides by DNA ligase III when acting on their respective substrates, even at the highest concentration of A12B4C3 tested (50 μ M). In contrast the human PNKP phosphatase activity is almost 100% inhibited by this concentration of A12B4C3 (101).



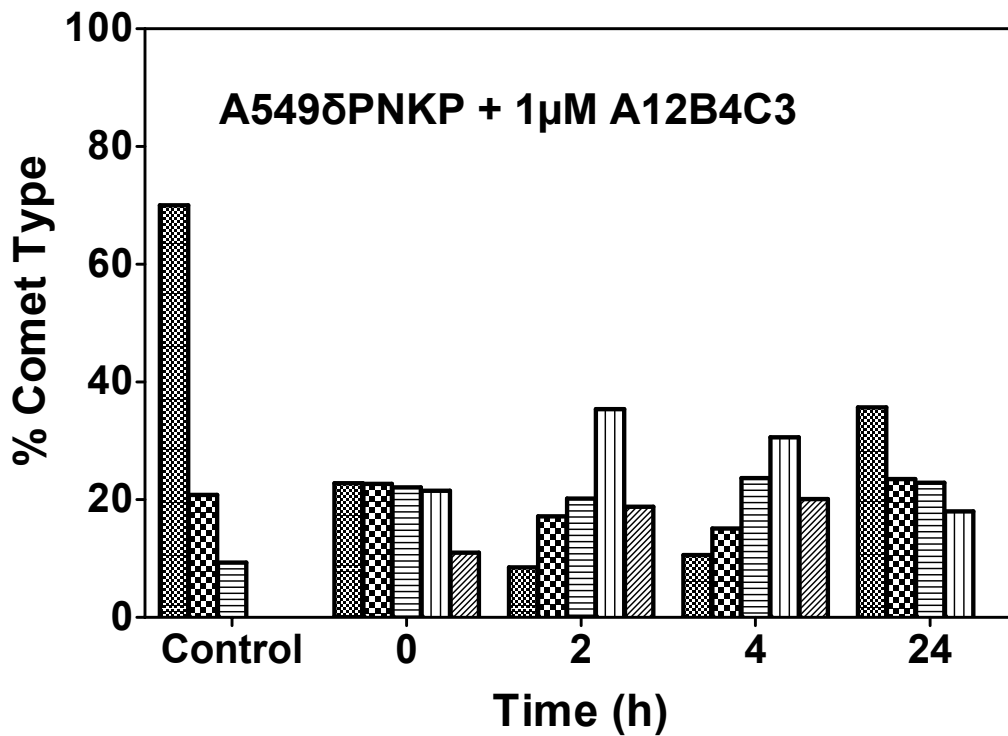
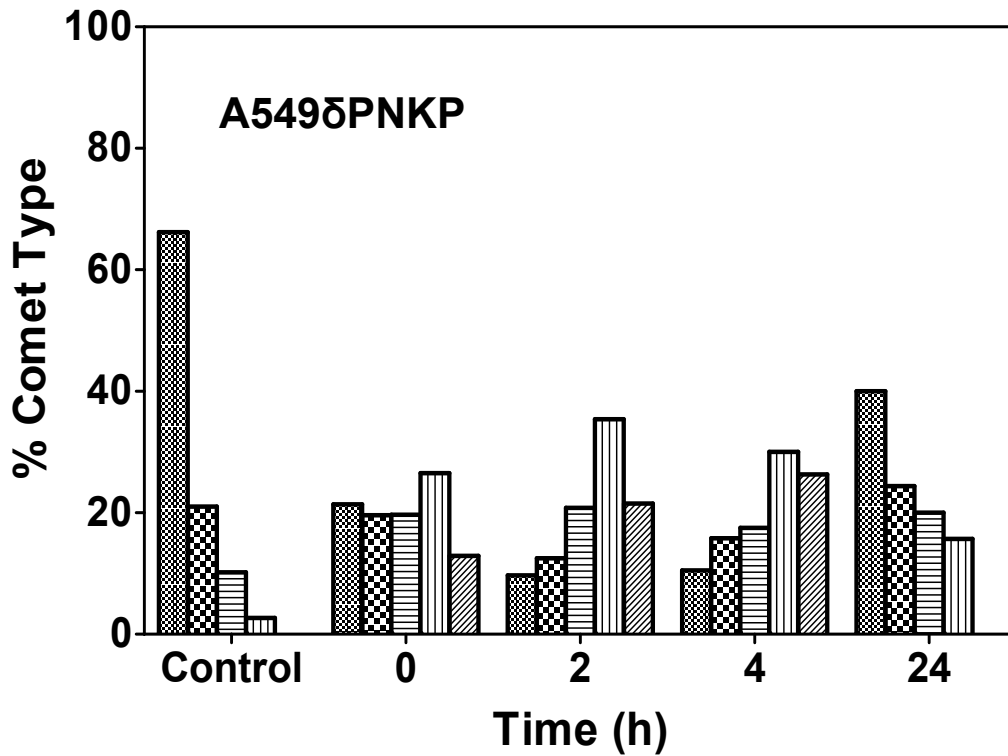


Figure 3.5. Double strand breaks before (control) and at the indicated times after 5-Gy irradiation measured by the comet assay under neutral conditions. Comets were categorized as described in the legend to Figure 3.4.

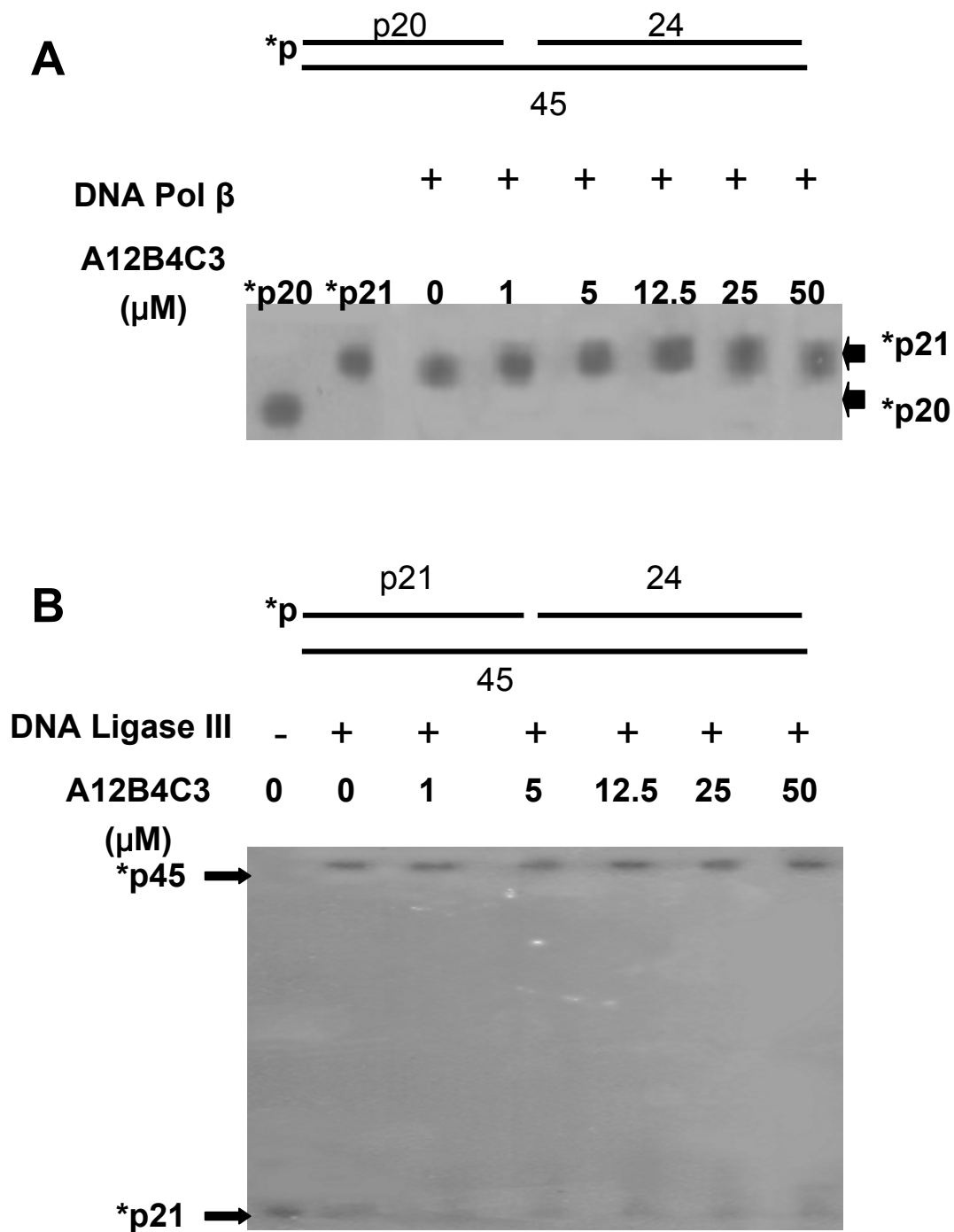


Figure 3.6. Influence of A12B4C3 on human SSBR proteins. (A) DNA polymerase β activity was assessed by measuring the single nucleotide extension of the 5'- ^{32}P -labeled 20mer component of a duplex substrate with a one-nucleotide gap. (B) DNA ligase III activity was measured on the basis of linkage of the 5'- ^{32}P -labeled 21mer component of a nicked substrate to the 24mer to produce a 45mer. In both cases the enzyme was pre-incubated with A12B4C3 and the compound was present throughout the reaction.

3.4.4 Mode of PNKP phosphatase inhibition by A12B4C3.

The mode of enzyme inhibition by A12B4C3 was determined by a Lineweaver-Burk analysis of the substrate concentration dependence on the reaction. Phosphatase activity was determined using a previously described colorimetric assay in which the substrate is a 20mer single-stranded oligonucleotide bearing a terminal 3'-phosphate group (101). To ascertain the mechanism of A12B4C3 inhibition, the assay was carried out using a fixed enzyme concentration while varying the concentration of inhibitor (5, 10 and 20 μM). A plot of $1/S$ vs $1/V$ is shown in Figure 3.7. The observed velocity V , which is a measure of the color development, decreased as the inhibitor concentration was increased, while the K_m value remained the same. This type of response is the hallmark of a non-competitive inhibitor.

Inhibitors that act non-competitively do not impede the binding of the enzyme to its substrate and thus have the potential to form a ternary complex with the enzyme and substrate. We examined this possibility employing fluorescence spectroscopy, which also provided a means of obtaining binding constants of PNKP to the inhibitor and to a 3'-phosphorylated DNA substrate. Since binding of the inhibitor or the substrate to PNKP partially quenches the protein Trp fluorescence at 332 nm following excitation at 295 nm, the binding affinity (K_d) can be determined by following fluorescence quenching as a function of ligand concentration (79). A representative plot of relative fluorescence intensity *versus*

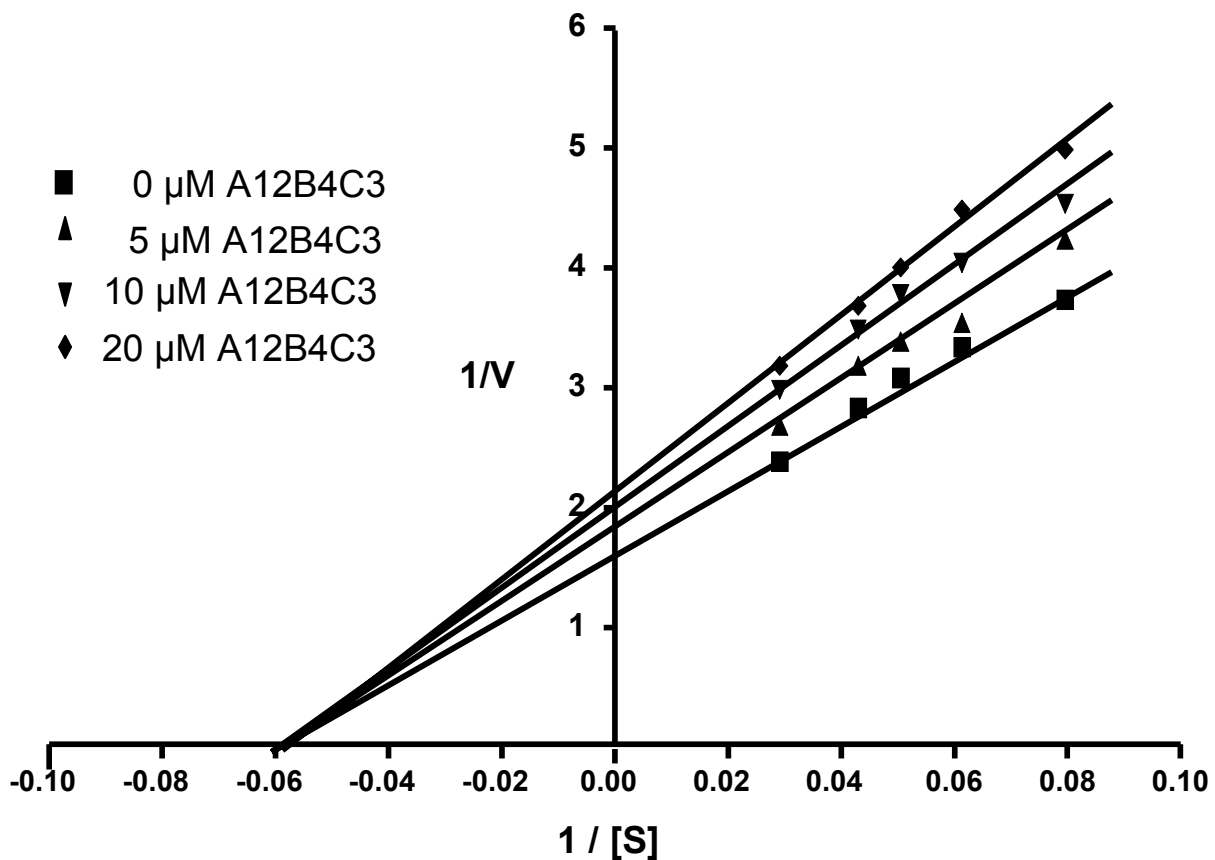


Figure 3.7. Lineweaver-Burk analysis of the inhibition of PNKP phosphatase activity using 0 μM (■), 5 μM (▲), 10 μM (▼), or 20 μM (◆) A12B4C3 and varying concentrations of 20mer 3'-P substrate. Data shown are the mean \pm S.E.M. of four independent experiments. Slopes were plotted against the concentration of A12B4C3. Intersection of the plot on the substrate concentration axis gave a K_m of 16 μM .

the concentration of A12B4C3 is shown in Figure 3.8A (inset). Nonlinear regression analysis of the binding data revealed unimodal binding with a K_d value of $0.37 \pm 0.03 \mu\text{M}$. We similarly measured the binding of PNKP to a single-stranded oligonucleotide bearing a phosphate at the 3'-terminus and biotin at the 5'-terminus. The latter group blocks the binding of PNKP to the 5'-terminus. We determined that PNKP bound this substrate with a K_d value of $0.6 \pm 0.05 \mu\text{M}$ (Figure 3.8B). Addition of the 3'-phosphorylated substrate to PNKP resulted in $20 \pm 2 \%$ quenching of Trp fluorescence. Addition of A12B4C3 to PNKP in the presence of the substrate induced a further quenching of $17 \pm 2 \%$ fluorescence, suggesting that the inhibitor was capable of binding to PNKP in the presence of its substrate. A similar result was obtained when the order of addition was changed. Thus, addition of A12B4C3 to PNKP resulted in $18 \pm 2\%$ quenching and the subsequent addition of the substrate yielded a further $20 \pm 2 \%$ quenching. These data clearly demonstrate that the substrate and inhibitor can form a ternary complex with PNKP and confirm that the A12B4C3 acts as a noncompetitive inhibitor.

3.4.5 A12B4C3 has no effect on ATP binding to PNKP

We have previously shown that A12B4C3 had a modest inhibitory effect on PNKP kinase activity. We therefore examined the influence of the inhibitor on the binding of ATP to PNKP by fluorescence titration (Figure 3.9). The K_d values for ATP binding in the absence and presence of A12B4C3 were 0.9 ± 0.1 and $1.0 \pm 0.1 \mu\text{M}$, respectively, indicating that the inhibitor exhibited no significant effect on ATP binding by the enzyme.

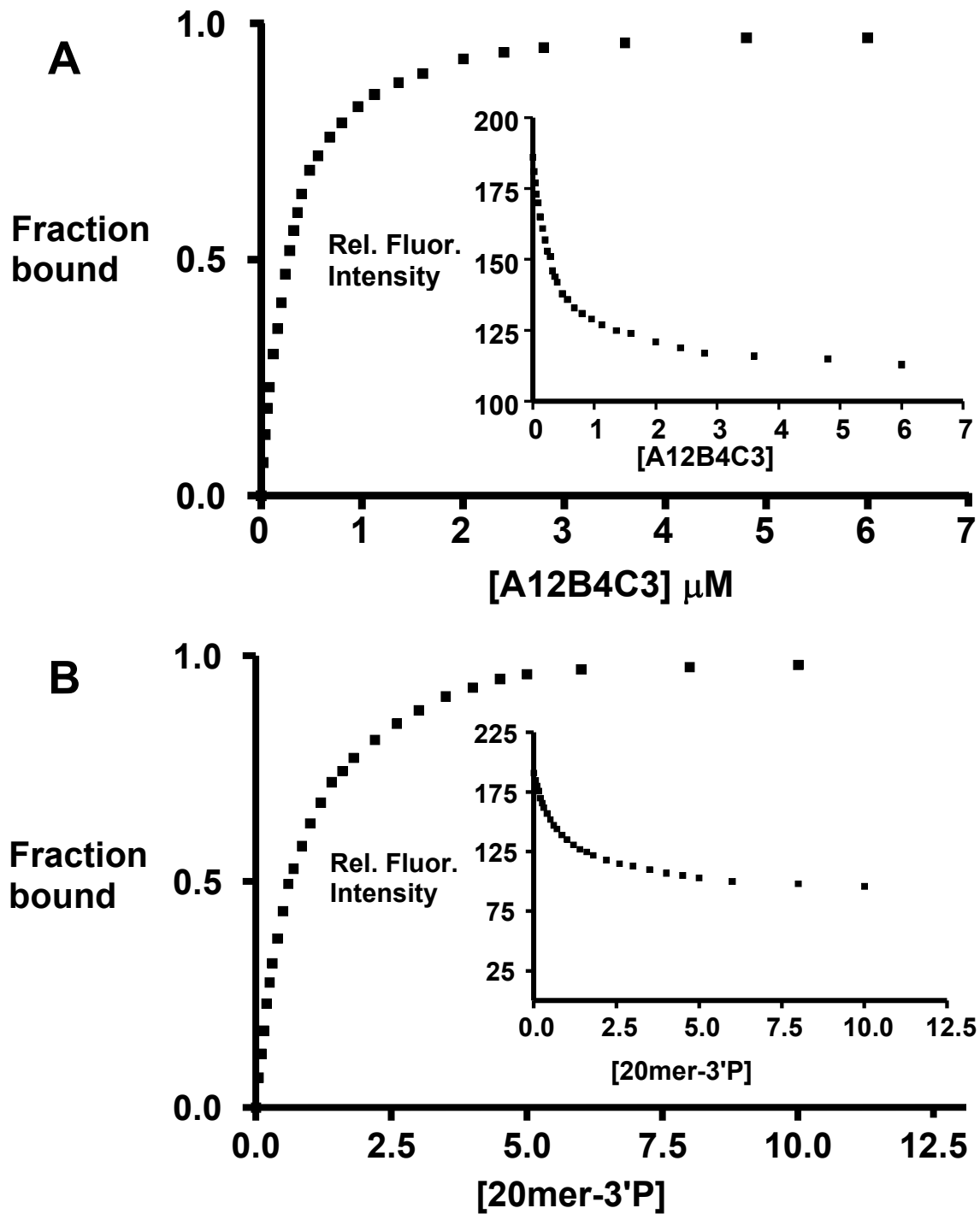


Figure 3.8. Fluorescence titration of PNKP with (A) A12B4C3 and (B) with 20mer-3'P oligonucleotide. PNKP (0.5 μM) in 50 mM Tris-HCl (pH 7.5), 100 mM NaCl, and 5 mM MgCl_2 was excited at 295 nm, and the fluorescence intensity was monitored at 332 nm (see inset). The fraction bound (i.e. relative fluorescence (Rel. Fluor.) intensity *versus* ligand concentration is plotted. (Produced by Dr. Rajam S. Mani)

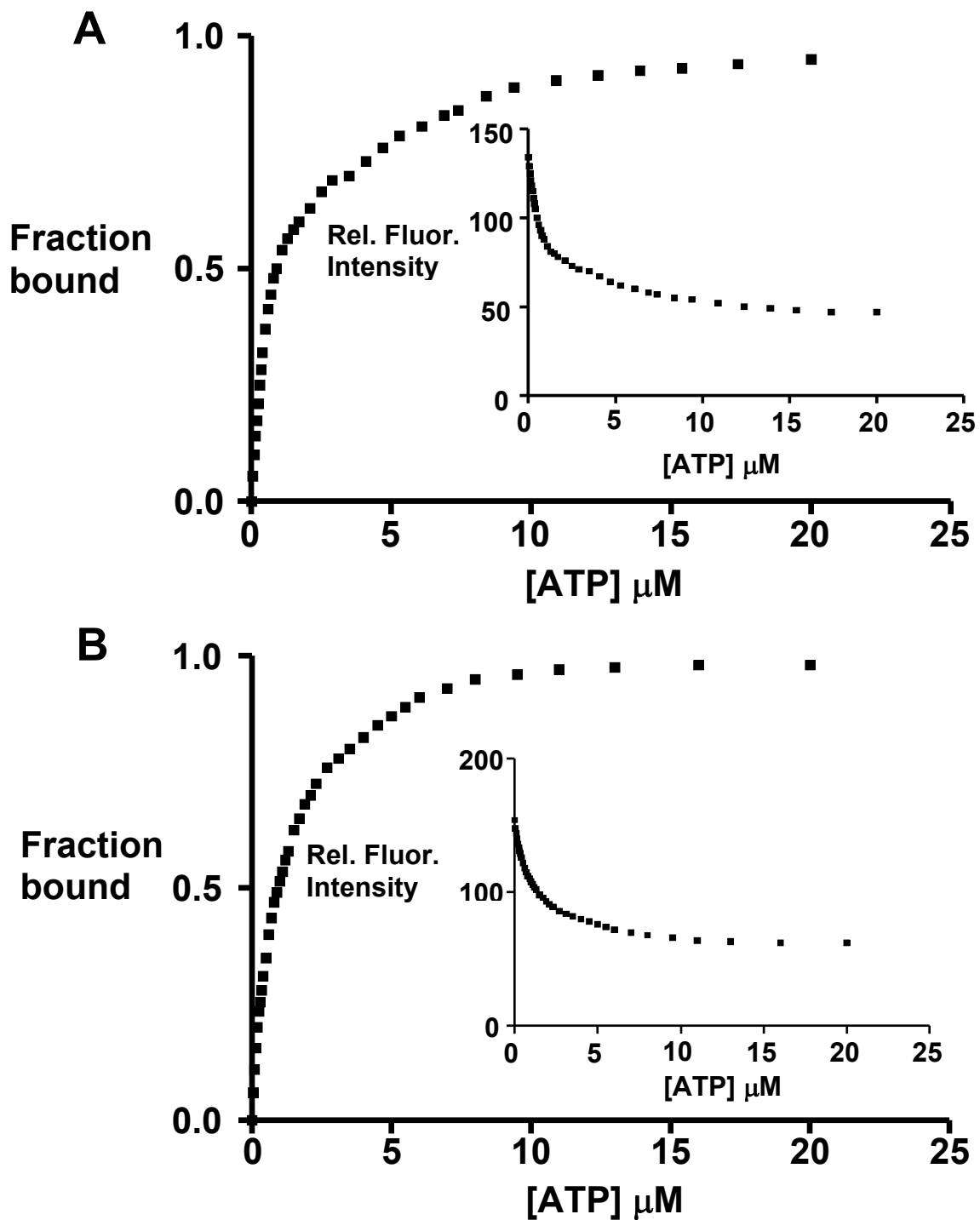


Figure 3.9. Fluorescence titration of PNKP vs ATP in the absence (A) and presence (B) of A12B4C3 (2 μM). PNKP (0.5 μM) in 50 mM Tris-HCl (pH 7.5), 100 mM NaCl, and 5 mM MgCl_2 was excited at 295 nm, and the fluorescence intensity was monitored at 332 nm (see inset). The fraction bound (i.e. relative fluorescence (Rel. Fluor.) intensity *versus* ligand concentration) is plotted. (Produced by Dr. Rajam S. Mani)

3.4.6 Effect of A12B4C3 binding on PNKP conformation

Circular dichroism, UV difference spectroscopy, steady-state fluorescence and fluorescence resonance energy transfer measurements were carried out to study the effect of A12B4C3 binding on the secondary and tertiary structure of PNKP.

3.4.6.1 Circular dichroism

Information concerning the secondary structure of PNKP was obtained from far-UV-CD data, and a typical far-UV-CD spectrum of PNKP is shown in Figure 3.10. PNKP exhibited two large, negative CD bands centered around 209 and 219 nm, indicating the presence of α -helical organization. The observed molar ellipticities, $[\theta]_M$, at these two wavelengths were -10080 ± 300 and -9200 ± 300 deg cm² dmol⁻¹, respectively. The CD spectra were analyzed according to the method of Chen et al. (98). The protein possessed ~28% α -helix and ~37% β -structure, and the remaining ~35% represented random structure. It is evident from Figure 3.10 that the addition of 2 μ M A12B4C3 induced a conformational change in PNKP; the molar ellipticity values $[\theta]_M$ at 209 and 219 nm were reduced to -8050 ± 300 and -7050 ± 300 deg cm² dmol⁻¹, respectively. Analysis of the CD data indicated a decrease in α -helical and β -structures accompanied by an increase in random structure. The calculated values were 22% α -helix and 30% β -structure while the random structure corresponded to 48%.

3.4.6.2 Ultraviolet difference spectroscopy

The local environments of aromatic residues in a protein can affect its UV absorption spectrum. If the solvent polarity around an aromatic ring decreases,

absorbance maxima will be shifted to longer wavelengths (red shift), and this will result in an increase in molar absorptivity (hyperchromic effect). On the other hand, if the solvent polarity around an aromatic ring increases, absorbance maxima will be shifted to shorter wavelengths (blue shift) and molar absorptivity will decrease (96,102,103). Figure 3.11 shows the difference spectrum of PNKP when A12B4C3 was added to the sample cell and the contents were mixed, thereby allowing the interaction to proceed, whereas in the reference cell the protein and the buffer containing A12B4C3 were not mixed. The concentration of protein and A12B4C3 was identical in both cells. The negative difference peak at 290 nm was characteristic of a blue shift of the tryptophan absorption band. The negative trough at 282 nm resulted from a blue shift of the tyrosine absorption band, and these blue shifts associated with tryptophan and tyrosine residues were interpreted as arising from an increased exposure of these aromatic groups to solvent (104).

3.4.6.3 Fluorescence resonance energy transfer

Acrylodan (AC), which reacts specifically with Cys groups in proteins, was used to label mutant PNKP WFX402 as described previously (79). PNKP WFX402-AC is a mutant in which every tryptophan except Trp402 has been replaced by phenylalanine was functionally active when tested for its phosphatase and kinase activities and retained ~85 % of its activities compared with unlabeled PNKP. The degree of labeling of PNKP WFX402 with AC was 1.4 ± 0.2 mol of AC/mol of PNKP WFX402. When the labeled protein was excited at 380 nm, the emission maximum occurred at 500 nm. The emission spectrum of PNKP, when

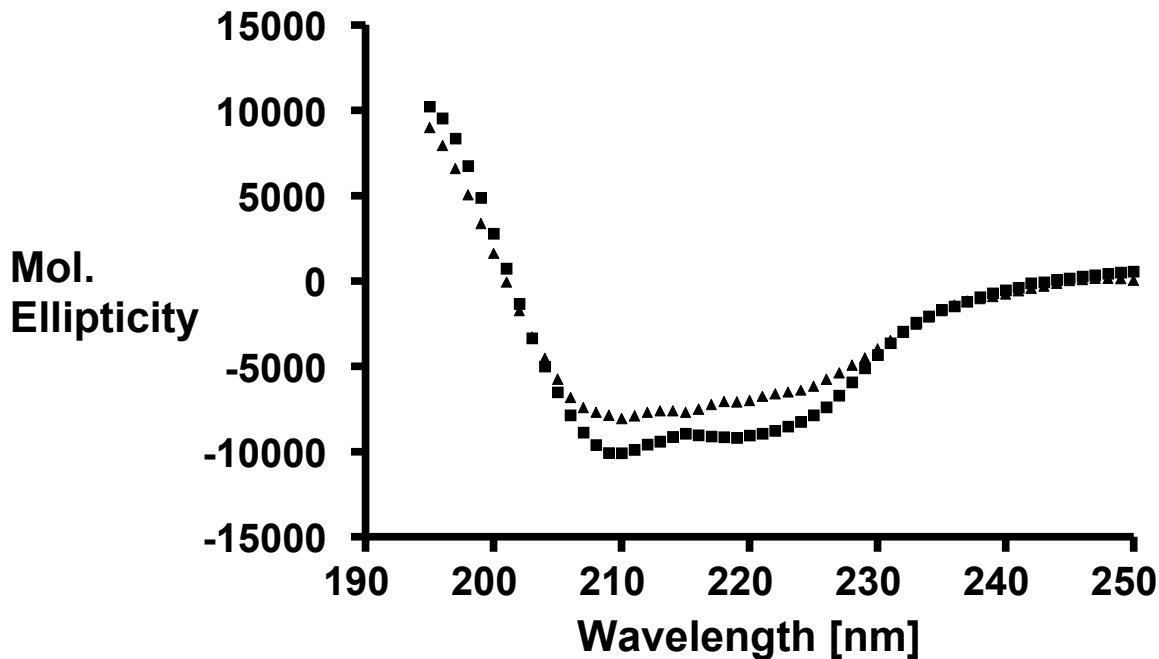


Figure 3.10. Influence of A12B4C3 binding on PNKP protein conformation. Far-UV CD spectrum of PNKP (0.5 mg/ml) in 50 mM Tris, pH 7.5, 100 mM NaCl, and 5 mM MgCl₂ (■) and PNKP (0.5 mg/ml) with 2 μM A12B4C3 inhibitor (▲). (Produced by Dr. Rajam S. Mani)

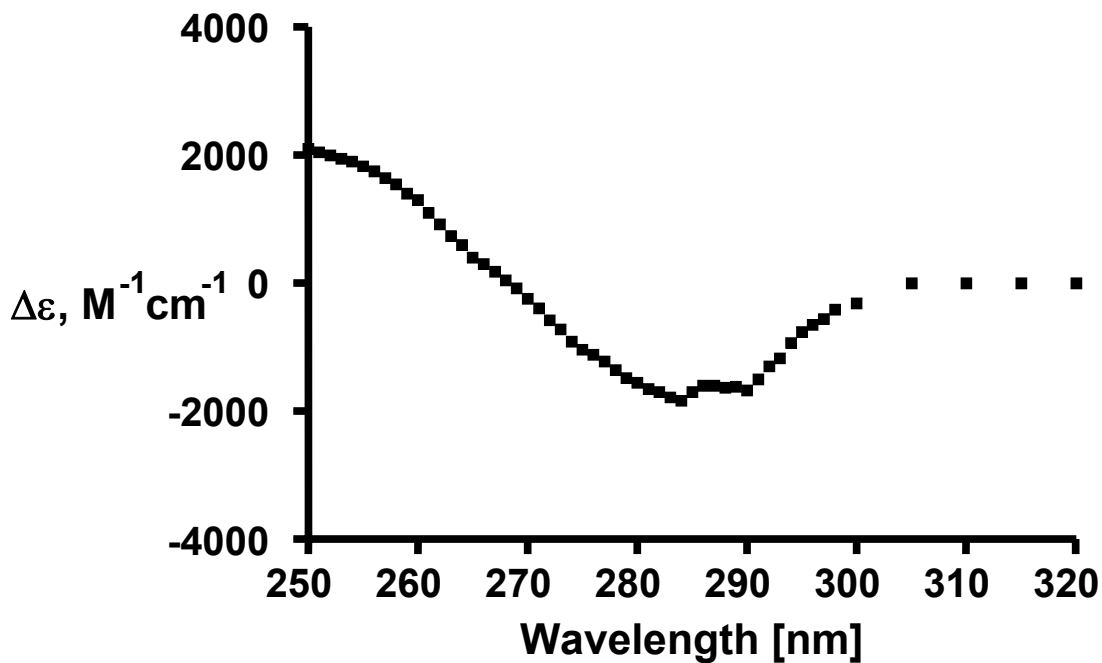


Figure 3.11. UV difference spectrum of PNKP produced by 2 μM A12B4C3 inhibitor. The concentration of PNKP used was 0.5 mg/ml in 50 mM Tris, pH 7.5, 100 mM NaCl, and 5 mM MgCl₂. The units are expressed as the difference in molar absorption, Δε. (Produced by Dr. Rajam S. Mani)

excited at 295 nm at which Tyr and Phe have no absorption and Trp is the only stimulated fluorophore, is shown in Figure 3.12A. The emission maximum was 332 nm. The presence of the AC label quenched Trp fluorescence at 332 nm, and this was accompanied by the appearance of a fluorescence peak around 500 nm. Since, free AC does not fluoresce under these conditions, the observed peak at 500 nm represented Trp-excited AC fluorescence and demonstrated energy transfer to AC. Figure 3.12B shows the emission spectrum of mutant PNKP WFX402 and the absorption spectrum of AC-labeled PNKP WFX402. There was substantial overlap of the absorbance and emission spectra. The overlap integral J , calculated according to eqn 3, was $2.81 \times 10^{-14} \text{ cm}^3 \text{ M}^{-1}$. Assuming $\kappa^2 = 2/3$, $n = 1.4$, and the quantum yield of the donor emission (PNKP) in the absence of the acceptor equals 0.10, the Förster critical distance R_0 was 27.45 Å for PNKP WFX402-AC. The transfer efficiency was 0.25. The determined values of E and R_0 were used to calculate R , the apparent average distance (32.90 Å) separating the Trp residue 402 from the AC-labeled Cys residues (Table 3.1). The emission spectrum of AC-labeled PNKP WFX402, excited at 295 nm, is shown in Figure 3.12C. The observed fluorescence at 332 nm was due to Trp residue 402 and the fluorescence peak at 500 nm corresponds to Trp-sensitized AC fluorescence. Addition of a 3'-phosphorylated/5'-biotinylated 20mer quenched the Trp fluorescence of PNKP WFX402-AC, suggesting an increase in transfer efficiency and providing evidence for a conformational change in PNKP WFX402-AC upon substrate binding. The effects on transfer efficiencies were measured by determining quantum yields of PNKP WFX402-AC in the absence and presence

of substrate, according to eqn 4. The transfer efficiencies were determined to be 0.25 for PNKP WFX402-AC and 0.31 for PNKP WFX402-AC in the presence of the 20mer. The average distances (R values) in angstroms between Trp402 and Cys residues were determined from the measured E values according to eqn 5. The average distance R for PNKP WFX402-AC was 32.90 Å, and this distance was reduced to 31.35 Å upon binding the 20mer (Table 3.1). The R value for the ternary complex involving PNKP WFX402-AC, 20mer, and A12B4C3 inhibitor was 31.92 Å, suggesting that a conformational change in the binary complex occurred

3.4.7 Localization of A12B4C3 interaction site with PNKP

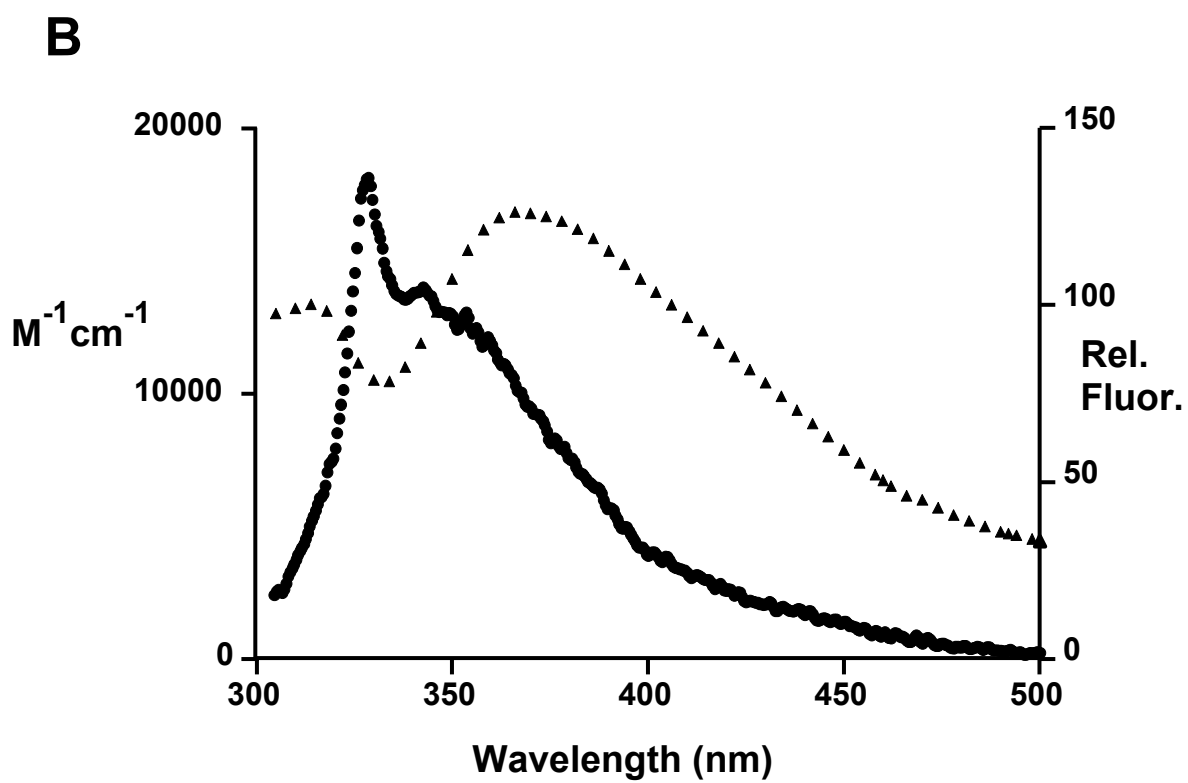
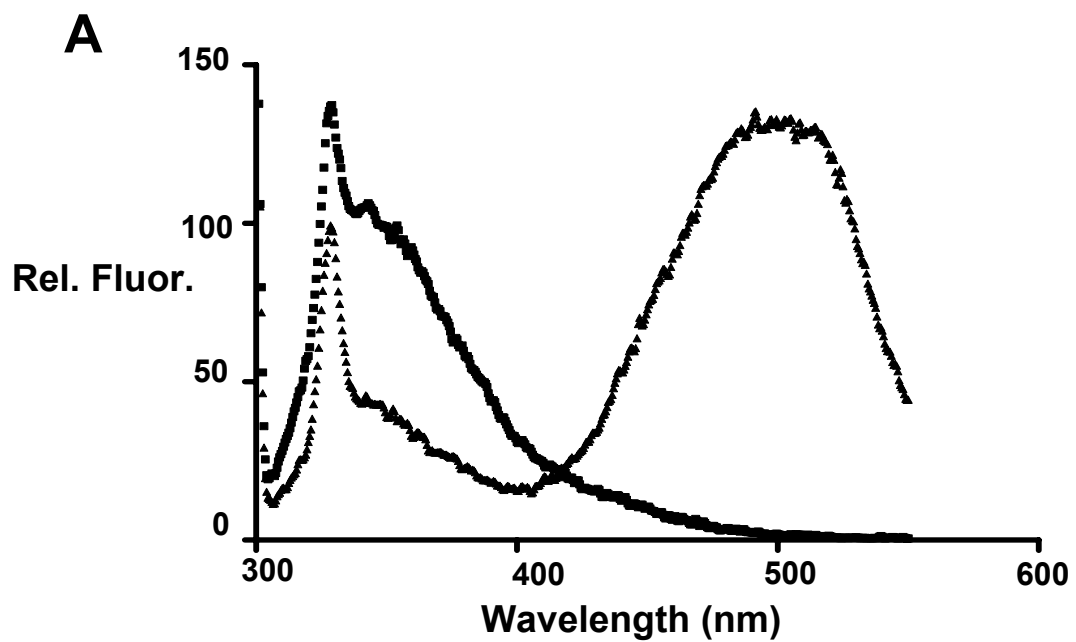
In an earlier study (79), we showed that the observed Trp fluorescence quenching caused by DNA binding results mainly from the perturbation of Trp402. For this reason, we made the following mutants, W402F and W331F in which Trp in position 402 or 331 were replaced by a Phe, in addition to WFX402. All three mutants retained good 3'-phosphatase activity. The observed inhibitory effects of A12B4C3 on these mutants are presented in Table 3.2. A12B4C3 was effective in inhibiting the phosphatase activity, as well as in quenching the Trp fluorescence, of W331F. However, when added to W402F, A12B4C3 had no effect on its phosphatase activity and there was also no quenching of its Trp fluorescence, clearly implying no interaction with this mutant PNKP. In contrast, when A12B4C3 was added to WFX 402, A12B4C3 inhibited its phosphatase activity and Trp fluorescence was also reduced. The observed effect on its

Table 3.1Fluorescence Energy Transfer Parameters of AC-Labeled PNKP-WFX402 mutant^a

	Overlap integral $J^b(\text{cm}^3 \text{M}^{-1})$	Critical distance $R_0(\text{Å})$	Efficiency of transfer $E^c(\%)$	Distance between Trp and Cys $R(\text{Å})$
WFX402	2.82×10^{-14}	27.50	25	32.95
WFX402 + DNA	2.79×10^{-14}	27.40	31	31.30
WFX402:DNA+A12B4C3	2.76×10^{-14}	27.38	28.5	31.95
WFX402+A12B4C3	2.74×10^{-14}	27.35	22	34.10
WFX402:A12B4C3+DNA	2.75×10^{-14}	27.37	30	31.40

^aAll measurements were carried out at 25 °C in 50 mM Tris (pH 7.5), 100 mM NaCl, and 5 mM MgCl₂.

^bDetermined as described in Materials and Methods. ^cEnergy transfer efficiency calculated from changes in fluorescence intensity. The relative errors in the R values are $\pm 0.1 \text{ Å}$. (Produced by Dr. Rajam S. Mani)



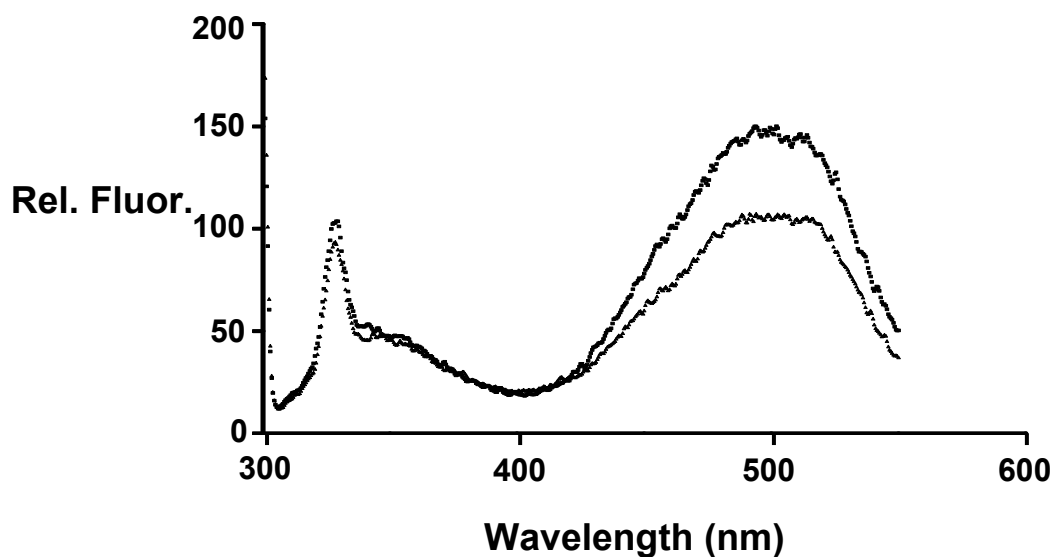
C

Figure 3.12. (A) Fluorescence emission spectra of PNKP (■) and PNKP-AC(▲). The concentration of hPNKP was 0.2 μ M in 50 mM Tris, pH 7.5, 100 mM NaCl, and 5 mM MgCl₂. The concentration of AC added was 0.16 μ M. The excitation wavelength was 295 nm. (B) Overlap of the Trp emission spectrum of mutant PNKP WFX402 (●) excited at 295 nm with the absorption spectrum of AC-labeled PNKP WFX402 (▲). The right ordinate gives fluorescence intensities measured in arbitrary units; the left ordinate is calibrated in terms of the molar absorbance of the PNKP WFX 402-AC complex. (C) Fluorescence emission spectra of PNKP WFX 402-AC (■) and with 1 μ M of 20mer-3'P oligonucleotide (▲). The excitation wavelength was 295 nm, and the concentration of the AC-labeled PNKP WFX 402 was 0.2 μ M. when A12B4C3 bound to PNKP WFX402-AC in the presence of the oligonucleotide. In a follow-up experiment, A12B4C3 was first added to PNKP WFX402-AC and subsequently the oligonucleotide was added to this binary complex. In this instance also, there was clear evidence for a ternary complex formation, implying that the binding of the DNA substrate and A12B4C3 is mutually exclusive, i.e. they bind at different sites on PNKP. (Produced by Dr. Rajam S. Mani)

and the observed quenching in Trp fluorescence arises from Trp402.

3.5 DISCUSSION

We previously identified A12B4C3 from a library of polysubstituted imido-piperidines based on its ability to inhibit the phosphatase activity of PNKP *in vitro* (101). The compound sensitized wild-type A549 cells to ionizing radiation, but not PNKP-knockdown (A549 δ PNKP) cells, suggesting that PNKP is its cellular target. However to confirm this, we further compared the properties of A12B4C3-treated cells to A549 δ PNKP cells, in particular their response to the topoisomerase I and II poisons, camptothecin and etoposide. The 3'-phosphate and 5'-hydroxyl strand-break termini generated in camptothecin-treated cells require the remedial action of PNKP, unlike the termini generated by etoposide. A549 cells treated with A12B4C3, like A549 δ PNKP cells, responded in accord with the expectation that the inhibitor would sensitize the cells to camptothecin but not etoposide (Figure 3.2). In addition, A12B4C3 did not sensitize the A549 δ PNKP cells to camptothecin (Figure 3.2), providing evidence to substantiate PNKP as the cellular target for the inhibitor.

Since PNKP depletion has been shown to slow the rates of SSBR and DSBR (15), we anticipated that the inhibitor would elicit the same response. Measurement of SSBR and DSBR by single-cell gel electrophoresis following exposure of cells to ionizing radiation indicated that A12B4C3 does indeed slow strand rejoining in cells (Figures 3.4 and 3.5), and the demonstration that

Table 3.2

Effect of A12B4C3 binding on wild type and mutant PNKP phosphatase activity and Trp fluorescence

PNKP	% Phosphatase Activity	% Inhibition	% Trp Quenching
Wild-type	100	100	18
W331F	90	95	17
W402F	85	~6	~3
WFX402	85	90	18

—

the inhibitor has no effect on two other key SSBR proteins, DNA Pol β and DNA ligase III, strongly implicates PNKP inhibition as the compound's mode of action.

Our biochemical and biophysical analyses clearly revealed that A12B4C3 acts as a non-competitive inhibitor that allosterically regulates the phosphatase activity of human PNKP. This provides an explanation for our previous observations regarding the specificity of the inhibitor. The phosphatase domain in human PNKP encompasses residues 146 to 336 and has a fold typical of the haloacid dehydrogenase (HAD) superfamily (16,22,24). DNA phosphatases from other species also belong to the HAD superfamily and have conserved residues that are involved in catalysis or in binding the Mg^{2+} and the phosphate moiety of the substrate and phosphoaspartate intermediate. The inhibitory effect of A12B4C3 when tested against a number of closely related phosphatases such as the PNKP enzymes isolated from bacteriophage T4, *Schizosaccharomyces pombe* and mouse, which belong to the HAD superfamily, exhibited strong specificity towards the mammalian PNKPs (101). It would seem less likely for a competitive inhibitor to show this degree of specificity. This is because competitive inhibitors interact with the catalytic site of the enzyme and this site shares a high degree of similarity with many other enzymes.

A12B4C3 also inhibits the kinase activity of PNKP, albeit to a lesser degree than the phosphatase activity (101). The kinase (Phe 341 - Glu 520) and the phosphatase domain (Gly 146 - Glu 337) together constitute the catalytic fragment, which carries out the enzymatic activities of PNKP (24). The kinase and the phosphatase domains in the catalytic fragment contact one another by two

short polypeptides: the intradomain linker (Leu 338 - Ala 340) and the C-terminal tail (Gln 517- Gly 521), which interacts with the phosphatase domain. The individual catalytic domains need to be within the catalytic fragment to retain their functional activities and proper folding. The catalytic domains could not be separated by proteolysis (24). This intimate association between the kinase and the phosphatase domains could explain why binding of A12B4C3 at or near Trp402 in the kinase domain is able to inhibit both activities of human PNKP by inducing a conformational change in the protein.

A12B4C3 exhibited strong affinity ($K_d = 0.37 \pm 0.03 \mu\text{M}$) for PNKP and the IC_{50} value obtained was $0.06 \mu\text{M}$ (101). In spite of being a non-competitive inhibitor, the IC_{50} value for A12B4C3 is comparable to the reported values for other inhibitors targeting DNA repair proteins. For example, SU11752, which selectively inhibits DNA-PK by competing with ATP, has an IC_{50} value of $0.13 \mu\text{M}$ (105), and recently developed pyrrolocarbazole lactam-based inhibitors of poly(ADP-ribose) polymerase, which compete against NAD^+ , were found to have IC_{50} values in the range of $0.02 - 0.1 \mu\text{M}$ (106).

In summary, we have further characterized the nature of the inhibition of PNKP by the imido-piperidine A12B4C3, showing it to be a tight-binding non-competitive inhibitor that interacts with Trp402. Since it sensitizes cells to camptothecin as well as ionizing radiation, A12B4C3, or derivatives of this compound, may have potential clinical benefit in countering the resistance of cancer cells to these agents. Data from this study will assist in the design of more

potent derivatives of A12B4C3 and help to define the protein binding pocket responsible for the interaction with PNKP.

3.6 Acknowledgements

Special acknowledgments must go out to Dr. Rajam Mani, who performed all the biophysical experiments and helped greatly in the writing of this paper. Recognition must also go out to Todd Mereniuk for his help in completing the comet assays and to Mesfin Fanta who helped purify the PNKP enzymes for use in all the experiments. In addition, I would like to thank Caesar Virgen for creating the PNKP mutants, which were essential for determining A12B4C3 mechanism of action. Special thanks go to Dr. Sam Wilson (Research Triangle Park, North Carolina) for providing DNA polymerase β , Dr Grigory Dianov (The Gray Institute for Radiation Oncology and Biology, University of Oxford) for providing DNA Ligase III and Dr. Dennis Hall (Department of Chemistry, University of Alberta) and his post-doctoral fellow Dr. Jean-Marie Grassot for providing the inhibitor A12B4C3. Lastly, I would like to acknowledge my supervisor Dr. Michael Weinfeld who was vital for the completion of this work.

Chapter IV

Discussion, Future Directions and Significance

4.1 DISCUSSION

The discovery that cancer cells depleted of hPNKP by targeted shRNA almost doubled the sensitivity to radiation and chemotherapy lead us to hypothesize that small molecule inhibitors to hPNKP may also be able to increase the sensitivity to radiation and chemotherapy. We initially began by consulting with a synthetic chemist Dr. Dennis Hall (Department of Chemistry, University of Alberta), who had created a small molecule library (85), which we were able to obtain and test. However, before we could test these compounds we needed to develop a high throughput-screening assay that could identify positive inhibitors to either the phosphatase or kinase activity of hPNKP.

This required a chemical based assay rather than an immunoassay and preferentially a fluorescence based approach since we initially intended to screen libraries containing approximately 10^4 compounds. We therefore decided to employ a modified version of the superquenching assay developed by QTL Biosystems (Santa Fe, NM) (90). This assay utilized the quenching of a terminal phosphate on a 20mer oligonucleotide to determine the extent of either phosphatase or kinase activity. After screening approximately 200 small molecules we identified five compounds A12B4C3, A1B4C3, A6B4C3, A26B11C2, and A39B1C2 that significantly inhibited hPNKP phosphatase activity (Figure 2.1C). To confirm that the QTL high throughput-screening assay was correctly identifying potential hPNKP phosphatase inhibitors we made use of a conventional radiogel assay. The radiogel assay measured the conversion of a radiolabeled oligo p*20p to p*20. All five inhibitors were confirmed on the

radiogel and the most potent was found to be A12B4C3 and further testing of its dose-response properties were undertaken. As shown in Figure 2.3, A12B4C3 had a substantial affect on hPNKP phosphatase activity up to 0.1 μM . To more closely analyze how potent A12B4C3 is as a hPNKP phosphatase inhibitor, we employed a colorimetric assay that measured the release of inorganic phosphate with the addition of malachite green. The inorganic phosphate binds to malachite green causing a chemical change in its structure, which resulted in a change in color from orange to green. Using the colorimetric assay we found that A12B4C3 had an IC_{50} of 0.06 μM , which was notably better than the second most potent inhibitor A6B4C3, which had an IC_{50} of 0.3 μM (Figure 2.4C).

A major drawback of many small molecule inhibitors is their lack of specificity to their intended target. The primary reason for this failure is due to the small molecules targeting the active site of the enzyme, which is conserved in many enzymes. Gefitinib is an example of a small molecule inhibitor that targets the ATP binding pocket (active site) of the epidermal growth factor receptor (EGFR) tyrosine kinase domain (107). For our analysis of A12B4C3 specificity we made use of three evolutionarily related PNKPs from T4 bacteriophage, *S. pombe*, and mouse and showed that A12B4C3 had minimal effect on inhibiting the phosphatase activity of all except mouse PNKP (Table 2.1). This is not surprising since mouse PNKP shares approximately 80% identity to hPNKP. In addition to examining phosphatases from the haloacid dehalogenase superfamily, we broadened our testing to two abundant protein phosphatase, PP-1 and calcineurin, that are part of the serine/threonine family, which are involved in a

wide-range of signal transduction pathways (92). We discovered A12B4C3 had absolutely no effect on inhibiting the phosphatase activity of either PP-1 or calcineurin (Figure 2.5A). Additionally, hPNKP kinase activity is slightly inhibited by A12B4C3 (Figure 2.5B) and this data suggests that the inhibitor acts in a noncompetitive manner disrupting the structure of the enzyme.

Cell-based assays examined the possibility that A12B4C3 could act as a radiosensitizer. Ionizing radiation damages DNA and creates breaks with incorrect 5'-hydroxyl and 3'-phosphate termini. hPNKP is responsible for repairing these damaged ends and in previous work, cancer cells depleted of hPNKP by targeted shRNA showed significant radiosensitivity. We utilized A549 lung and MDA-MB-231 breast carcinoma cells to test radiosensitization by A12B4C3 and discovered that it approximately doubled the radiation-induced cell killing (Figure 2.6B and 2.6C). Furthermore, in cells where hPNKP is depleted no statistical increase in killing was observed when the inhibitor was added. This indicated that the cellular target of A12B4C3 is primarily hPNKP.

Further analysis of A12B4C3's effects on cancer cells looked at the chemosensitizing properties of A12B4C3 and compared the results in both A549 treated and A549 δ PNKP treated cells. Chemotherapeutic agents such as topoisomerase I and II poisons, camptothecin and etoposide, respectively were utilized to ascertain A12B4C3 chemosensitizing properties. The 3'-phosphate and 5'-hydroxyl strand-break termini generated in camptothecin-treated cells require the remedial action of PNKP, unlike the termini generated by etoposide. A549 cells treated with A12B4C3, like A549 δ PNKP cells, responded in accord with the

expectation that the inhibitor would sensitize the cells to camptothecin but not etoposide (Figure 3.2). In addition, A12B4C3 did not sensitize the A549δPNKP cells to camptothecin (Figure 3.2), providing evidence to further substantiate PNKP as the cellular target for the inhibitor. Since PNKP depletion has been shown to slow the rates of SSBR and DSBR (15), we anticipated that the inhibitor would elicit the same response. Measurement of SSBR and DSBR by single-cell gel electrophoresis following exposure of cells to ionizing radiation indicated that A12B4C3 does indeed slow strand rejoining in cells (Figures 3.4 and 3.5), and the demonstration that the inhibitor has no effect on two other key SSBR proteins, DNA Pol β and DNA ligase III (figure 3.6A and 3.6B), strongly implicates PNKP inhibition as the compound's mode of action.

Our biochemical and biophysical analyses clearly revealed that A12B4C3 acts as a non-competitive inhibitor that allosterically alters the catalytic domain of human PNKP. This provides an explanation for our previous observation (section 2.4.4 chapter II) regarding the specificity of the inhibitor. The phosphatase domain in human PNKP encompasses residues 146 to 336 and has a fold typical of the haloacid dehydrogenase (HAD) superfamily (16,22,24). DNA phosphatases from other species also belong to the HAD superfamily and have conserved residues that are involved in catalysis or in binding the Mg²⁺ and the phosphate moiety of the substrate and phosphoaspartate intermediate. The inhibitory effect of A12B4C3 when tested against a number of closely related phosphatases such as the PNKP enzymes isolated from bacteriophage T4, *Schizosaccharomyces pombe* and mouse, which belong to the HAD superfamily, exhibited strong

specificity towards the mammalian PNKPs (101). It would seem less likely for a competitive inhibitor to show this degree of specificity. Competitive inhibitors do not show high specificity because they target the catalytic site of the enzyme, which is highly conserved in large numbers of proteins. This results in the competitive inhibitor being able to interact with a considerable number of enzymes. This is a major drawback because the drug must be administered in a higher concentration to see an effect, which could be toxic because of all the off-target interactions.

A12B4C3 also inhibits the kinase activity of PNKP, albeit to a lesser degree than the phosphatase activity (101). The kinase (Phe 341 - Glu 520) and the phosphatase subdomains (Gly 146 - Glu 337) together constitute the catalytic domain, which carries out the enzymatic activities of PNKP (24). The kinase and the phosphatase subdomains in the catalytic domain contact one another by two short polypeptides: the intradomain linker (Leu 338 - Ala 340) and the C-terminal tail (Gln 517- Gly 521), which interacts with the phosphatase domain. For reference the crystal structure of mammalian PNKP is shown in Figure 4.1. In addition, A12B4C3 is added to Figure 4.1 to indicate where we suggest A12B4C3 binds. The subdomains need to be within the catalytic domain to retain their functional activities and proper folding. The catalytic subdomains could not be separated by proteolysis (24). This intimate association between the kinase and the phosphatase domains could explain why binding of A12B4C3 at or near Trp402 (Figure 4.1 and Figure 4.2) in the kinase domain is able to inhibit both activities of human PNKP by inducing a conformational change in the protein.

With the help of Dr. Jack Tuszynski (Department of Oncology, University of Alberta) and his graduate student Khaled Barakat, we were able to model a potential interaction between A12B4C3 and Trp402 in the kinase domain of hPNKP (Figure 4.2). The computer model was created using a docking method where the binding energy of A12B4C3 to all sites on PNKP was measured. The binding energies were ranked and the lowest binding energies were predicted to be the potential binding site of A12B4C3 to PNKP.

In summary, we describe the initial identification and characterization of a potent hPNKP phosphatase inhibitor A12B4C3, which showed high specificity to hPNKP and had limited toxicity at high doses. The nature of the inhibition of hPNKP by the imido- piperidine A12B4C3, showed it to be a tight-binding non-competitive inhibitor that interacts with Trp402. Since it sensitizes cells to camptothecin as well as ionizing radiation, A12B4C3, or derivatives of this compound, may have potential clinical benefit in countering the resistance of cancer cells to radiation or chemotherapy. In addition, A12B4C3 may also enhance the efficacy of these cancer treatments which may enable more cancers to be cured. Structure-activity relationship testing has lead to the hypothesis that the nitro group on the aromatic ring of A12B4C3 is primarily responsible for inhibiting the phosphatase activity of hPNKP. Substitution of the nitro group with other similar chemical groups such as a methyl, ester, sulfone, or carboxylic acid have proven unsuccessful in reproducing the potent phosphatase inhibition of A12B4C3.

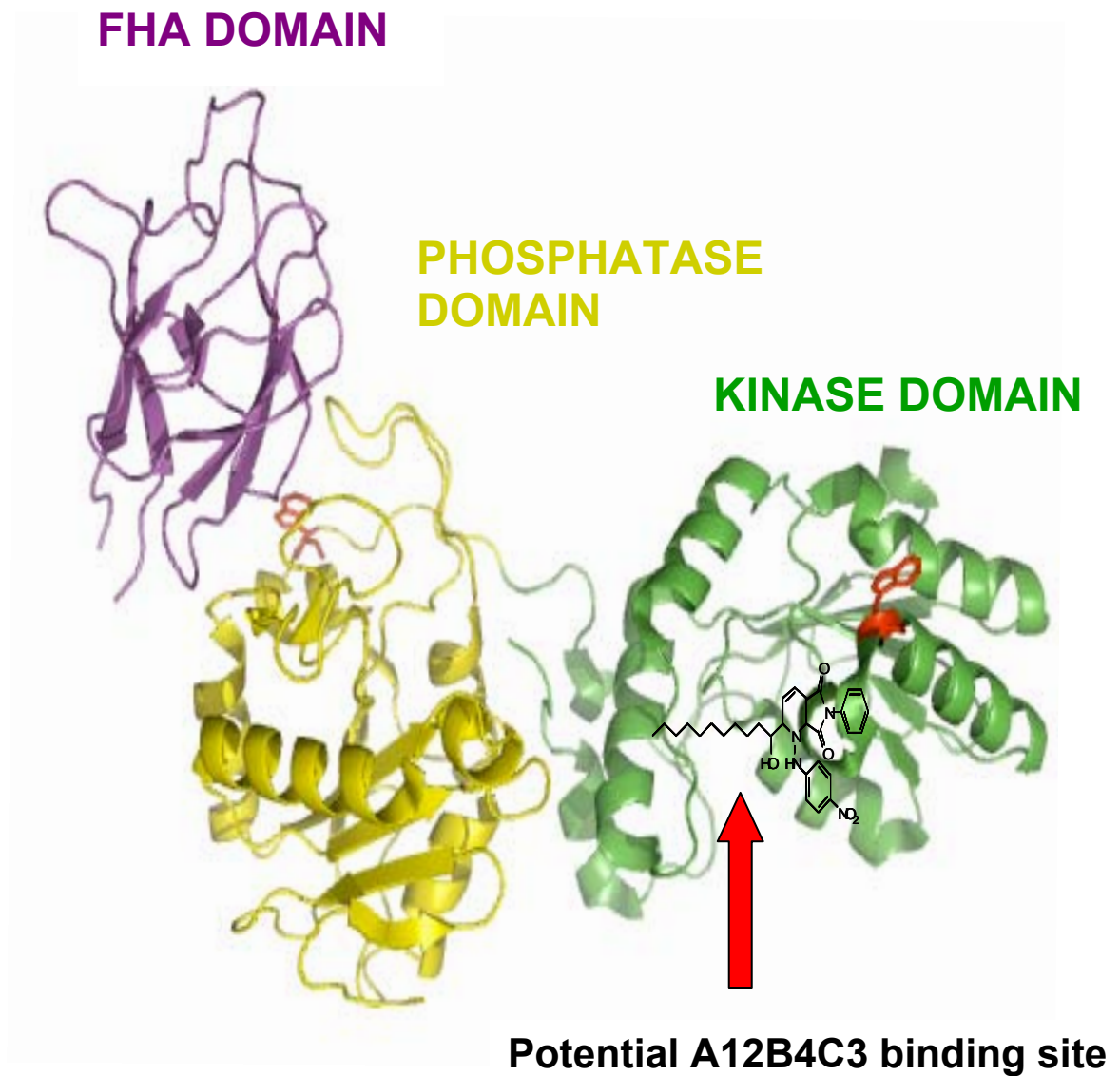
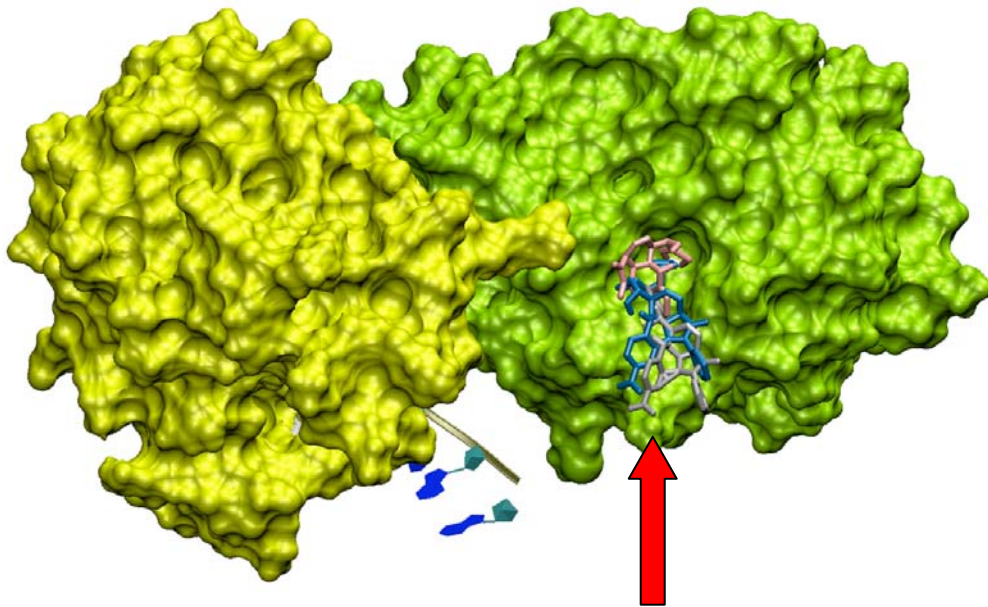


Figure 4.1. Crystal structure of murine PNKP, provided by Dr Mark Glover (Department of Biochemistry, University of Alberta). The FHA domain is indicated in purple, the phosphatase domain in yellow and the kinase domain in green. The red residues indicate tryptophans that were mutated to phenylalanines (W331F and W402F). W331F is located in the phosphatase domain, while W402 F is located in the kinase domain.

**PHOSPHATASE
DOMAIN**

KINASE DOMAIN



Potential A12B4C3 binding site

Figure 4.2. Computer modeling indicates that A12B4C3 binds strongly with residue Trp 402 of hPNKP. The phosphatase domain and kinase domain of hPNKP are indicated in yellow and green respectively. This image was provided by Khaled Barakat, PhD Candidate, University of Alberta and Dr. Jack Tuszynski (Department of Oncology, University of Alberta).

4.2 FUTURE DIRECTIONS

The discovery and initial characterization of A12B4C3 has led to the prospect of further examining A12B4C3 as a cancer drug to be used in combination with radio- and chemotherapy to enhance their efficacy or to be used alone as a single agent in a synthetically lethal approach. However, we hypothesize that A12B4C3 is unlikely to be a suitable drug for humans due to its chemical makeup, which is very reactive and not suitable for delivery to humans. Nonetheless, additional experiments must be performed in order to confirm or deny our hypothesis and to gauge A12B4C3 effectiveness as a possible future drug in the battle against cancer. These experiments fall under 4 main categories, 1) classification of how A12B4C3 inhibition affects SSBR and DSBR complexes *in vitro*; 2) pharmacological testing of A12B4C3 using both pharmacokinetic and pharmacodynamic approaches, along with animal studies; 3) construction of a drug delivery system for A12B4C3 and 4) testing a sub-library of A12B4C3 derivatives to find a more “druggable” compound.

4.2.1 Studying A12B4C3’s effect on SSBR and DSBR complexes

Having used radio-gel examination of A12B4C3 inhibition of SSBR enzymes DNA polymerase β and DNA ligase III, and observing that both polymerase and ligase activities are unchanged in the presence of the inhibitor, we will pursue A12B4C3 inhibitory effects of hPNKP when its part of either the SSBR or DSBR complex. As mentioned in section 1.2, PNKP forms a complex with Pol β , LIG3 and XRCC1 to repair SSBs, and with XRCC4 and DNA-PK to repair DSBs and these complexes may not be able to form when A12B4C3 is

present or may form inappropriately, which maybe an additional reason why A12B4C can radiosensitize lung and breast cancer cells. The data gathered here will allow us to grasp a more detailed outlook as to how A12B4C3 inhibition of hPNKP phosphatase activity has on formation of SSBR or DSBR complexes and to the extent this has on cell survival. And determination of A12B4C3 effects of hPNKP when its part of repair complexes leads to increased radio- and chemosensitivity *in vitro*. Radio-gel examination using double-stranded oligonucleotides with both SSBR and DSBR complexes will be utilized to see how effective A12B4C3 inhibits PNKP phosphatase activity when PNKP is part of a repair complex. In addition, discussions with Dr Jack Tuszynski (Dept of Oncology, University of Alberta) will help determine whether computer modeling can be applied to see how A12B4C3 effects PNKP inhibition when its part of SSBR or DSBR complexes.

4.2.2 Pharmacological and Animal Studies for A12B4C3

The use of A12B4C3 as a radio- and chemosensitizer in cancer cell lines has shown that it can be a potentially important drug in the treatment of cancer. However, in order to increase our understanding of the radio- and chemosensitization of A12B4C3 to cancer cells, we will observe its influence on irradiation and chemotherapy of tumour xenografts grown in mice. However, before tumour xenografts models can be undertaken the pharmacological characteristics of A12B4C3 must be examined.

Analyzing the pharmacological qualities of A12B4C3 will encompass testing pharmacokinetic and pharmacodynamic properties. The response to a drug

is delayed relative to the time of drug introduction. To determine the drug's effect, models must be utilized to predict the outcome. Recently, transit compartment models were shown to capture this time delay for chemotherapeutic drugs (108,109). It is important to determine how much of the drug is being absorbed in tissue, the rate of its distribution and finally its elimination from the body. The distribution of a drug is governed by many factors including blood flow to different organs, diffusion, protein and tissue binding, and high lipid solubility (109). Simeoni and colleagues have proposed a semi-mechanistic pharmacokinetic/pharmacodynamic (PK/PD) model to assess the antitumour effect in xenografts in mice (110-112). Following this model one can calculate the threshold concentration C_T derived from xenografts and can correlate this value with the active dose in humans. Furthermore, we plan to combine anticancer agents, (ionizing radiation or camptothecin derivatives and A12B4C3) to obtain a better response with reduced adverse effects. However, assessing the nature and intensity of combination drug therapy in vivo is challenging. In spite of this, using the PK/PD modeling approach, as described above, may allow better selection for the most advantageous combination therapies. In addition, Bigioni et al., 2008 used a combination index assay analyzed by the median effect plot (113) to ascertain the effects of drug combinations in terms of synergy, additivity or antagonism (113-115). Making use of both parameters from Simeoni et al., 2009 and Bigioni et al., 2008, we can improve the probability of determining the most effective dose of A12B4C3 to be used in mouse xenografts model systems.

We have observed that hPNKP inhibition results in significant radio- and chemosensitivity in cancer cell lines (95,116). To further investigate this effect tumour growth inhibition assays using SCID nude mice bearing palpable, subcutaneous human tumour cell xenografts will be used to help determine the effect that A12B4C3 has in decreasing tumour volume when combined with radio- or chemotherapy.

4.2.3 Development of a Drug Delivery System for A12B4C3

There are two main concepts in drug delivery systems, active targeting and passive targeting. Active targeting involves monoclonal antibodies or ligands that specifically bind to tumour cells. However, this application of active drug delivery is restricted to tumours that express high levels and/or unique targets on their cellular membranes. Conversely, passive targeting is achieved through the enhanced permeability and retention (EPR) effect (117). The EPR effect is based on a solid tumours inability to clear accumulated macromolecules due to a number of factors, including ineffective lymphatic drainage, poor vascular scaffolding, and increased vascularity (118). Importantly, polymeric micelles have shown to improve therapeutic performance and modify the toxicity profile of encapsulated drugs by changing their pharmacokinetic characteristics. And, recently their benefit in enhancing the absorption of incorporated drugs has been shown in a number of clinical trials e.g. NK-911 micelles with doxorubicin encapsulated (119). Working in collaboration with Dr. Afsaneh Lavasanifar (Faculty of Pharmacy and Pharmaceutical Sciences, University of Alberta) we plan to create two unique polymeric micelles that have A12B4C3 encapsulated.

One micelle will contain specific lipids on the outside to actively target the integrins overexpressed by tumour endothelial cells. It is well documented that certain integrins, especially $\alpha_5\beta_1$ and $\alpha_5\beta_6$, are overexpressed on tumour endothelial cells and metastatic cancer cells (120). Construction of block copolymer micelles with A12B4C3 encapsulated will be prepared and tested on tumours that overexpress $\alpha_5\beta_1$ and $\alpha_5\beta_6$ integrins. Cellular uptake and intracellular release of the compound will be measured by HPLC. The second micelle constructed will not contain these lipids and rely on the passive targeting EPR effect to target solid tumour tissues. The reasoning behind developing both active and passive micelles is because not all tumours will have integrins overexpressed on their cellular membrane and for these tumours use of the passive micelles may be a better alternative.

Another approach to deliver A12B4C3 to tumours is attaching it to albumin, which is an abundant protein normally seen in people to carry nutrients throughout the body. An example of this approach is seen with the anti-cancer agent Paclitaxel, which is commonly used to treat metastatic breast cancer (121). Paclitaxel has been coupled to albumin in a formulation called Abraxane. The advantage of binding drugs to albumin is that most drugs require solvents to dissolve the drug and these chemicals can be harmful to the patient. Drugs attached to albumin on the other hand do not require these chemicals and can reduce the risk of hypersensitivity-related side effects (121). The main rationale for using albumin to help deliver A12B4C3 to cancer cells is that A12B4C3 has been shown to bind strongly to albumin (Dr. Daniel Durocher personal

communication). Our goal is to have an Abraxane-like version for A12B4C3, which can be better utilized to treat cancer with reduced side effects.

4.2.4 Testing a sub-library of A12B4C3

In order to obtain a more potent derivative of A12B4C3, we plan to design and test a sub-library of compounds. These compounds will be designed and synthesized in collaboration with Dr. Dennis Hall (Department of Chemistry, University of Alberta) and Dr. Jack Tuszynski (Department of Biochemistry, University of Alberta) to assess which moieties of A12B4C3 would be best to modify to obtain an enhanced ability to inhibit hPNKP phosphatase activity and improve solubility. Testing of these compounds will be performed using a similar approach as described in chapter II (95).

4.3 SIGNIFICANCE

There is still considerable room for improvement to radio-and chemotherapy in the treatment of cancer. DNA repair inhibitors represent an excellent potential complement to both of these therapeutic modalities. In addition, one of our goals is to develop A12B4C3 into a single agent anti-cancer drug. This is possible due to the concept of synthetic lethality (described in section 1.5 chapter I), which takes advantage of mutations that arise in specific types of cancers. The discovery of synthetically lethal partnerships with hPNKP is currently being investigated in Dr. Michael Weinfeld's lab. Preliminary data suggest that hPNKP may be an important target in a wide-range of cancers. However, further examination is required to understand the realistic potential of this line of investigation.

Chapter V

References

1. Bradley, M.O. and Kohn, K.W. (1979) X-ray induced DNA double strand break production and repair in mammalian cells as measured by neutral filter elution. *Nucleic Acids Res*, **7**, 793-804.
2. Caldecott, K.W. (2008) Single-strand break repair and genetic disease. *Nat Rev Genet*, **9**, 619-631.
3. Fromme, J.C., Banerjee, A. and Verdine, G.L. (2004) DNA glycosylase recognition and catalysis. *Curr Opin Struct Biol*, **14**, 43-49.
4. Megnin-Chanet, F., Bollet, M.A. and Hall, J. (2010) Targeting poly(ADP-ribose) polymerase activity for cancer therapy. *Cell Mol Life Sci*, **67**, 3649-3662.
5. Lima, C.D., Wang, J.C. and Mondragon, A. (1994) Three-dimensional structure of the 67K N-terminal fragment of E. coli DNA topoisomerase I. *Nature*, **367**, 138-146.
6. Hartlerode, A.J. and Scully, R. (2009) Mechanisms of double-strand break repair in somatic mammalian cells. *Biochem J*, **423**, 157-168.
7. Lieber, M.R. (2010) The mechanism of double-strand DNA break repair by the nonhomologous DNA end-joining pathway. *Annu Rev Biochem*, **79**, 181-211.
8. Rothkamm, K., Kruger, I., Thompson, L.H. and Lobrich, M. (2003) Pathways of DNA double-strand break repair during the mammalian cell cycle. *Mol Cell Biol*, **23**, 5706-5715.
9. Hinz, J.M., Yamada, N.A., Salazar, E.P., Tebbs, R.S. and Thompson, L.H. (2005) Influence of double-strand-break repair pathways on radiosensitivity throughout the cell cycle in CHO cells. *DNA Repair (Amst)*, **4**, 782-792.
10. Meek, K., Dang, V. and Lees-Miller, S.P. (2008) DNA-PK: the means to justify the ends? *Adv Immunol*, **99**, 33-58.
11. Nick McElhinny, S.A. and Ramsden, D.A. (2004) Sibling rivalry: competition between Pol X family members in V(D)J recombination and general double strand break repair. *Immunol Rev*, **200**, 156-164.
12. Whitehouse, C.J., Taylor, R.M., Thistlethwaite, A., Zhang, H., Karimi-Busheri, F., Lasko, D.D., Weinfeld, M. and Caldecott, K.W. (2001) XRCC1 stimulates human polynucleotide kinase activity at damaged DNA termini and accelerates DNA single-strand break repair. *Cell*, **104**, 107-117.
13. Wiederhold, L., Leppard, J.B., Kedar, P., Karimi-Busheri, F., Rasouli-Nia, A., Weinfeld, M., Tomkinson, A.E., Izumi, T., Prasad, R., Wilson, S.H. *et al.* (2004) AP endonuclease-independent DNA base excision repair in human cells. *Mol Cell*, **15**, 209-220.
14. Chappell, C., Hanakahi, L.A., Karimi-Busheri, F., Weinfeld, M. and West, S.C. (2002) Involvement of human polynucleotide kinase in double-strand break repair by non-homologous end joining. *EMBO J*, **21**, 2827-2832.
15. Rasouli-Nia, A., Karimi-Busheri, F. and Weinfeld, M. (2004) Stable down-regulation of human polynucleotide kinase enhances spontaneous mutation frequency and sensitizes cells to genotoxic agents. *Proc Natl Acad Sci U S A*, **101**, 6905-6910.

16. Karimi-Busheri, F., Daly, G., Robins, P., Canas, B., Pappin, D.J., Sgouros, J., Miller, G.G., Fakhrai, H., Davis, E.M., Le Beau, M.M. *et al.* (1999) Molecular characterization of a human DNA kinase. *J Biol Chem*, **274**, 24187-24194.
17. Weinfeld, M., Mani, R.S., Abdou, I., Aceytuno, R.D. and Glover, J.N. Tidying up loose ends: the role of polynucleotide kinase/phosphatase in DNA strand break repair. *Trends Biochem Sci*, **36**, 262-271.
18. Koch, C.A., Agyei, R., Galicia, S., Metalnikov, P., O'Donnell, P., Starostine, A., Weinfeld, M. and Durocher, D. (2004) Xrcc4 physically links DNA end processing by polynucleotide kinase to DNA ligation by DNA ligase IV. *Embo J*, **23**, 3874-3885.
19. Lieber, M.R., Ma, Y., Pannicke, U. and Schwarz, K. (2003) Mechanism and regulation of human non-homologous DNA end-joining. *Nat Rev Mol Cell Biol*, **4**, 712-720.
20. Shen, J., Gilmore, E.C., Marshall, C.A., Haddadin, M., Reynolds, J.J., Eyaid, W., Bodell, A., Barry, B., Gleason, D., Allen, K. *et al.* (2010) Mutations in PNKP cause microcephaly, seizures and defects in DNA repair. *Nat Genet*, **42**, 245-249.
21. www.genecards.org (2011) polynucleotide kinase 3'-phosphatase.
22. Jilani, A., Ramotar, D., Slack, C., Ong, C., Yang, X.M., Scherer, S.W. and Lasko, D.D. (1999) Molecular cloning of the human gene, PNKP, encoding a polynucleotide kinase 3'-phosphatase and evidence for its role in repair of DNA strand breaks caused by oxidative damage. *J Biol Chem*, **274**, 24176-24186.
23. Karimi-Busheri, F., Lee, J., Tomkinson, A.E. and Weinfeld, M. (1998) Repair of DNA strand gaps and nicks containing 3'-phosphate and 5'-hydroxyl termini by purified mammalian enzymes. *Nucleic Acids Res*, **26**, 4395-4400.
24. Bernstein, N.K., Williams, R.S., Rakovszky, M.L., Cui, D., Green, R., Karimi-Busheri, F., Mani, R.S., Galicia, S., Koch, C.A., Cass, C.E. *et al.* (2005) The molecular architecture of the mammalian DNA repair enzyme, polynucleotide kinase. *Mol Cell*, **17**, 657-670.
25. Aravind, L. and Koonin, E.V. (1998) The HD domain defines a new superfamily of metal-dependent phosphohydrolases. *Trends Biochem Sci*, **23**, 469-472.
26. Wang, L.K., Lima, C.D. and Shuman, S. (2002) Structure and mechanism of T4 polynucleotide kinase: an RNA repair enzyme. *EMBO J*, **21**, 3873-3880.
27. Jemal, A., Siegel, R., Ward, E., Hao, Y., Xu, J., Murray, T. and Thun, M.J. (2008) Cancer statistics, 2008. *CA Cancer J Clin*, **58**, 71-96.
28. Anand, P., Kunnumakkara, A.B., Sundaram, C., Harikumar, K.B., Tharakan, S.T., Lai, O.S., Sung, B. and Aggarwal, B.B. (2008) Cancer is a preventable disease that requires major lifestyle changes. *Pharm Res*, **25**, 2097-2116.
29. Croce, C.M. (2008) Oncogenes and cancer. *N Engl J Med*, **358**, 502-511.

30. Knudson, A.G., Jr. (1971) Mutation and cancer: statistical study of retinoblastoma. *Proc Natl Acad Sci U S A*, **68**, 820-823.
31. Sherr, C.J. (2004) Principles of tumor suppression. *Cell*, **116**, 235-246.
32. Hanahan, D. and Weinberg, R.A. (2000) The hallmarks of cancer. *Cell*, **100**, 57-70.
33. Beasley, M., Driver, D. and Dobbs, H.J. (2005) Complications of radiotherapy: improving the therapeutic index. *Cancer Imaging*, **5**, 78-84.
34. Horiot, J.C., Le Fur, R., N'Guyen, T., Chenal, C., Schraub, S., Alfonsi, S., Gardani, G., Van Den Bogaert, W., Danczak, S., Bolla, M. *et al.* (1992) Hyperfractionation versus conventional fractionation in oropharyngeal carcinoma: final analysis of a randomized trial of the EORTC cooperative group of radiotherapy. *Radiother Oncol*, **25**, 231-241.
35. Stuschke, M. and Pottgen, C. (2010) Altered fractionation schemes in radiotherapy. *Front Radiat Ther Oncol*, **42**, 150-156.
36. Sutherland, B.M., Bennett, P.V., Sidorkina, O. and Laval, J. (2000) Clustered damages and total lesions induced in DNA by ionizing radiation: oxidized bases and strand breaks. *Biochemistry*, **39**, 8026-8031.
37. Ward, J.F. (1995) Radiation mutagenesis: the initial DNA lesions responsible. *Radiat Res*, **142**, 362-368.
38. Ward, J.F. (1994) The complexity of DNA damage: relevance to biological consequences. *Int J Radiat Biol*, **66**, 427-432.
39. Goodhead, D.T. (1994) Initial events in the cellular effects of ionizing radiations: clustered damage in DNA. *Int J Radiat Biol*, **65**, 7-17.
40. Kodym, R. and Horth, E. (1995) Determination of radiation-induced DNA strand breaks in individual cells by non-radioactive labelling of 3' OH ends. *Int J Radiat Biol*, **68**, 133-139.
41. Perry, M.C. (2008) *The chemotherapy source book*. 4th ed. Wolters Kluwer Health/Lippincott Williams & Wilkins, Philadelphia.
42. Ferguson, L.R. and Baguley, B.C. (1996) Mutagenicity of anticancer drugs that inhibit topoisomerase enzymes. *Mutat Res*, **355**, 91-101.
43. Holden, J.A. (2001) DNA topoisomerases as anticancer drug targets: from the laboratory to the clinic. *Curr Med Chem Anticancer Agents*, **1**, 1-25.
44. Capranico, G., Ferri, F., Fogli, M.V., Russo, A., Lotito, L. and Baranello, L. (2007) The effects of camptothecin on RNA polymerase II transcription: roles of DNA topoisomerase I. *Biochimie*, **89**, 482-489.
45. Creemers, G.J., Lund, B. and Verweij, J. (1994) Topoisomerase I inhibitors: topotecan and irinotecan. *Cancer Treat Rev*, **20**, 73-96.
46. Druker, B.J., Tamura, S., Buchdunger, E., Ohno, S., Segal, G.M., Fanning, S., Zimmermann, J. and Lydon, N.B. (1996) Effects of a selective inhibitor of the Abl tyrosine kinase on the growth of Bcr-Abl positive cells. *Nat Med*, **2**, 561-566.
47. Drew, Y. and Plummer, R. (2010) The emerging potential of poly(ADP-ribose) polymerase inhibitors in the treatment of breast cancer. *Curr Opin Obstet Gynecol*, **22**, 67-71.
48. Telli, M.L. and Ford, J.M. (2010) PARP Inhibitors in Breast Cancer. *Clin Adv Hematol Oncol*, **8**, 629-635.

49. Campbell, L., Blackhall, F. and Thatcher, N. (2010) Gefitinib for the treatment of non-small-cell lung cancer. *Expert Opin Pharmacother*, **11**, 1343-1357.
50. Bustinza-Linares, E., Kurzrock, R. and Tsimberidou, A.M. (2010) Salirasib in the treatment of pancreatic cancer. *Future Oncol*, **6**, 885-891.
51. Drew, Y. and Plummer, R. The emerging potential of poly(ADP-ribose) polymerase inhibitors in the treatment of breast cancer. *Curr Opin Obstet Gynecol*, **22**, 67-71.
52. Mendes-Pereira, A.M., Martin, S.A., Brough, R., McCarthy, A., Taylor, J.R., Kim, J.S., Waldman, T., Lord, C.J. and Ashworth, A. (2009) Synthetic lethal targeting of PTEN mutant cells with PARP inhibitors. *EMBO Mol Med*, **1**, 315-322.
53. Salmena, L., Carracedo, A. and Pandolfi, P.P. (2008) Tenets of PTEN tumor suppression. *Cell*, **133**, 403-414.
54. Abbotts, R. and Madhusudan, S. Human AP endonuclease 1 (APE1): from mechanistic insights to druggable target in cancer. *Cancer Treat Rev*, **36**, 425-435.
55. Wilson, D.M., 3rd and Simeonov, A. (2010) Small molecule inhibitors of DNA repair nuclease activities of APE1. *Cell Mol Life Sci*, **67**, 3621-3631.
56. Yoo, D.G., Song, Y.J., Cho, E.J., Lee, S.K., Park, J.B., Yu, J.H., Lim, S.P., Kim, J.M. and Jeon, B.H. (2008) Alteration of APE1/ref-1 expression in non-small cell lung cancer: the implications of impaired extracellular superoxide dismutase and catalase antioxidant systems. *Lung Cancer*, **60**, 277-284.
57. Agrawal, M., Garg, R.J., Kantarjian, H. and Cortes, J. Chronic myeloid leukemia in the tyrosine kinase inhibitor era: what is the "best" therapy? *Curr Oncol Rep*, **12**, 302-313.
58. Johnson, N. and Shapiro, G.I. Cyclin-dependent kinases (cdks) and the DNA damage response: rationale for cdk inhibitor-chemotherapy combinations as an anticancer strategy for solid tumors. *Expert Opin Ther Targets*, **14**, 1199-1212.
59. Cheung, C.H., Coumar, M.S., Hsieh, H.P. and Chang, J.Y. (2009) Aurora kinase inhibitors in preclinical and clinical testing. *Expert Opin Investig Drugs*, **18**, 379-398.
60. Yap, T.A., Sandhu, S.K., Carden, C.P. and de Bono, J.S. (2011) Poly(ADP-ribose) polymerase (PARP) inhibitors: Exploiting a synthetic lethal strategy in the clinic. *CA Cancer J Clin*, **61**, 31-49.
61. Dobzhansky, T. (1946) Genetics of Natural Populations. Xiii. Recombination and Variability in Populations of *Drosophila Pseudoobscura*. *Genetics*, **31**, 269-290.
62. Farmer, H., McCabe, N., Lord, C.J., Tutt, A.N., Johnson, D.A., Richardson, T.B., Santarosa, M., Dillon, K.J., Hickson, I., Knights, C. *et al.* (2005) Targeting the DNA repair defect in BRCA mutant cells as a therapeutic strategy. *Nature*, **434**, 917-921.
63. Bryant, H.E., Schultz, N., Thomas, H.D., Parker, K.M., Flower, D., Lopez, E., Kyle, S., Meuth, M., Curtin, N.J. and Helleday, T. (2005) Specific

- killing of BRCA2-deficient tumours with inhibitors of poly(ADP-ribose) polymerase. *Nature*, **434**, 913-917.
64. Turner, N.C., Lord, C.J., Iorns, E., Brough, R., Swift, S., Elliott, R., Rayter, S., Tutt, A.N. and Ashworth, A. (2008) A synthetic lethal siRNA screen identifying genes mediating sensitivity to a PARP inhibitor. *EMBO J*, **27**, 1368-1377.
 65. Madhusudan, S. and Middleton, M.R. (2005) The emerging role of DNA repair proteins as predictive, prognostic and therapeutic targets in cancer. *Cancer Treat Rev*, **31**, 603-617.
 66. O'Connor, M.J., Martin, N.M. and Smith, G.C. (2007) Targeted cancer therapies based on the inhibition of DNA strand break repair. *Oncogene*, **26**, 7816-7824.
 67. Drew, Y. and Calvert, H. (2008) The potential of PARP inhibitors in genetic breast and ovarian cancers. *Ann N Y Acad Sci*, **1138**, 136-145.
 68. Madhusudan, S., Smart, F., Shrimpton, P., Parsons, J.L., Gardiner, L., Houlbrook, S., Talbot, D.C., Hammonds, T., Freemont, P.A., Sternberg, M.J. *et al.* (2005) Isolation of a small molecule inhibitor of DNA base excision repair. *Nucleic Acids Res*, **33**, 4711-4724.
 69. Marchand, C., Lea, W.A., Jadhav, A., Dexheimer, T.S., Austin, C.P., Inglese, J., Pommier, Y. and Simeonov, A. (2009) Identification of phosphotyrosine mimetic inhibitors of human tyrosyl-DNA phosphodiesterase I by a novel AlphaScreen high-throughput assay. *Mol Cancer Ther*, **8**, 240-248.
 70. Hickson, I., Zhao, Y., Richardson, C.J., Green, S.J., Martin, N.M., Orr, A.I., Reaper, P.M., Jackson, S.P., Curtin, N.J. and Smith, G.C. (2004) Identification and characterization of a novel and specific inhibitor of the ataxia-telangiectasia mutated kinase ATM. *Cancer Res*, **64**, 9152-9159.
 71. Zhao, Y., Thomas, H.D., Batey, M.A., Cowell, I.G., Richardson, C.J., Griffin, R.J., Calvert, A.H., Newell, D.R., Smith, G.C. and Curtin, N.J. (2006) Preclinical evaluation of a potent novel DNA-dependent protein kinase inhibitor NU7441. *Cancer Res*, **66**, 5354-5362.
 72. Plummer, R., Jones, C., Middleton, M., Wilson, R., Evans, J., Olsen, A., Curtin, N., Boddy, A., McHugh, P., Newell, D. *et al.* (2008) Phase I study of the poly(ADP-ribose) polymerase inhibitor, AG014699, in combination with temozolomide in patients with advanced solid tumors. *Clin Cancer Res*, **14**, 7917-7923.
 73. Henner, W.D., Rodriguez, L.O., Hecht, S.M. and Haseltine, W.A. (1983) gamma Ray induced deoxyribonucleic acid strand breaks. 3' Glycolate termini. *J Biol Chem*, **258**, 711-713.
 74. Lennartz, M., Coquerelle, T., Bopp, A. and Hagen, U. (1975) Oxygen--effect on strand breaks and specific end-groups in DNA of irradiated thymocytes. *Int J Radiat Biol Relat Stud Phys Chem Med*, **27**, 577-587.
 75. Buchko, G.W. and Weinfeld, M. (1993) Influence of nitrogen, oxygen, and nitroimidazole radiosensitizers on DNA damage induced by ionizing radiation. *Biochemistry*, **32**, 2186-2193.

76. Friedberg, E.C., Aguilera, A., Gellert, M., Hanawalt, P.C., Hays, J.B., Lehmann, A.R., Lindahl, T., Lowndes, N., Sarasin, A. and Wood, R.D. (2006) DNA repair: from molecular mechanism to human disease. *DNA Repair (Amst)*, **5**, 986-996.
77. Krokan, H.E., Nilsen, H., Skorpen, F., Otterlei, M. and Slupphaug, G. (2000) Base excision repair of DNA in mammalian cells. *FEBS Lett*, **476**, 73-77.
78. Loizou, J.I., El-Khamisy, S.F., Zlatanou, A., Moore, D.J., Chan, D.W., Qin, J., Sarno, S., Meggio, F., Pinna, L.A. and Caldecott, K.W. (2004) The protein kinase CK2 facilitates repair of chromosomal DNA single-strand breaks. *Cell*, **117**, 17-28.
79. Mani, R.S., Fanta, M., Karimi-Busheri, F., Silver, E., Virgen, C.A., Caldecott, K.W., Cass, C.E. and Weinfeld, M. (2007) XRCC1 stimulates polynucleotide kinase by enhancing its damage discrimination and displacement from DNA repair intermediates. *J Biol Chem*, **282**, 28004-28013.
80. Karimi-Busheri, F., Rasouli-Nia, A., Allalunis-Turner, J. and Weinfeld, M. (2007) Human polynucleotide kinase participates in repair of DNA double-strand breaks by nonhomologous end joining but not homologous recombination. *Cancer Res*, **67**, 6619-6625.
81. Das, A., Wiederhold, L., Leppard, J.B., Kedar, P., Prasad, R., Wang, H., Boldogh, I., Karimi-Busheri, F., Weinfeld, M., Tomkinson, A.E. *et al.* (2006) NEIL2-initiated, APE-independent repair of oxidized bases in DNA: Evidence for a repair complex in human cells. *DNA Repair (Amst)*, **5**, 1439-1448.
82. Plo, I., Liao, Z.Y., Barcelo, J.M., Kohlhagen, G., Caldecott, K.W., Weinfeld, M. and Pommier, Y. (2003) Association of XRCC1 and tyrosyl DNA phosphodiesterase (Tdp1) for the repair of topoisomerase I-mediated DNA lesions. *DNA Repair (Amst)*, **2**, 1087-1100.
83. Dobson, C.J. and Allinson, S.L. (2006) The phosphatase activity of mammalian polynucleotide kinase takes precedence over its kinase activity in repair of single strand breaks. *Nucleic Acids Res*, **34**, 2230-2237.
84. Bernstein, N.K., Karimi-Busheri, F., Rasouli-Nia, A., Mani, R., Dianov, G., Glover, J.N. and Weinfeld, M. (2008) Polynucleotide kinase as a potential target for enhancing cytotoxicity by ionizing radiation and topoisomerase I inhibitors. *Anticancer Agents Med Chem*, **8**, 358-367.
85. Ulaczyk-Lesanko, A., Pelletier, E., Lee, M., Prinz, H., Waldmann, H. and Hall, D.G. (2007) Optimization of three- and four-component reactions for polysubstituted piperidines: application to the synthesis and preliminary biological screening of a prototype library. *J Comb Chem*, **9**, 695-703.
86. Mani, R.S., Karimi-Busheri, F., Fanta, M., Cass, C.E. and Weinfeld, M. (2003) Spectroscopic studies of DNA and ATP binding to human polynucleotide kinase: evidence for a ternary complex. *Biochemistry*, **42**, 12077-12084.

87. Meijer, M., Karimi-Busheri, F., Huang, T.Y., Weinfeld, M. and Young, D. (2002) Pnk1, a DNA kinase/phosphatase required for normal response to DNA damage by gamma-radiation or camptothecin in *Schizosaccharomyces pombe*. *J Biol Chem*, **277**, 4050-4055.
88. Misik, A.J., Perreault, K., Holmes, C.F. and Fliegel, L. (2005) Protein phosphatase regulation of Na⁺/H⁺ exchanger isoform I. *Biochemistry*, **44**, 5842-5852.
89. Wei, Q. and Lee, E.Y. (1997) Expression and reconstitution of calcineurin A and B subunits. *Biochem Mol Biol Int*, **41**, 169-177.
90. Rininsland, F., Xia, W., Wittenburg, S., Shi, X., Stankewicz, C., Achyuthan, K., McBranch, D. and Whitten, D. (2004) Metal ion-mediated polymer superquenching for highly sensitive detection of kinase and phosphatase activities. *Proc Natl Acad Sci U S A*, **101**, 15295-15300.
91. Chen, L., McBranch, D.W., Wang, H.L., Helgeson, R., Wudl, F. and Whitten, D.G. (1999) Highly sensitive biological and chemical sensors based on reversible fluorescence quenching in a conjugated polymer. *Proc Natl Acad Sci U S A*, **96**, 12287-12292.
92. Villafranca, J.E., Kissinger, C.R. and Parge, H.E. (1996) Protein serine/threonine phosphatases. *Curr Opin Biotechnol*, **7**, 397-402.
93. Breslin, C. and Caldecott, K.W. (2009) DNA 3'-phosphatase activity is critical for rapid global rates of single-strand break repair following oxidative stress. *Mol Cell Biol*, **29**, 4653-4662.
94. Nitiss, J.L. and Wang, J.C. (1996) Mechanisms of cell killing by drugs that trap covalent complexes between DNA topoisomerases and DNA. *Mol Pharmacol*, **50**, 1095-1102.
95. Freschauf, G.K., Karimi-Busheri, F., Ulaczyk-Lesanko, A., Mereniuk, T.R., Ahrens, A., Koshy, J.M., Rasouli-Nia, A., Pasarj, P., Holmes, C.F., Rininsland, F. *et al.* (2009) Identification of a small molecule inhibitor of the human DNA repair enzyme polynucleotide kinase/phosphatase. *Cancer Res*, **69**, 7739-7746.
96. Mani, R.S., Karimi-Busheri, F., Cass, C.E. and Weinfeld, M. (2001) Physical properties of human polynucleotide kinase: hydrodynamic and spectroscopic studies. *Biochemistry*, **40**, 12967-12973.
97. Mani, R.S., Karimi-Busheri, F., Fanta, M., Caldecott, K.W., Cass, C.E. and Weinfeld, M. (2004) Biophysical characterization of human XRCC1 and its binding to damaged and undamaged DNA. *Biochemistry*, **43**, 16505-16514.
98. Chen, Y.H., Yang, J.T. and Chau, K.H. (1974) Determination of the helix and beta form of proteins in aqueous solution by circular dichroism. *Biochemistry*, **13**, 3350-3359.
99. Forster, t. (ed.) (1965) *in Modern Quantum Chemistry, Istanbul Lectures*. Academic Press, New York.
100. Selvin, P.R. (1995) Fluorescence resonance energy transfer. *Methods Enzymol*, **246**, 300-334.
101. Freschauf, G.K., Karimi-Busheri, F., Ulaczyk-Lesanko, A., Mereniuk, T.R., Ahrens, A., Koshy, J.M., Rasouli-Nia, R., Pasarj, P., Holmes,

- C.F.B., Rininsland, F., Hall, D.G., and Weinfeld, M. . (in press) Isolation of a small molecule inhibitor of the human DNA repair enzyme polynucleotide kinase/phosphatase. *Cancer Research*.
102. Leach, S.J. (ed.) (1969) in *Physical Principles and Techniques of Protein Chemistry*. Academic Press, New York.
 103. Mani, R.S., Shelling, J.G., Sykes, B.D. and Kay, C.M. (1983) Spectral studies on the calcium binding properties of bovine brain S-100b protein. *Biochemistry*, **22**, 1734-1740.
 104. Donovan, J.W. (1973) Ultraviolet difference spectroscopy--new techniques and applications. *Methods Enzymol*, **27**, 497-525.
 105. Ismail, I.H., Martensson, S., Moshinsky, D., Rice, A., Tang, C., Howlett, A., McMahan, G. and Hammarsten, O. (2004) SU11752 inhibits the DNA-dependent protein kinase and DNA double-strand break repair resulting in ionizing radiation sensitization. *Oncogene*, **23**, 873-882.
 106. Wells, G.J., Bihovsky, R., Hudkins, R.L., Ator, M.A. and Husten, J. (2006) Synthesis and structure-activity relationships of novel pyrrolocarbazole lactam analogs as potent and cell-permeable inhibitors of poly(ADP-ribose)polymerase-1 (PARP-1). *Bioorg Med Chem Lett*, **16**, 1151-1155.
 107. Sordella, R., Bell, D.W., Haber, D.A. and Settleman, J. (2004) Gefitinib-sensitizing EGFR mutations in lung cancer activate anti-apoptotic pathways. *Science*, **305**, 1163-1167.
 108. Lobo, E.D. and Balthasar, J.P. (2002) Pharmacodynamic modeling of chemotherapeutic effects: application of a transit compartment model to characterize methotrexate effects in vitro. *AAPS PharmSci*, **4**, E42.
 109. Mager, D.E., Wyska, E. and Jusko, W.J. (2003) Diversity of mechanism-based pharmacodynamic models. *Drug Metab Dispos*, **31**, 510-518.
 110. Simeoni, M., Magni, P., Cammia, C., De Nicolao, G., Croci, V., Pesenti, E., Germani, M., Poggesi, I. and Rocchetti, M. (2004) Predictive pharmacokinetic-pharmacodynamic modeling of tumor growth kinetics in xenograft models after administration of anticancer agents. *Cancer Res*, **64**, 1094-1101.
 111. Rocchetti, M., Poggesi, I., Germani, M., Fiorentini, F., Pellizzoni, C., Zugnoni, P., Pesenti, E., Simeoni, M. and De Nicolao, G. (2005) A pharmacokinetic-pharmacodynamic model for predicting tumour growth inhibition in mice: a useful tool in oncology drug development. *Basic Clin Pharmacol Toxicol*, **96**, 265-268.
 112. Magni, P., Simeoni, M., Poggesi, I., Rocchetti, M. and De Nicolao, G. (2006) A mathematical model to study the effects of drugs administration on tumor growth dynamics. *Math Biosci*, **200**, 127-151.
 113. Bigioni, M., Benzo, A., Irrissuto, C., Lopez, G., Curatella, B., Maggi, C.A., Manzini, S., Crea, A., Caroli, S., Cubadda, F. *et al.* (2008) Antitumour effect of combination treatment with Sabarubicin (MEN 10755) and cis-platin (DDP) in human lung tumour xenograft. *Cancer Chemother Pharmacol*, **62**, 621-629.

114. Chou, T.C. and Talalay, P. (1984) Quantitative analysis of dose-effect relationships: the combined effects of multiple drugs or enzyme inhibitors. *Adv Enzyme Regul*, **22**, 27-55.
115. Kaufmann, S.H., Peereboom, D., Buckwalter, C.A., Svingen, P.A., Grochow, L.B., Donehower, R.C. and Rowinsky, E.K. (1996) Cytotoxic effects of topotecan combined with various anticancer agents in human cancer cell lines. *J Natl Cancer Inst*, **88**, 734-741.
116. Freschauf, G.K., Mani, R.S., Mereniuk, T.R., Fanta, M., Virgen, C.A., Dianov, G.L., Grassot, J.M., Hall, D.G. and Weinfeld, M. (2010) Mechanism of action of an imidopiperidine inhibitor of human polynucleotide kinase/phosphatase. *J Biol Chem*, **285**, 2351-2360.
117. Matsumura, Y. and Maeda, H. (1986) A new concept for macromolecular therapeutics in cancer chemotherapy: mechanism of tumoritropic accumulation of proteins and the antitumor agent smancs. *Cancer Res*, **46**, 6387-6392.
118. Matsumura, Y. (2008) Polymeric micellar delivery systems in oncology. *Jpn J Clin Oncol*, **38**, 793-802.
119. Nakanishi, T., Fukushima, S., Okamoto, K., Suzuki, M., Matsumura, Y., Yokoyama, M., Okano, T., Sakurai, Y. and Kataoka, K. (2001) Development of the polymer micelle carrier system for doxorubicin. *J Control Release*, **74**, 295-302.
120. Hecht, J.L., Dolinski, B.M., Gardner, H.A., Violette, S.M. and Weinreb, P.H. (2008) Overexpression of the alphavbeta6 integrin in endometrial cancer. *Appl Immunohistochem Mol Morphol*, **16**, 543-547.
121. Mirtsching, B., Cosgriff, T., Harker, G., Keaton, M., Chidiac, T. and Min, M. (2010) A Phase II Study of Weekly Nanoparticle Albumin-Bound Paclitaxel With or Without Trastuzumab in Metastatic Breast Cancer. *Clin Breast Cancer*, 1-8.

**Appendix A – Supplementary Material and
Analysis from Chapter II (Kinase Inhibitors)**

A.1 INTRODUCTION

As described in chapter I, hPNKP is involved in repairing both SSBs and DSBs and depletion of hPNKP in cells targeted by shRNA, can increase the radio- and chemosensitivity of cancer cells (15). This finding stimulated our lab into the identification and further characterization of a potent hPNKP phosphatase inhibitor, A12B4C3 (95). We found that A12B4C3 was highly specific to hPNKP and could double the radio- and chemosensitivity of A549 lung adenocarcinoma cells (95,116). Additional molecular and biophysical results demonstrated that A12B4C3 slowed both SSBR and DSBR and was determined to be a non-competitive inhibitor that when bound to hPNKP caused an allosteric conformational change resulting in hPNKP phosphatase inhibition (116). Taking into account these findings we have started to look for small molecule inhibitors of hPNKPs kinase activity. The rationale behind this thinking is that a PNKP kinase inhibitor may enhance therapies that predominantly produce 5-hydroxyl termini, such as Top1 poisons. In addition, it has been shown that the phosphatase activity of hPNKP is dominant to the kinase activity (83), and normal cells exposed to A12B4C3 may be affected in a more negative manner than cells exposed to a hPNKP kinase inhibitor because of its recessive activity. We have currently identified two hPNKP kinase inhibitors.

A.2 RESULTS

A.2.1 Screen of imidopiperidine compounds for PNKP Kinase Inhibitors

To identify candidate hPNKP kinase inhibitors a fluorescence based screening assay, which utilized the superquenching of fluorescently labeled 5'-DNA phosphates to determine the amount of kinase inhibition of hPNKP was

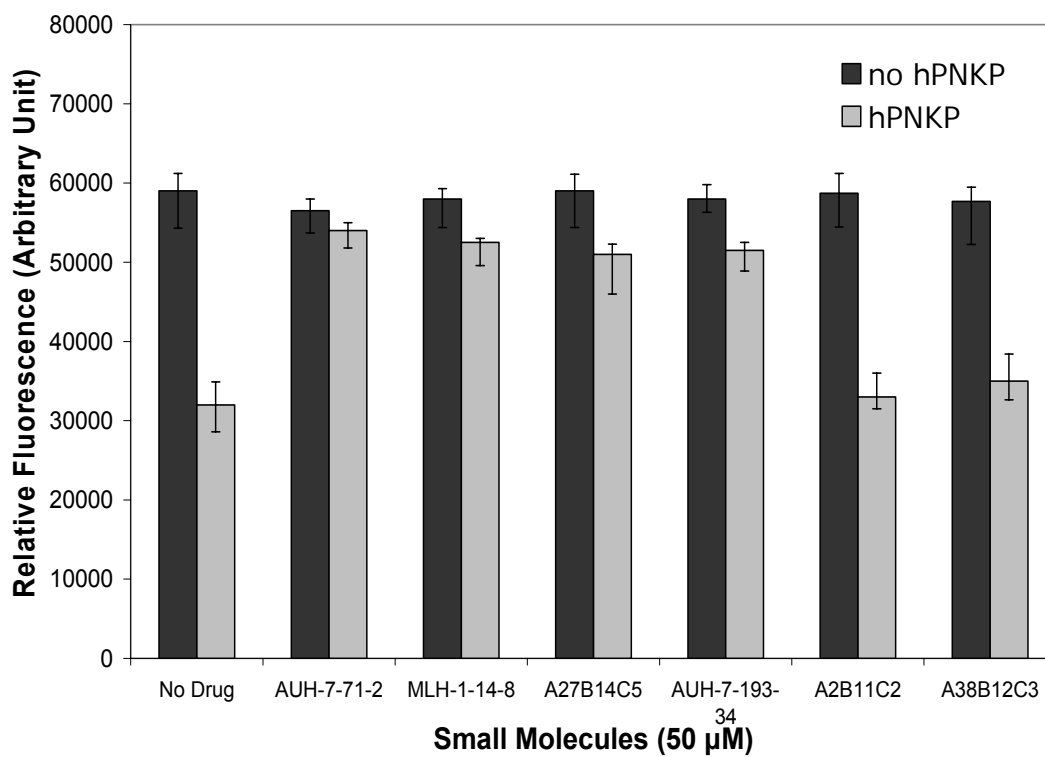


Figure A.1. Results of the fluorescence screening assay for six of the compounds tested. A2B11C2 and A38B12C3 are examples of negative kinase inhibitors due to substantial quenching of fluorescence. AUH-7-71-2, MLH-1-14-8, A27B14C5, and AUH-7-193-34 all displayed no inhibition of fluorescence quenching. The data are drawn from one experiment of triplicate data point's \pm SEM.

employed (90). This screening assay was modified slightly from a previous report, which outlined the identification of novel hPNKP phosphatase inhibitors (95). The modification encompassed the use of a 3'-fluorexcently tagged oligonucleotides with a 5'-OH group. This simple modification allowed the screening of kinase inhibitors to hPNKP possible. We tested approximately 300 polysubstituted piperidines (85) for their capacity to inhibit the kinase activity of hPNKP. We identified four compounds AUH-7-71-2, MLH-1-14-8, A27B14C5, and AUH-7-193-34, which were observed to cause substantial inhibition of hPNKPs kinase activity as shown in Figure A.1. Results for A2B11C2 and A38B12C3 are shown as examples of compounds that had minimal kinase inhibitory effect (Figure A.1).

A.2.2 Confirmation of Kinase Inhibition

To confirm the positive results from the fluorescence based high throughput screen we examined the transfer of ³²P-labeled phosphate from radiolabeled ATP to an oligonucleotide. As shown in Figure A.2, all four inhibitors, AUH-7-71-2, MLH-1-14-8, A27B14C5, and AUH-7-193-34, did indeed inhibit the kinase activity of hPNKP at 50 μM.

A.2.3 Specificity of AUH-7-71-2, MLH-1-14-8, A27B14C5, and AUH-7-193-34

To examine the specificity of the positive kinase inhibitors we made use of the PiColorLock assay (described in section 2.3.4 Chapter II). We discovered that all four kinase inhibitors had most a modest effect on inhibiting the phosphatase activity of hPNKP (Figure A.3).

Small Molecules 50 μ M

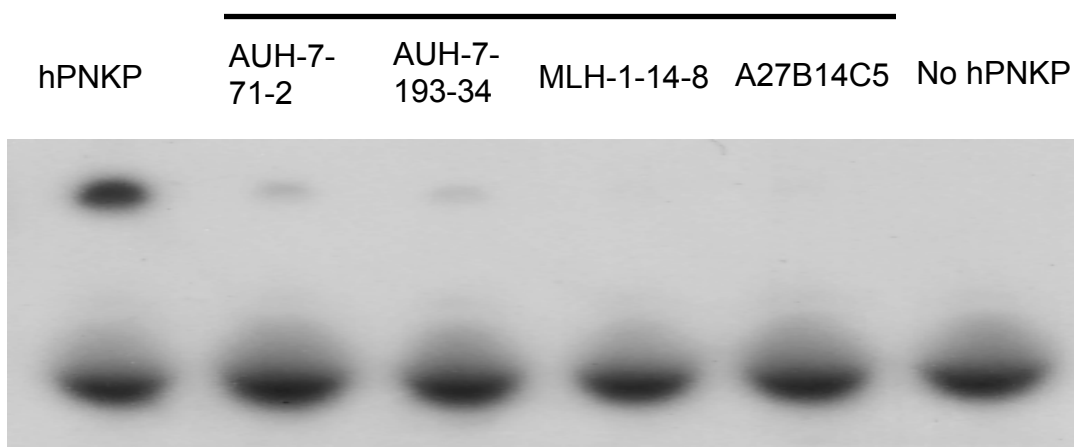


Figure A.2. Confirmation of inhibition of hPNKP kinase activity by conventional radio-gel assay. Kinase activity was measured by the transfer of radiolabeled phosphate [γ - 32 P]ATP. Addition of positive inhibitors, AUH-7-71-2, MLH-1-14-8, A27B14C5, and AUH-7-193-34 reduced the amount of phosphate transferred. The figure confirms that all four positive inhibitors identified in the high throughput screen do strongly inhibit hPNKP kinase activity.

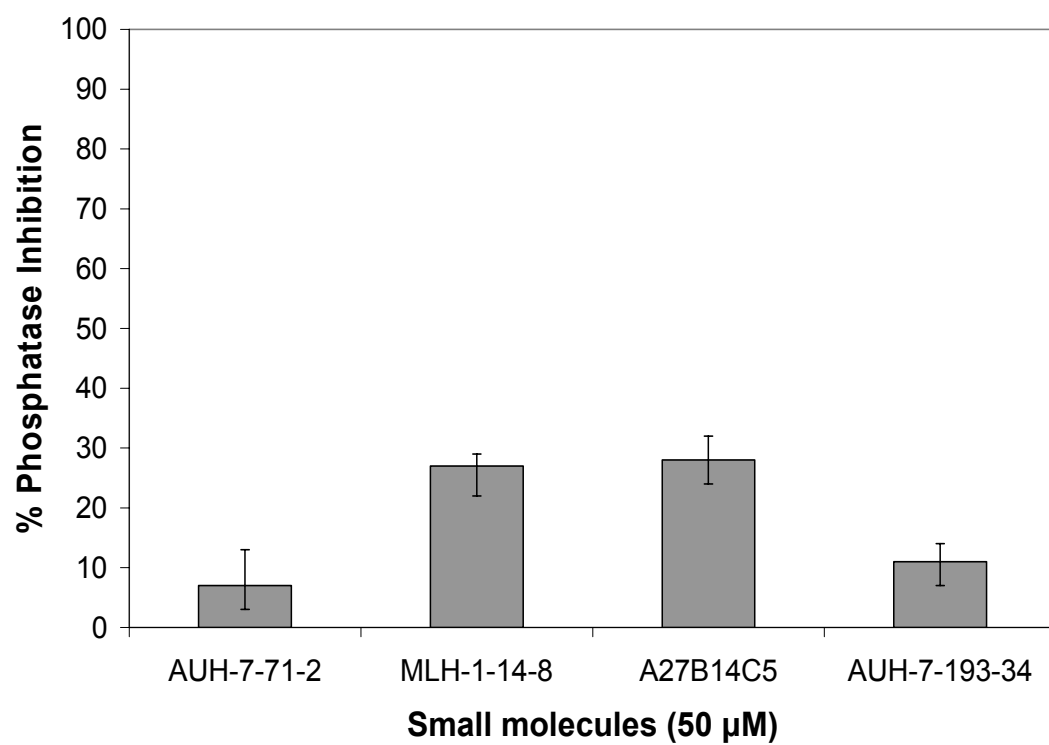


Figure A.3. Determining specificity of kinase inhibitors by measuring 3'-phosphatase activity by the PiColorlock Gold assay. All four kinase inhibitors AUH-7-71-2, MLH-1-14-8, A27B14C5, and AUH-7-193-34 had minimal effect on hPNKP phosphatase activity. The data are drawn from three sets of determinations \pm SEM.

A.2.4 Cytotoxicity of MLH-1-14-8 and A27B14C5

To determine if MLH-1-14-8 and A27B14C5 were good candidates to be used as radio- and chemosensitizers they were tested for their inherent toxicity. Cytotoxicity was measured by cell proliferation assay after exposure of A549 human lung adenocarcinoma cells to increasing doses of the compound for 72 h (Figure A.4). We observed a significant dose-dependent reduction in cell proliferation immediately after 10 μ M for both MLH-1-14-8 and A27B14C5. No significant effect on cell proliferation was detected after exposure with either 10 μ M MLH-1-14-8 or 10 μ M A27B14C5.

A.2.5 Radiosensitization by MLH-1-14-8

We then examined the capacity of MLH-1-14-8 to act as a radiosensitizer. A27B14C5 was not tested due to insufficient quantities of the compound. A549 cells were incubated with 1 μ M MLH-1-14-8 for 2 h prior to irradiation and then maintained in the presence of the compound for a further 24 h. The survival curves indicated that exposure to MLH-1-14-8 moderately increased the radiosensitivity of A549 cells (Figure A.5). Importantly, MLH-1-14-8 failed to sensitize the PNKP-depleted cells, suggesting that hPNKP may be the principle target of MLH-1-14-8 in the cell.

A.3 DISCUSSION

Appendix A describes the identification of hPNKP kinase inhibitors and the subsequent preliminary characterization of these compounds. After screening almost 300 polysubstituted piperidines, four kinase inhibitors were identified, AUH-7-71-2, MLH-1-14-8, A27B14C5, and AUH-7-193-34, and further testing

was undertaken. MLH-1-14-8 and A27B14C5 were clearly the two most potent inhibitors with approximately 100% kinase inhibition at 50 μ M (Figure A.2).

An important issue with all small molecules is their specificity. We examined the ability of the four kinase inhibitors to inhibit the phosphatase activity of hPNKP. We discovered that all four kinase inhibitors had considerably less influence on the phosphatase activity than the kinase activity of PNKP (Figure A.3)

Next we analyzed the toxicity levels of the two most potent kinase inhibitors by utilizing a cell proliferation assay. We discovered that both MLH-1-14-8 and A27B14C5 had minimal toxicity at low μ M doses (Figure A.4). Radiosensitizing studies showed that MLH-1-14-8 at 1 μ M could modestly increase the radiosensitivity of A549 lung adenocarcinoma cells (Figure A.5). Moreover, when MLH-1-14-8 was added to A549 δ PNKP cells no further significant increase in radiosensitization was observed. Characterization of A27B14C5 radiosensitizing properties has not yet been undertaken due to insufficient quantities of the compound.

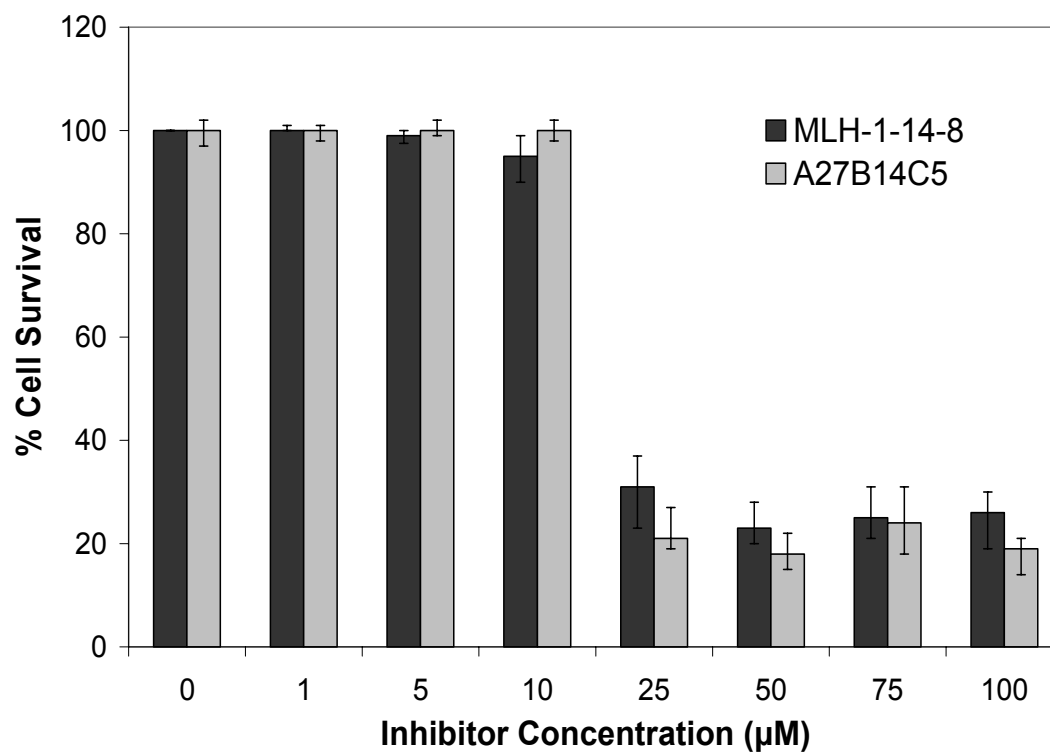


Figure A.4. Cytotoxicity of MLH-1-14-8 and A27B14C5 alone measured by 72-h exposure of A549 lung adenocarcinoma cells to increasing concentrations of the compound and determination of cell proliferation as described in section 2.3.9. The data are drawn from three independent determinations \pm SEM.

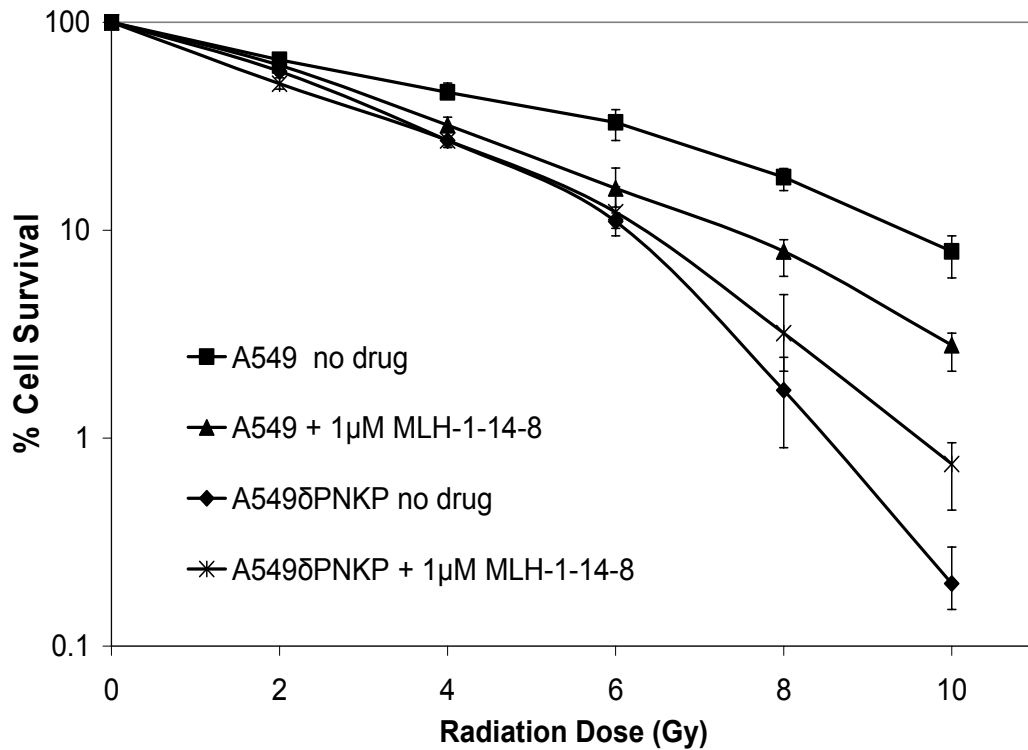


Figure A.5. Influence of MLH-1-14-8 on the radiosensitivity of wild-type A549 cells and PNKP-deficient cells (A549δPNKP). Cells were exposed to 1 µM MLH-1-14-8 2 h before irradiation and then maintained in the same media for a further 24 h. The media was then replaced with fresh media without the drug. Radiosensitization was determined by the colony-forming assay as described in section 2.3.10. The survival curves are based on three independent sets of determinations ± SEM.